On Finite Element and Control Volume Upwinding Methods for High Peclet Number Flows

by

Dena Hendriana

Submitted to the Department of Mechanical Engineering
in partial fulfillment of the requirements for the degree of

Master of Science in Mechanical Engineering

at the

MASSACHUSETTS INSTITUTE OF TECHNOLOGY

May 1994

Author . . . .
Department of Mechanical Engineering
May 6, 1994

Certified by . . . .
Klaus-Jürgen Bathe
Professor of Mechanical Engineering
Thesis Supervisor

Accepted by . . . .
Ain Ants Sonin
Chairman, Graduate Committee

On Finite Element and Control Volume Upwinding Methods for High Peclet Number Flows

by

Dena Hendriana

Submitted to the Department of Mechanical Engineering
on May 6, 1994, in partial fulfillment of the
requirements for the degree of
Master of Science in Mechanical Engineering

Abstract

The standard Galerkin finite element method is unstable for the solution of high Peclet/Reynolds number flows. Upwinding procedures have been proposed to stabilize the method. This thesis attempts to identify the optimum upwinding scheme used in the quadrilateral four-node finite element. We achieve this by comparing several previously published upwinding techniques via testing their stability and accuracy in two numerical convection-diffusion problems. Our experiment shows that for some of the upwinding procedures, we can only find an exact nodal solution in one-dimensional analysis, but not in two-dimensional analysis. With this limitation, we find that the positive-coefficient upwinding scheme provides the best stability and accuracy characteristics.

Thesis Supervisor: Klaus-Jürgen Bathe
Title: Professor of Mechanical Engineering

Acknowledgments

Contents

List of Figures

List of Tables

10

Chapter 1

Introduction

The finite element method has been used extensively in simulating physical situations. The main reason for this is that the finite element method is flexible to represent complex geometric domains. Where analytical solutions are difficult or impossible to obtain, the finite element method can provide good solutions in simulating physical situations governed by well established mathematical equations. The finite element method has been used abundantly in structural mechanics. Its development is still being continued to extend its application in complex fluid mechanics as reflected in research published during the recent years.

The finite element method for solving fluid mechanics problems is usually based on the Eulerian formulation in which a fixed position control volume is used to derive the governing equations. This leads to the governing equation to contain a convective term that has first order spatial derivatives. Using the Galerkin finite element procedure on the governing equation, the convective term creates a skew matrix which is the source of nonphysical oscillations. These nonphysical oscillations therefore are a result of the discretization of the first order spatial derivative in the convective term when the convective term dominates the other terms in the governing equation.

Many methods have been proposed to circumvent the numerical oscillations. These methods are called upwinding. The idea in upwinding is that the node in the upstream direction gives more weight to the solution than the node in the downstream direction.

Research on upwinding procedures started in the 1950's. While the basic idea of upwinding was already proposed by Courant et al. [9] in 1952, the techniques for more general control volume type methods and for finite element procedures are still under active development. Some important procedures have been proposed by Hughes et al. [5, 12, 13, 14, 20], Zienkiewicz et al. [8], Donea et al. [11], Schneider et al. [22], Patankar [21], etc. These methods are quite efficient in certain applications, with the use of specific discretizations, but improvements and generalizations for finite element analysis with optimal accuracy characteristics are still sought.

The basic upwinding technique applies the forward difference method, of first order accuracy, to the convective term for stable calculation which replaces the central difference method obtained from the Galerkin finite element procedure. However, it turns out that by using the forward difference method, the numerical results are not satisfactory since they are overly diffused. To improve accuracy, an adjusted variable, which is a function of the Reynolds number or the Peclet number, is introduced in upwinding methods. As a result, an exact nodal solution is obtained for one dimensional analysis.

For two dimensional cases, the idea of upwinding can not be easily applied. Various methods have been proposed to implement the basic idea of upwinding to two dimensional analyses. In this thesis, we shall discuss various upwinding methods specifically with respect to their use in two dimensional analyses.

1.1 Thesis Organization

This thesis is divided into six chapters. Chapter 1 is an introduction to the topic considered in this thesis. Chapter 2 summarizes the basic governing equation — the heat transfer equation in fluid mechanics — which leads to the common convection-diffusion equation. Derivation of the finite element method used for this equation, along with an explanation of the assumptions made, is also presented in this chapter.

Chapter 3 discusses upwinding schemes used to solve the convection-diffusion problems in one dimension. In this chapter, solutions to the convection-diffusion

problems for a domain that is subdivided into a uniform mesh obtained by using various upwinding schemes are compared. The schemes being discussed are the Galerkin method, full upwinding scheme which applies the forward difference method, the exponential scheme, the Petrov-Galerkin, and the Galerkin least squares method. A third order accuracy upwinding scheme is also discussed here.

Discussion on the upwinding schemes for the two dimensional analyses are explored in chapter 4. Basic ideas of individual schemes will also be explained. The schemes presented are basically extensions of the upwinding schemes discussed in chapter 3. Comparisons among the schemes will be presented.

In chapter 5, we explain test problems used in measuring the accuracy and the stability of the previously explained upwinding schemes. Explanation of the domain, meshes, specified velocity fields, and the boundary conditions of the test problems is given. The expected solutions to the test problems are described and compared to the numerical results obtained by using the various upwinding schemes.

Chapter 6 presents the solutions to the test problems using the upwinding schemes and conclusions. Discussion of the individual results is given. The results are also compared to the ADINA-F solutions using the macro triangular four node elements available in this general fluid flow finite element program.

Finally, chapter 7 presents the conclusions of the study.

Chapter 2

Basic Equation

Consider the general heat transfer equation in fluid mechanics

$$\rho c_p \left(\frac{\partial \theta}{\partial t} + v_i \frac{\partial \theta}{\partial x_i} \right) = \frac{\partial}{\partial x_i} \left(\kappa \frac{\partial \theta}{\partial x_i} \right) + q^B \tag{2.1}$$

where ρ, c_p, θ, v_i, κ and q^B are the fluid density, the heat capacity, temperature, the velocity in the x_i direction, the thermal conductivity and the heat source, respectively. Assuming κ to be constant, rewriting equation 2.1 leads to the usual convection-diffusion equation,

$$\theta_{,t} + \underline{v} \cdot \underline{\nabla} \theta = \alpha \nabla^2 \theta + q \tag{2.2}$$

where $()_{,t}$ denotes differentiation with respect to time; $\underline{\nabla}$ denotes spatial differentiation, $\underline{v}$, α and q are the velocity field, diffusivity $(\alpha = \frac{\kappa}{\rho c_p})$ and the source term $(q = \frac{q^B}{\rho c_p})$, respectively. In this model, α is assumed to be constant.

2.1   Finite Element Formulation

Consider a domain (Ω) which lies in $R^{n_{sd}}$ space dimensions and $x = \{x_i\}$ where $i = 1, 2, ..., n_{sd}$ are the coordinate axes of the system in the $R^{n_{sd}}$ space. The time t considered is in the interval $]0, T[$, where T is a specified time. Let eqn. 2.2 be the governing equation in the domain (Ω). The domain is discretized into n_{el} subdomains

14

(Ω^e) where

$$\Omega = \bigcup_{e=1}^{n_{el}} \Omega^e$$

$$\emptyset = \bigcap_{e=1}^{n_{el}} \Omega^e$$

The domain has a boundary (S) and is divided into S_u and S_f

$$S = S_u \bigcup S_f$$

$$\emptyset = S_u \bigcap S_f$$

where the essential boundary condition is applied on S_u and the natural boundary condition on S_f.

In the element, the temperature (θ) is described by nodal point temperatures and its distribution across the element is defined using interpolation functions (v_h). The interpolation functions are in the solution function space (V_h) defined as the following

$$V_h = \{v_h \mid v_h \in (H^1)^{n_{sd}}, v_h = g_h \text{ on } S_u\}$$

where H^1 is the Sobolev space and g_h is the essential boundary condition that is applied on S_u.

Introducing the interpolation matrix $\mathbf{H}$ and the gradient matrix $\mathbf{B}$ that are used to approximate the function and the gradient of θ in a typical element,

$$\theta = \mathbf{H}\hat{\theta} \qquad (2.3)$$

$$\nabla\theta = \mathbf{B}\hat{\theta}$$

where $\hat{\theta}$ is a vector of nodal value θ.

The weighting function (w) is in the weighting function space that is defined as follows

$$W_h = \{w_h \mid w_h \in (H^1)^{n_{sd}}, w_h = 0 \text{ on } S_u\}$$

15

The classical Galerkin procedure applied to the basic convection-diffusion equation (eqn. 2.2) with any weighting function (w) gives

$$\int_{Vol} w\left(\theta_{,t} + \underline{v} \cdot \underline{\nabla}\theta - \alpha\nabla^2\theta - q\right) dVol = 0 \qquad (2.4)$$

Applying integration by parts and the divergence rule to eqn. 2.4, we obtain

$$\int_{Vol} w\,\theta_{,t}\,dVol \;+\; \int_{Vol} w\,\underline{v}\cdot\underline{\nabla}\theta\,dVol + \int_{Vol} \underline{\nabla}w\alpha\underline{\nabla}\theta\,dVol$$
$$= \int_{Vol} wq\,dVol + \int_{S_u} wq^{\cdot}\,dS_u \qquad (2.5)$$

where $q^{\cdot}$ is the natural boundary condition.

Equation 2.5 leads to the finite element matrix equation as follows

$$\mathbf{M}\dot{\hat{\theta}} + \mathbf{K_c}\hat{\theta} + \mathbf{K_d}\hat{\theta} \;=\; \mathbf{R_b} + \mathbf{R_s} \qquad (2.6)$$

where $\hat{\theta}$ is the nodal temperature vector, $\mathbf{M}$, $\mathbf{K_c}$, $\mathbf{K_d}$, $\mathbf{R_b}$, and $\mathbf{R_s}$ are the mass matrix, the stiffness matrix from the convective term, the stiffness matrix from the diffusive term, the load vector from the source term and the load vector from the boundary conditions, respectively. The finite element matrix equation must be solved to obtain the numerical solution for the convection-diffusion problem with specified boundary conditions.

In one dimensional analysis, a two-node element may be used with linear interpolation functions. The interpolation functions for each node are defined as follows

$$h_1 = \frac{1}{2}(1+r)$$
$$h_2 = \frac{1}{2}(1-r)$$

where r is the local coordinate. The Jacobian scalar is required to relate the local coordinate (r) to the global coordinate (x). Fig. 2-1 shows the linear interpolation functions in the element.

The interpolation matrix $\mathbf{H}$ and the gradient matrix $\mathbf{B}$ for this element are defined
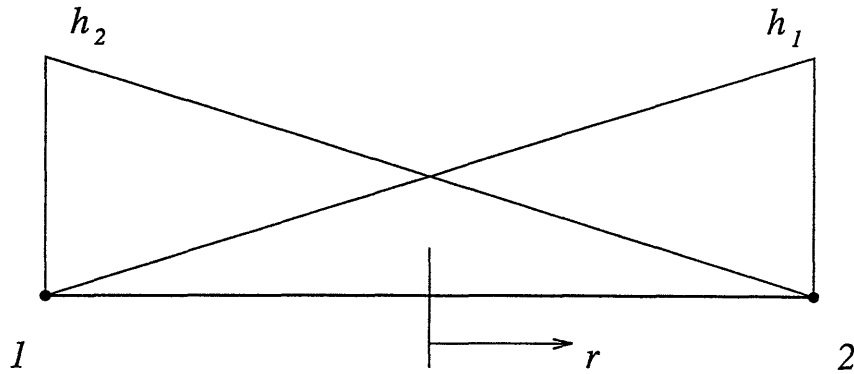
Figure 2-1: Interpolation function for two-node element

as follows

$$\mathbf{H} = [h_1 \ h_2] \tag{2.7}$$

$$\mathbf{B} = \left[\frac{\partial h_1}{\partial x} \ \frac{\partial h_2}{\partial x}\right]$$

For two dimensional analysis, a quadrilateral four-node element is considered. The interpolation functions for this element are bilinear functions that are defined as follows

$$h_1 = \frac{1}{4}(1 + r)(1 + s)$$

$$h_2 = \frac{1}{4}(1 - r)(1 + s)$$

$$h_3 = \frac{1}{4}(1 - r)(1 - s)$$

$$h_4 = \frac{1}{4}(1 + r)(1 - s)$$

where r and s are the local coordinates in the element which are shown in fig. 2-2. The local coordinate system is employed to generalize formulations for any shape of quadrilateral elements obtained from the discretization process of a complex geometric domain. As a consequence, Jacobian matrix is required to connect the local coordinate system with the global coordinate system. Using the local coordinate system, any

17
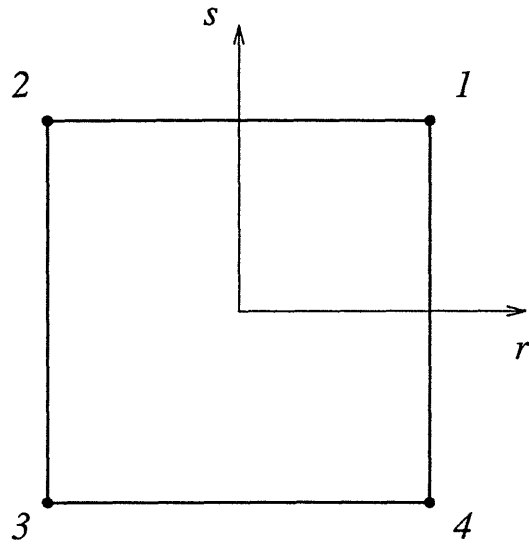
Figure 2-2: Local coordinate r and s for four-node element.

shape of quadrilateral of elements can be treated as 2x2 square elements.

The interpolation matrix $\mathbf{H}$ and the gradient matrix $\mathbf{B}$ for two dimensional case are defined as follows

$$\mathbf{H} = [h_1 \ h_2 \ h_3 \ h_4]$$

$$\mathbf{B} = \begin{bmatrix} \frac{\partial h_1}{\partial x} & \frac{\partial h_2}{\partial x} & \frac{\partial h_3}{\partial x} & \frac{\partial h_4}{\partial x} \\ \frac{\partial h_1}{\partial y} & \frac{\partial h_2}{\partial y} & \frac{\partial h_3}{\partial y} & \frac{\partial h_4}{\partial y} \end{bmatrix}$$

Chapter 3

Various Upwinding Schemes in One Dimensional Analysis

In this chapter, the one dimensional convection-diffusion equation is considered and some upwinding schemes for one dimensional application are discussed. Consider the convection-diffusion equation (eqn. 2.2) for one dimensional case, assuming steady state condition and zero source term,

$$v\theta_{,x} = \alpha\theta_{,xx} \qquad (3.1)$$

When the finite element method without upwinding schemes is applied to a simple problem, which is governed by the equation above, oscillations in the numerical solution is observed; however when the numerical method is used with upwinding schemes, the oscillation difficulty is eliminated. A uniform mesh domain to be considered with the element length Δx and its linear interpolation functions is shown in fig 3-1.

3.1 Classical Galerkin method

The classical Galerkin method uses the weighting functions that are in the same space as the interpolation functions. By applying the Galerkin method to eqn. 3.1,
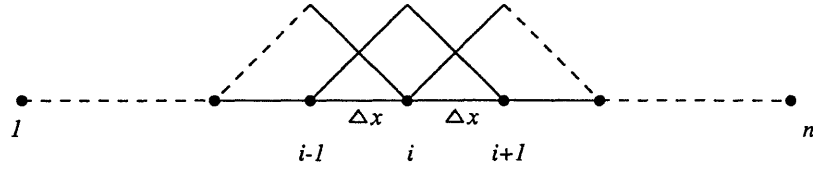
Figure 3-1: Uniform mesh for i^{th} node and its interpolation functions.

we obtain the following equation,

$$\int_{Vol} w\,(v\frac{d\theta}{dx} - \alpha\frac{d^2\theta}{dx^2})\,dVol = 0 \tag{3.2}$$

Solving eqn. 3.2 leads to the following discrete form for the ith node (i within the boundary) of a uniform mesh with element size $\triangle x$,

$$v\frac{-\theta_{i-1} + \theta_{i+1}}{2\triangle x} = \alpha\frac{\theta_{i-1} - 2\theta_i + \theta_{i+1}}{\triangle x^2} \tag{3.3}$$

which can be simplified to obtain the following equation

$$(-1 - \frac{Pe^e}{2})\theta_{i-1} + 2\theta_i + (-1 + \frac{Pe^e}{2})\theta_{i+1} = 0 \tag{3.4}$$

where $\theta_{i-1}, \theta_i,$ and θ_{i+1} are the nodal values of θ at stations $i - 1, i,$ and $i + 1$, respectively. Pe^e is the element peclet number , $Pe^e = \dfrac{v\,\triangle x}{\alpha}$.

It can be seen that the use of the Galerkin method gives the same result as of the central difference method for the spatial derivatives. The coefficients of θ from the diffusive term (in the right hand side of eqn. 3.3) are symmetric with respect to i and this gives a stable numerical solution. However, the coefficients of θ from the convective term (in the left hand side of eqn. 3.3) are anti-symmetric. When the convective term dominates, this anti-symmetry coefficients create instability in the finite element solution which is indicated by oscillations. For demonstration of the oscillations, consider the following problem.

Sample Problem

A one dimensional domain with total lenght=1 is divided into 20 uniform elements. Let the convection-diffusion equation (eqn.3.1) govern in the domain. The velocity field is prescribed by $v = 1$ uniformly, and constant diffusivity is assumed, $\alpha = 10^{-2}$, (The global Peclet number is 100). The boundary conditions are defined as follows

$$\theta = 1 \text{ at } x = 0$$
$$\theta = 0 \text{ at } x = 1$$

In one dimensional case, the boundary S_f, where the natural boundary condition
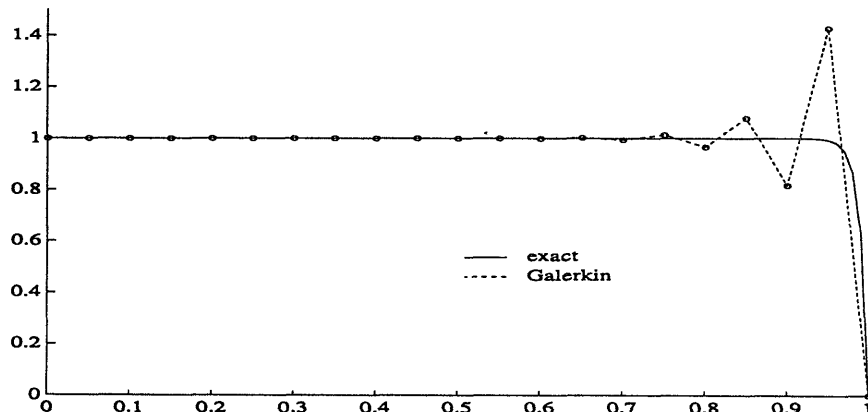
Figure 3-2: Solution of the convection-diffusion problem using the classical Galerkin method.

is applied, represents a nodal point instead of a surface. In the sample problem, the essential boundary condition is applied to the left and right boundaries, so the problem does not contain S_f.

Fig. 3-2 shows the numerical result of the problem using the Galerkin method. In the solution, oscillations occur near the boundary layer at $x = 1$.

3.2 Full Upwinding Scheme

To avoid the numerical oscillations in the finite element solution of convection-diffusion problems when Peclet number is high, researchers have modified an upwinding method that is available in the finite difference method for use in the finite element method. Originally, the upwinding method was proposed by Courant et al. [9]. Using this method, the central difference approximation that is obtained using the classical Galerkin method for the first spatial derivatives in the convective term is replaced by the forward difference approximation. Essentially, this method places more weight on the coefficient of θ for the node in the upstream direction and relaxes the weight on the node in the downstream direction. For a uniform mesh with element length $\triangle x$ and $v > 0$, full upwinding scheme gives the following discrete equation for the ith node

$$v\frac{-\theta_{i-1} + \theta_i}{\triangle x} = \alpha\frac{\theta_{i-1} - 2\theta_i + \theta_{i+1}}{\triangle x^2} \tag{3.5}$$

$$(-1 - Pe^e)\theta_{i-1} + (2 + Pe^e)\theta_i - \theta_{i+1} = 0 \tag{3.6}$$

When $v < 0$, full the upwinding scheme gives the following discrete equation for the ith node

$$v\frac{-\theta_i + \theta_{i+1}}{\triangle x} = \alpha\frac{\theta_{i-1} - 2\theta_i + \theta_{i+1}}{\triangle x^2} \tag{3.7}$$

$$-\theta_{i-1} + (2 - Pe^e)\theta_i + (-1 + Pe^e)\theta_{i+1} = 0 \tag{3.8}$$

Using the full upwinding scheme, the sample problem defined in the end of Section 3.1 is solved and the result is shown in fig. 3-3.

The numerical solutions of the convection-diffusion problems are always stable when the full upwinding scheme is used. However, the solutions are not satisfactory because they are too diffusive. This is because the use of the full upwinding method leads to the use of the forward difference approximation that has a lower accuracy than the central difference approximation obtained by the Galerkin method. The forward difference method has a first order of accuracy whereas the central difference method has a second order accuracy. In order to improve the numerical results, other upwinding schemes are proposed.
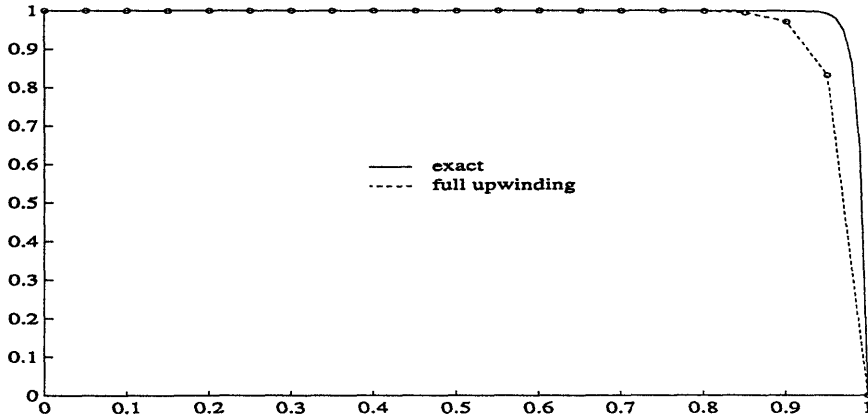
Figure 3-3: Solution of the convection-diffusion problem using full upwinding method.

3.3 Exponential Upwinding Scheme

This upwinding scheme has been derived based on the control volume finite element method (CVFEM) argument [21]. Originally, this method was proposed by Spalding in [24]. In CVFEM, a domain is divided into a number of control volumes. In every control volume, the governing equation is satisfied that leads to satisfying the governing equation throughout the whole domain. Let the eqn. 3.1 be the governing equation in a domain that is subdivided into control volumes uniformly. Consider the ith node in the domain where the control volume is applied (see fig. 3-4). Rewrite eqn. 3.1 in the following way

$$\frac{df}{dx} = 0 \tag{3.9}$$

$$f = v\theta - \alpha\frac{d\theta}{dx}$$

where f is the flux of convective and diffusive terms. In the control volume method, the fluxes enter from the left and right boundaries. The boundaries are located

between nodes (see fig. 3-4). Integrating eqn. 3.9 over the control volume, we obtain

$$f_{i+\frac{1}{2}} - f_{i-\frac{1}{2}} = 0 \tag{3.10}$$

where $f_{i+\frac{1}{2}}$ and $f_{i-\frac{1}{2}}$ are the fluxes at the right and left boundaries.
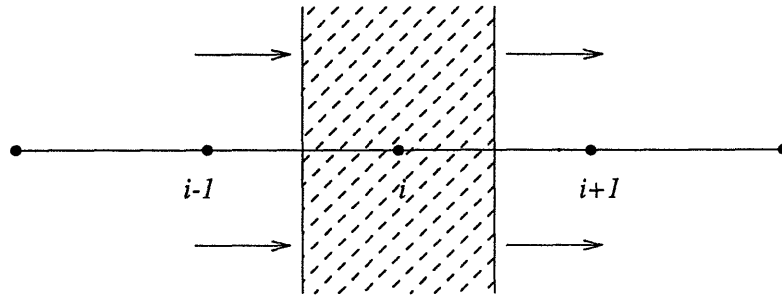
Figure 3-4: Control volume applied to the ith node

The original control volume method uses linear interpolation functions to approximate the value of θ at the control volume boundaries (see fig. 3-5), so

$$f_{i+\frac{1}{2}} = v\frac{\theta_{i+1} + \theta_i}{2} - \alpha\frac{\theta_{i+1} - \theta_i}{\triangle x} \tag{3.11}$$

$$f_{i-\frac{1}{2}} = v\frac{\theta_i + \theta_{i-1}}{2} - \alpha\frac{\theta_i - \theta_{i-1}}{\triangle x} \tag{3.12}$$

By substituting eqn. 3.11 and 3.12 into eqn. 3.10, we obtain

$$v\frac{-\theta_{i-1} + \theta_{i+1}}{2} - \alpha\frac{\theta_{i-1} - 2\theta_i + \theta_{i+1}}{\triangle x} = 0 \tag{3.13}$$

If this equation is divided by $\triangle x$, it can be seen that the control volume method using linear interpolation functions leads to a solution that is equivalent to solution found by the central difference method for the convective and diffusive terms. It is already discussed that the central difference approximation is not stable when the convective term dominates the diffusive term. In order to make the solution stable, the flux f at the control volume boundaries need to be evaluated in a different way.
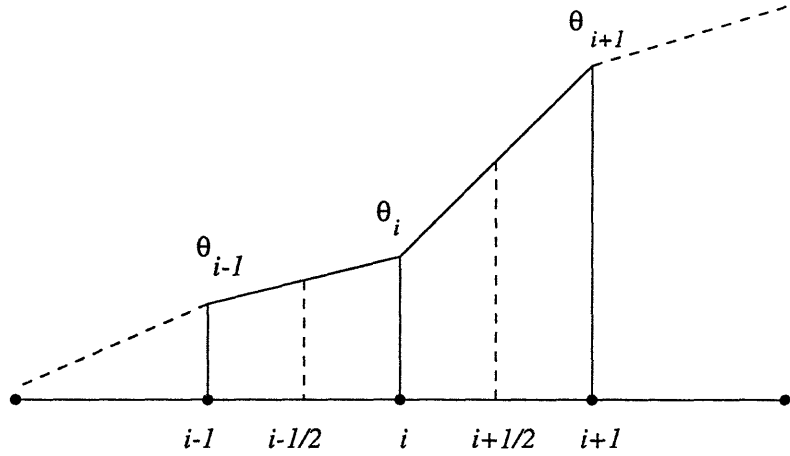
Figure 3-5: Linear interpolation function of θ in the control volume method.

Instead of using linear interpolation functions, the exact solution of the convection-diffusion equation (eqn. 3.1) is used to evaluate the value of θ at the boundaries. The exact value of θ and its derivative with respect to x for the left boundary are

$$\theta\Big|_{i-\frac{1}{2}} = \theta_{i-1} + \frac{(\theta_i - \theta_{i-1})(\exp(\frac{Pe^e}{2}) - 1)}{\exp(Pe^e) - 1} \tag{3.14}$$

$$\frac{d\theta}{dx}\Big|_{i-\frac{1}{2}} = \frac{(\theta_i - \theta_{i-1})\frac{Pe^e}{\Delta x}\exp(\frac{Pe^e}{2})}{\exp(Pe^e) - 1} \tag{3.15}$$

For the right boundary, the exact value of θ and its derivative have similar form of equations as the equations above, except that the subscript $i - 1$ and i need to be replaced by i and $i + 1$. Inserting these equations into eqn. 3.9, we obtain

$$f_{i-\frac{1}{2}} = v\left[\theta_{i-1} + \frac{\theta_{i-1} - \theta_i}{exp(Pe^e) - 1}\right] \tag{3.16}$$

$$f_{i+\frac{1}{2}} = v\left[\theta_i + \frac{\theta_i - \theta_{i+1}}{exp(Pe^e) - 1}\right] \tag{3.17}$$

Finally after inserting eqn. 3.16 and 3.17 into 3.10, this scheme gives the equation for the node i,

$$(-e^{Pe^e})\theta_{i-1} + (1 + e^{Pe^e})\theta_i - \theta_{i+1} = 0 \tag{3.18}$$

25

Using this scheme, an exact nodal solution is obtained. This is expected since the exact solution of the governing equation is incorporated in the formulation. Note that the coefficients of θ in eqn. 3.18 are functions of the Peclet number which depends on the value of the flow velocity, so the coefficient will vary depending on the velocity. Fig. 3-6 depicts the solution of the problem considered in the end of section 3.1 using the exponential upwinding scheme.
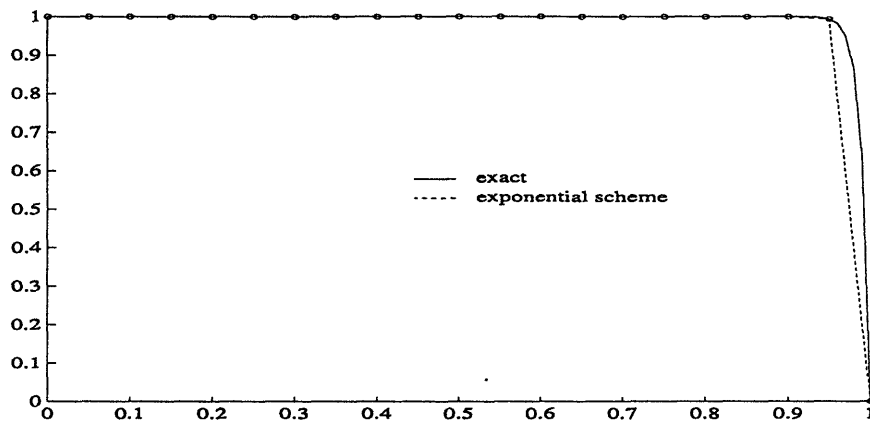
Figure 3-6: Solution of the convection-diffusion problem using the exponential scheme.

3.4 Petrov-Galerkin Method

In contrast to the classical Galerkin method, the Petrov-Galerkin method uses a different weighting function which is not in the same space as the interpolation function. This method was originally proposed by Christie et al. [8]. The weighting function in this scheme is designed to include the upwinding effect. Its modification is based on the idea of allowing more weight to the node in the upstream direction and reducing the weight to the node in the downstream direction. The modified weighting function is defined as follows

$$\overline{w} = w + p \tag{3.19}$$

26

where $\overline{w}$ is the modified weighting function; w is the original weighting function (which is the same as the interpolation function) and p is a perturbation function. The perturbation function is defined as follows

$$p = \gamma \frac{\triangle x}{2} \frac{dh}{dx} \qquad (3.20)$$

γ is a coefficient to control the magnitude of the perturbation function; $\triangle x$ is the element length and h is the interpolation function. The value of the coefficient is between -1 to 1. Fig. 3-7 shows the modified weighting function for a typical linear interpolation element.
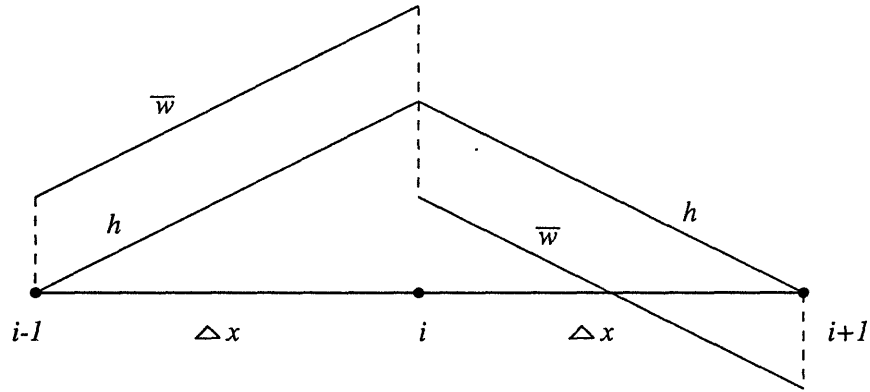
Figure 3-7: The weighting function ($\overline{w}$) and the related interpolation function (h).

Applying this weighting function to the governing equation (eqn. 3.1) while using integration by parts and the divergence rule, we obtain

$$\int_{Vol} \overline{w} \left(v\theta_{,x} - \alpha\theta_{,xx} \right) dVol = 0$$

and hence

$$\int_{Vol} \overline{w} \, v\theta_{,x} \, dVol + \int_{Vol} \overline{w}_{,x} \alpha\theta_{,x} \, dVol = \int_{S_f} \overline{w} \, q^* \, dS_f \qquad (3.21)$$

where q^* is the natural boundary condition. Note that in the second term of eqn. 3.21,

$\overline{w}_{,x} = w_{,x}$ for the following reason

$$\overline{w}_{,x} = w_{,x} + p_{,x}$$

$$p_{,x} = (\gamma\frac{\Delta x}{2}h_{,x})_{,x}$$

$$= \gamma\frac{\Delta x}{2}h_{,xx}$$

Since a linear interpolation function is used, $h_{,xx} = 0$ and therefore $\overline{w}_{,x} = w_{,x}$.

Consider the first term in eqn. 3.21,

$$\int_{Vol} \overline{w}\, v\theta_{,x}\, dVol = \int_{Vol} (w + \gamma\frac{\Delta x}{2}w_{,x})\, v\theta_{,x}\, dVol$$

$$= \int_{Vol} w\, v\theta_{,x}\, dVol + \int_{Vol} w_{,x}\tilde{\alpha}\theta_{,x}\, dVol \qquad (3.22)$$

where $\tilde{\alpha}$ is an artificial diffusivity

$$\tilde{\alpha} = \gamma\frac{\Delta x}{2}v$$

Rewriting eqn. 3.21

$$\int_{Vol} w\, v\theta_{,x}\, dVol + \int_{Vol} w_{,x}(\alpha + \tilde{\alpha})\theta_{,x}\, dVol = \int_{S_f} \overline{w}\, q^*\, dS_f \qquad (3.23)$$

gives the discrete equation for the ith node (that does not have the S_f boundary) in a uniform mesh which is as follows

$$(-1 - (1 + \gamma)\frac{Pe^e}{2})\theta_{i-1} + (2 + \gamma Pe^e)\theta_i + (-1 + (1 - \gamma)\frac{Pe^e}{2})\theta_{i+1} = 0 \qquad (3.24)$$

setting γ as [8],

$$\gamma = \coth(\frac{Pe^e}{2}) - \frac{2}{Pe^e} \qquad (3.25)$$

which is an adjustment to achieve the exact solution at the nodes; obtained by equating eqn. 3.24 with the exact solution of the governing equation (derivation of eqn. 3.25 is given in appendix A).

The result of the problem considered in section 3.1 using the Petrov-Galerkin method is given in fig. 3-8.
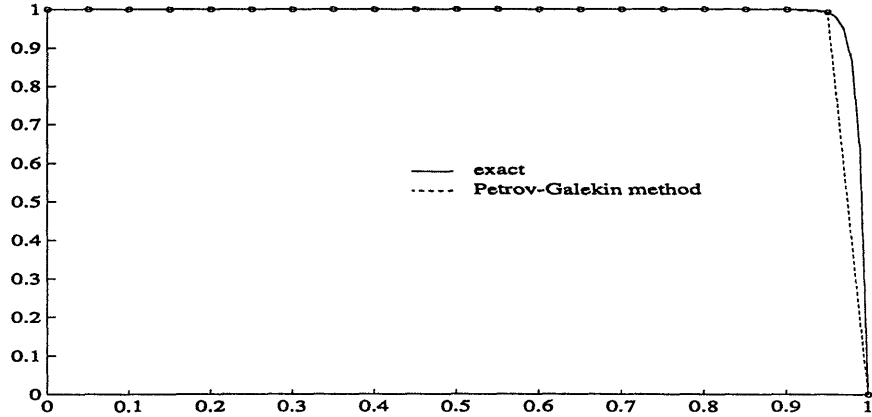
Figure 3-8: Solution to the convection-diffusion problem using the Petrov-Galerkin method.

3.5 Galerkin Least Squares Upwinding Scheme

In this upwinding scheme, least squares expressions [23] are included in the classical Galerkin method with a selected weight coefficient, τ, to control the magnitude of the new expression. The least squares functions for eqn. 3.1 are

$$
\begin{aligned}
L_{2m}\left[h_i\right] &= v\frac{dh_i}{dx} - \alpha\frac{d^2 h_i}{dx^2} \\
L_{2m}\left[\theta_h\right] &= v\frac{d\theta_h}{dx} - \alpha\frac{d^2 \theta_h}{dx^2}
\end{aligned}
\tag{3.26}
$$

where θ_h is the finite element solution of the unknown variable θ in the domain. Since linear interpolation functions are used, the latter terms on the right hand side of eqns. 3.26 are dropped.

After the Galerkin least squares method is applied to the governing equation, we

29

obtain

$$\int_{Vol} w \left(v\frac{d\theta}{dx} - \alpha\frac{d^2\theta}{dx^2} \right) dVol + \int_{Vol} (v\frac{dh}{dx})\tau(v\frac{d\theta}{dx}) \, dVol = 0 \qquad (3.27)$$

The last term in the equation above is the least squares term and τ is a variable to be adjusted in order to obtain the nodal exact solution. Solving eqn. 3.27 leads to the discrete equation for the ith node,

$$(-1 - \frac{Pe^e}{2} - \frac{\tau v^2}{\alpha})\theta_{i-1} + (2 + 2\frac{\tau v^2}{\alpha})\theta_i + (-1 + \frac{Pe^e}{2} - \frac{\tau v^2}{\alpha})\theta_{i+1} = 0 \qquad (3.28)$$

To obtain the nodal exact solution, the value of τ is evaluated as follows [23] (see appendix B for derivation)

$$\tau = \frac{h}{2v} \coth(\frac{Pe^e}{2}) - \frac{\alpha}{v^2} \qquad (3.29)$$

Fig. 3-9 shows the solution to the problem considered in sec. 3.1 using the Galerkin least squares method.
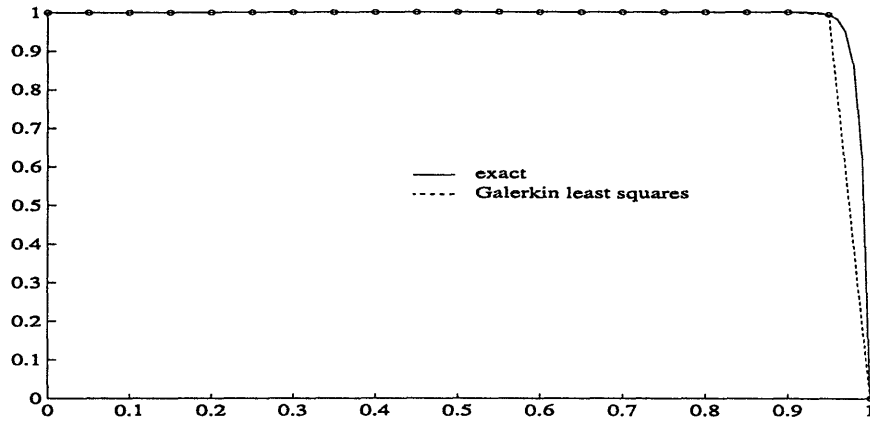
Figure 3-9: Solution to the convection-diffusion problem using the Galerkin least squares method.

Having to calculate an adjusted variable, such as τ in the Galerkin least squares method or γ in the Petrov-Galerkin method, is quite cumbersome. Therefore the following upwinding scheme is introduced.

3.6 Third Order Accuracy Upwinding Scheme

The third order accuracy upwinding scheme is similar to the Petrov-Galerkin method (in which the weighting function is modified using a perturbation function to allow more weight to the node in the upstream direction than the node in the downstream direction) with the exception that it uses a different perturbation function from the one used in the Petrov Galerkin method [16, 17, 18]. In this scheme, the perturbation function contains higher order spatial derivatives,

$$
\begin{aligned}
\overline{w} &= w + p \\
p &= -\frac{1}{3}\triangle x^2 \frac{d^2 w}{dx^2} - \frac{1}{12}\beta \triangle x^3 sign(v)\frac{d^3 w}{dx^3}
\end{aligned}
\tag{3.30}
$$

where $\triangle x, \beta$ and w are the element length, a variable to control the magnitude of the upwinding effect, and the original weighting function respectively. It is seen that this perturbation function is rather complicated. Therefore, for simplification, the modified weighting function is only applied on the convective term [18]. We then obtain

$$
\int_{Vol}(w + p)\,v\frac{d\theta}{dx}\,dVol - \int_{Vol} w\alpha \frac{d^2\theta}{dx^2}\,dVol = 0
\tag{3.31}
$$

Substituting eqn. 3.30 and applying integration by parts and the divergence rule, we have

$$
\int_{Vol}(wv\theta_{,x} - \frac{1}{3}\triangle x^2 w_{,xx}v\theta_{,x} - \frac{1}{12}\beta\triangle x^3 w_{,xxx}|v|\theta_{,x})dVol + \int_{Vol} w_{,x}\alpha\theta_{,x}dVol = \int_{S_f} wq^* dS_f
\tag{3.32}
$$

The weighting function contains third order spatial derivatives. Naturally, the interpolation function in an element needs to be at least a cubical function to be able to use the third order accuracy upwinding method. To apply this method to a linear interpolation element, auxiliary variables are introduced,

$$
\gamma = v\theta_{,x}
\tag{3.33}
$$

$$
\lambda = \triangle x^2 w_{,xx}
\tag{3.34}
$$

31

Hence, substituting eqn. 3.33 and eqn. 3.34 into eqn. 3.32, we obtain

$$\int_{Vol} (w\gamma - \frac{1}{3}\lambda v\theta_{,x} - \frac{1}{12}\lambda_{,x}\beta\triangle x|v|\theta_{,x})dVol + \int_{Vol} w_{,x}\alpha\theta_{,x}dVol = \int_{S_f} wq^{\cdot}dS_f \quad (3.35)$$

The classical Galerkin procedure is now applied to eqn. 3.33 and 3.34 weighted by $\bar{\gamma}$ and $\bar{\lambda}$ respectively,

$$\int_{Vol} \bar{\gamma}\gamma \, dVol = \int_{Vol} \bar{\gamma}v\theta_{,x} \, dVol \quad (3.36)$$

$$\int_{Vol} \bar{\lambda}\lambda \, dVol = -\int_{Vol} \bar{\lambda}_{,x}\triangle x^2 w_{,x} \, dVol + \int_{S_f} \bar{\lambda}q_\lambda^{\cdot} \, dS_f \quad (3.37)$$

where $q_\lambda^{\cdot}$ is the natural boundary condition for the auxiliary variable λ. Since we do not intend to calculate the solution of the auxiliary variable λ, the $q_\lambda^{\cdot}$ is ignored and can be assumed to be zero.

Considering the problem defined in sec. 3.1, where the essential boundary condition is applied to both sides, the last term in eqn. 3.35 becomes zero since there is no S_f boundary. In this upwinding method, the auxiliary variables are interpolated using the same interpolation functions used for the variable θ. Eqns. 3.35, 3.36 and 3.37 lead to the individual matrix equations

$$\mathbf{W}^{\mathbf{T}}\mathbf{A_1}\mathbf{\Gamma} - \mathbf{\Lambda}^{\mathbf{T}}\mathbf{A_2}\mathbf{\Theta} - \mathbf{\Lambda}^{\mathbf{T}}\mathbf{A_3}\mathbf{\Theta} + \mathbf{W}^{\mathbf{T}}\mathbf{K}\mathbf{\Theta} = 0 \quad (3.38)$$

$$\mathbf{M_o}\mathbf{\Gamma} = \mathbf{A_4}\mathbf{\Theta} \quad (3.39)$$

$$\mathbf{M_o}\mathbf{\Lambda} = -\mathbf{A_5}\mathbf{W} \quad (3.40)$$

where $\mathbf{W}, \mathbf{\Gamma}, \mathbf{\Lambda}$, and $\mathbf{\Theta}$ are the vectors of the nodal values w, γ, λ, and θ respectively. The weighting function w is treated in the same way as the auxiliary variables and its value is stored in the nodal values vector $\mathbf{W}$. The matrices in eqn. 3.38, 3.39, and 3.40 are defined as follows

$$\mathbf{A_1} = \int_{Vol} \mathbf{H}^{\mathbf{T}}\mathbf{H} \, dVol$$

$$\mathbf{A_2} = \int_{Vol} \mathbf{H}^{\mathbf{T}}\frac{1}{3}v\mathbf{B} \, dVol$$

32

$$A_3 = \int_{Vol} B^T \frac{\beta}{12} \triangle x B \, dVol$$

$$A_4 = \int_{Vol} H^T v B \, dVol$$

$$A_5 = \int_{Vol} B^T \triangle x^2 B \, dVol$$

$$K = \int_{Vol} B^T \alpha B \, dVol$$

where H and B are the interpolation and the gradient function matrices respectively. M_o is a "lumped matrix" because the boundary conditions and the solution of the auxiliary variables are not intended to be found [17]. Using the "lumped matrix" will also simplify calculations for this particular upwinding method.

Substituting eqns. 3.39 and 3.40 into 3.38 and simplifying the equation, we obtain

$$A^* \Theta + K^* \Theta = 0 \tag{3.41}$$

where A^* and K^* are the convective and diffusive matrices which are defined as follows

$$A^* = A_1 M_o^{-1} A_4 + A_5^T M_o^{-T} A_2 + A_5^T M_o^{-T} A_3 \tag{3.42}$$

$$K^* = K \tag{3.43}$$

The matrix multiplication defined in eqn. 3.42 must be done globally rather than on the element level. It means that the global matrices $A_1, A_2, A_3, A_4, A_5, K$ and M_o need to be assembled before matrix multiplication in eqn. 3.42 is performed. The size of every matrix is the same as that of the stiffness matrix K in other upwinding methods, such as the Petrov-Galerkin method. Thus, the computer memory required to run a computer program that implements the third order accuracy upwinding method is roughly 5 times larger than the memory required by a computer program that implements all of the other upwinding methods. Computer programs implementing these other upwinding methods, such as the Petrov-Galerkin method, require less computer memory because they perform the matrix multiplication on the

33
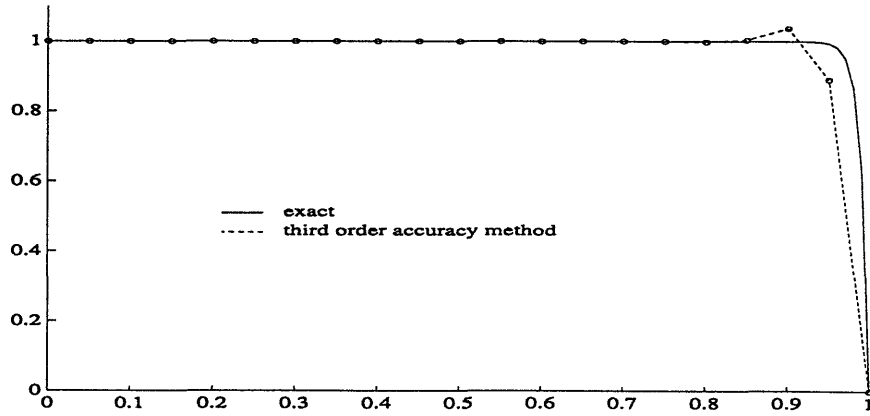
Figure 3-10: Solution of the convection-diffusion problem using the third order accuracy upwinding method.

element level.

Fig.3-10 shows the solution to the problem considered in section 3.1 using the third order accuracy upwinding method with $\beta = 1.5$. The author of this upwinding technique did not explain how to determine the value of β. However, from our experience, when the Peclet number is very high, $\beta = 1.5$ gives a minimum overshoot error at the boundary layer in the numerical solution. The boundary layer is characterized by a high gradient of the variable θ which occurs in the solution of the sample problem at $x = 1$.

3.7 Comparison of Upwinding Schemes in One Dimensional Analysis

The upwinding schemes that have been explained above will be compared in terms of discrete equations for the ith node in a uniform mesh and their results .

The discrete equation from the Galerkin method is

$$(-1 - \frac{Pe^e}{2})\theta_{i-1} + 2\theta_i + (-1 + \frac{Pe^e}{2})\theta_{i+1} = 0 \qquad (3.44)$$

This equation generates oscillations in the solutions to the convection-diffusion problems when Peclet number is high, $Pe^e > 2$.

The full upwinding scheme gives the discrete equation

$$(-1 - Pe^e)\theta_{i-1} + (2 + Pe^e)\theta_i - \theta_{i+1} = 0 \qquad (3.45)$$

which gives overly diffusive numerical solutions of convection-diffusion problems.

The exponential scheme gives the discrete equation

$$(-e^{Pe^e})\theta_{i-1} + (1 + e^{Pe^e})\theta_i - \theta_{i+1} = 0 \qquad (3.46)$$

The coefficients of the variable θ contains exponential functions which are very expensive to calculate. However, an exact nodal solution is obtained using this equation.

To compare the solution obtained from the Petrov-Galerkin method with those obtained from the other methods, substitute eqn. 3.25 into eqn. 3.24 and then multiply the resulting equation by $\dfrac{(e^{Pe^e} - 1)}{Pe^e}$ to get

$$(-e^{Pe^e})\theta_{i-1} + (1 + e^{Pe^e})\theta_i - \theta_{i+1} = 0 \qquad (3.47)$$

It turns out that this this equation is exactly the same as the discrete equation derived using the exponential scheme. This is expected since the formulation of both schemes include the exact solution of the convection-diffusion equation.

Derivations of the Petrov-Galerkin method and the exponential scheme are different. For the Petrov-Galerkin method, the derivation is based on the modification of the weighting function, while for the exponential scheme, the derivation is based on the control volume argument.

To compare the discrete equation obtained using the Galerkin least squares method with those obtained using the other upwinding schemes, insert eqn. 3.29 into eqn. 3.28

Table 3.1: Comparison of the exponential scheme, the Petrov-Galerkin method, the Galerkin least squares method and the third order accuracy method for one dimensional convection-diffusion problem with various source functions.

	Source term	Exponential	P-G	Gls	TOA
Uniform mesh	0	exact	exact	exact	non-exact
	constant	exact	exact	exact	non-exact
	linear	non-exact	exact	exact	non-exact
	general	non-exact $\neq$	non-exact $=$	non-exact	non-exact
Distorted mesh	0	exact	exact	exact	non-exact
	constant	non-exact	exact	exact	non-exact
	linear	non-exact $\neq$	non-exact $=$	non-exact	non-exact
	general	non-exact $\neq$	non-exact $=$	non-exact	non-exact

and then multiply the resulting equation by $\dfrac{(e^{Pe^{e}} - 1)}{Pe^{e}}$,

$$(-e^{Pe^{e}})\theta_{i-1} + (1 + e^{Pe^{e}})\theta_i - \theta_{i+1} = 0 \tag{3.48}$$

This equation is identical to those derived using the exponential scheme and the Petrov-Galerkin method.

Finally, the discrete equation obtained using the third order accuracy method is rather complicated and long. However, to put it briefly, Kondo [16, 17, 18] claims that the order of accuracy of the convective term is 3, so oscillations in the numerical solutions of the convection-diffusion problems can be reduced.

The solutions obtained using the exponential scheme, the Petrov-Galerkin scheme, the Galerkin least squares method and the third order accuracy method were compared in this work when the source term is non-zero. Calculations are performed for various source term functions and the results are shown in table. 3.1, where P-G - the Petrov-Galerkin method; Gls - the Galerkin least squares method; and TOA - the third order accuracy method. Based on this data, the exponential scheme has a lower accuracy compared to that of the Petrov-Galerkin and the Galerkin least squares schemes when the source term is non-zero. In a uniform mesh, both the Petrov-Galerkin and the Galerkin least squares methods give exact solutions to the problems with a linear source function whereas the exponential scheme does not give an exact

solution. Similarly, in a distorted mesh, the former two produce exact solutions to the problems with a constant source function while the exponential scheme does not. The fact that the Petrov-Galerkin and Galerkin least squares schemes have similar results is consistent with Hughes, Franca, and Hulbert's claim [12] that for linear interpolation elements, the Petrov-Galerkin method is identical to the Galerkin least squares method (see appendix C for the proof). However, for quadratic interpolation elements, those upwinding methods are no longer identical.

For the third order accuracy procedure, exact solutions cannot be found for any source function. This indicates that it has the lowest accuracy compared to the other three methods.

Chapter 4

Various Upwinding Schemes in Two Dimensional Analysis

In this chapter, the application of the upwinding schemes explained in Chapter 3 is extended to two dimensions. The procedure of upwinding schemes for the two dimensional analysis is analogous to that for the one dimensional analysis. Oscillations in numerical solutions to convection-diffusion problems for the two dimensional cases are more complicated than for the one dimensional cases. In general, using numerical methods to solve convection-diffusion problems in two dimensional cases cannot yield exact solutions — as is done in one dimensional analysis — with any upwinding scheme. In the two dimensional case, most of the upwinding schemes provide numerical solutions that still contain oscillations and a defect that is usually called the crosswind diffusion effect. This effect usually occurs when the velocity field is unaligned with the grid lines. The crosswind diffusion in numerical solutions is a spurious diffusion in the direction perpendicular to the streamline resulting in the deterioration of the numerical results. Thus this chapter will discuss the application of some of the previously published upwinding schemes in two dimensions as well as their characteristics. We restate that the governing equation for the convection-diffusion problem in two dimensional analysis (eqn. 2.2) is as follows

$$\theta_{,t} + \underline{v} \cdot \underline{\nabla}\theta = \alpha\nabla^2\theta + q \qquad (4.1)$$

where θ, $\underline{v}$, α, and q are the temperature, velocity field, diffusivity and the source terms, respectively.

4.1 Streamline Upwind/Petrov-Galerkin (SUPG)

This scheme is a two dimensional extension of the Petrov Galerkin method explained in chapter 3. Basically, an artificial diffusivity is introduced to reduce oscillations in the numerical solutions. The artificial diffusivity only has an effect in the streamline direction. This is based on the argument that the oscillations in the numerical solutions are generated by the high Peclet number in the streamline direction [5].
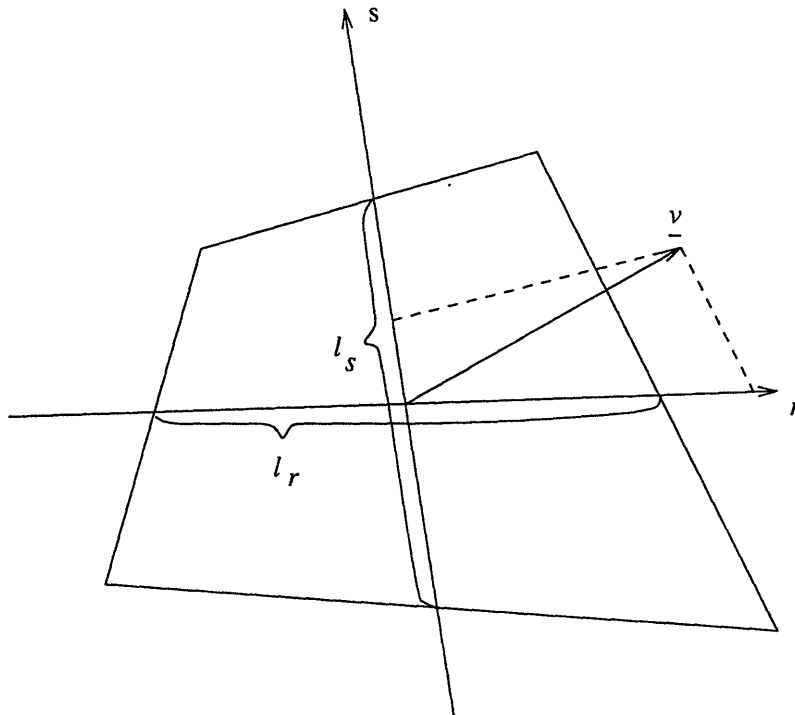
Figure 4-1: The average velocity vector in an element.

The method uses a directional Peclet number where the components of the total Peclet number in the local axes directions are calculated independently and are then added together to obtain the total Peclet number. In fig. 4-1, the velocity vector at

the origin of the element r and s local coordinates, is decomposed into v_r and v_s in r and s directions (The origin contains the average the velocity in the element). l_r and l_s are the average element lengths in r and s directions. Diffusivity is assumed to be isotropic and constant. The element Peclet numbers in r and s directions can be calculated as follows

$$Pe_r = \frac{v_r l_r}{\alpha}$$
$$Pe_s = \frac{v_s l_s}{\alpha}$$

Each direction can be treated the same as for a one dimensional case.

$$\lambda_r = \gamma_r \frac{l_r v_r}{2 \parallel \underline{v} \parallel}$$
$$\gamma_r = \coth(\frac{Pe_r}{2}) - \frac{2}{Pe_r}$$
$$\lambda_s = \gamma_s \frac{l_s v_s}{2 \parallel \underline{v} \parallel}$$
$$\gamma_s = \coth(\frac{Pe_s}{2}) - \frac{2}{Pe_s}$$
$$\parallel \underline{v} \parallel = \sqrt{v_r^2 + v_s^2}$$

λ_r and λ_r are added to obtain the total λ that corresponds to the original velocity direction $\underline{v}$ as follows

$$\lambda = \lambda_r \frac{v_r}{\parallel \underline{v} \parallel} + \lambda_s \frac{v_s}{\parallel \underline{v} \parallel}$$

Similar to the one dimensional case, perturbation function for the two dimensional case is defined as follows

$$p = \lambda \frac{\underline{v} \cdot \nabla w}{\parallel \underline{v} \parallel}$$
$$\parallel \underline{v} \parallel = \sqrt{v_x^2 + v_y^2}$$

where p and w are the perturbation function and the weighting function respectively. The modified weighting function includes the perturbation function for this scheme

defined as follows

$$\overline{w} = w + \lambda \frac{\underline{v} \cdot \underline{\nabla} w}{\| \underline{v} \|} \tag{4.2}$$

Applying the classical Galerkin procedure with the modified weighting function to eqn. 4.1, we obtain

$$\int_{Vol} \overline{w}(\theta_{,t} + \underline{v} \cdot \underline{\nabla}\theta - \alpha\nabla^2\theta - q) \, dVol = 0$$

After applying integration by parts and the divergence rule,

$$\int_{Vol} \overline{w}\theta_{,t} \, dVol + \int_{Vol} \overline{w}\underline{v} \cdot \underline{\nabla}\theta \, dVol + \int_{Vol} \underline{\nabla}\overline{w}\alpha\underline{\nabla}\theta \, dVol = \int_{Vol} \overline{w}q \, dVol + \int_{S_f} \overline{w}q^* \, dS_f \tag{4.3}$$

The second term can be rewritten as

$$\int_{Vol} \overline{w}\underline{v} \cdot \underline{\nabla}\theta \, dVol = \int_{Vol} w\underline{v} \cdot \underline{\nabla}\theta \, dVol + \int_{Vol} \underline{\nabla}w \cdot \underline{v}^T \frac{\lambda}{\| \underline{v} \|} \underline{v} \cdot \underline{\nabla}\theta \, dVol$$

So, the artificial diffusivity is

$$\tilde{\alpha} = \underline{v}^T \frac{\lambda}{\| \underline{v} \|} \underline{v}$$

This artificial diffusivity expression is similar to the one obtained using the Petrov-Galerkin method in the one dimensional case. If the flow is in one dimension, this artificial diffusivity reduces to that found by the Petrov-Galerkin method.

Comparable to the one dimensional case, $\underline{\nabla}\overline{w} = \underline{\nabla}w$ when a linear interpolation function is considered in the element. Eqn. 4.3 gives the discrete equation at the node (j, k) for a uniform two dimensional mesh shown in fig. 4-2 as follows

$$\{-2 - \frac{Pe_x^e}{2} + \frac{Pe_y^e}{2} - \frac{\gamma}{\alpha \| \underline{v} \|}(v_x^2 + v_y^2 - 3v_x v_y)\} \, \theta_{j-1,k+1} \quad +$$

$$\{-2 + 2Pe_y^e - \frac{\gamma}{\alpha \| \underline{v} \|}(-2v_x^2 + 4v_y^2)\} \, \theta_{j,k+1} \quad +$$

$$\{-2 + \frac{Pe_x^e}{2} + \frac{Pe_y^e}{2} - \frac{\gamma}{\alpha \| \underline{v} \|}(v_x^2 + v_y^2 + 3v_x v_y)\} \, \theta_{j+1,k+1} \quad +$$

$$\{-2 - 2Pe_x^e - \frac{\gamma}{\alpha \| \underline{v} \|}(4v_x^2 - 2v_y^2)\} \, \theta_{j-1,k} \quad +$$

41
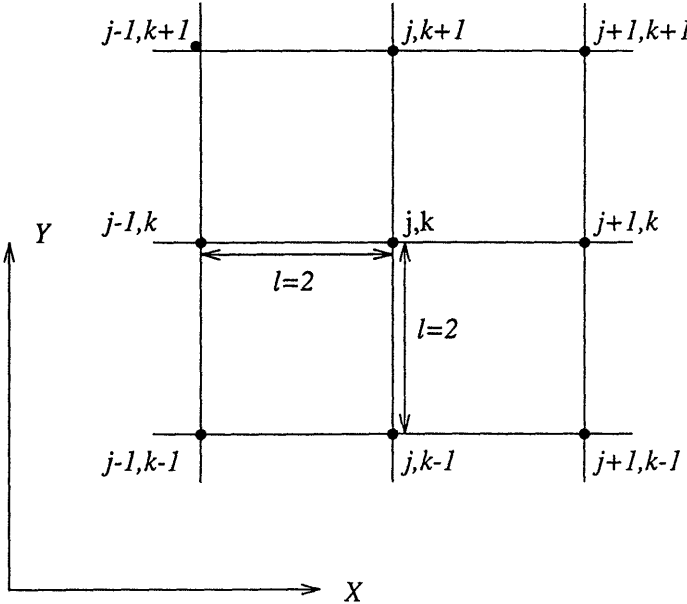
Figure 4-2: Node (j, k) in a uniform two dimensional mesh.

$$\{16 + \frac{\gamma}{\alpha \parallel \underline{v} \parallel}(8v_x^2 + 8v_y^2)\} \ \theta_{j,k} \quad +$$

$$\{-2 + 2Pe_x^e - \frac{\gamma}{\alpha \parallel \underline{v} \parallel}(4v_x^2 - 2v_y^2)\} \ \theta_{j+1,k} \quad +$$

$$\{-2 - \frac{Pe_x^e}{2} - \frac{Pe_y^e}{2} - \frac{\gamma}{\alpha \parallel \underline{v} \parallel}(v_x^2 + v_y^2 + 3v_x v_y)\} \ \theta_{j-1,k-1} \quad +$$

$$\{-2 - 2Pe_y^e - \frac{\gamma}{\alpha \parallel \underline{v} \parallel}(-2v_x^2 + 4v_y^2)\} \ \theta_{j,k-1} \quad +$$

$$\{-2 + \frac{Pe_x^e}{2} - \frac{Pe_y^e}{2} - \frac{\gamma}{\alpha \parallel \underline{v} \parallel}(v_x^2 + v_y^2 - 3v_x v_y)\} \ \theta_{j+1,k-1} \quad = \quad 0$$

This equation is of a similar form to the one dimensional equation obtained using the Petrov-Galerkin method (Eqn. 3.24). The equation is reduced to eqn. 3.24 for one dimensional case ($v_y = 0$). This is done by canceling all the v_y and Pe_y^e terms and collecting all coefficients of θ with the same j index. Eqn. 4.3 then leads to the finite element equation

$$\mathbf{M}\dot{\hat{\theta}} + \mathbf{K_c}\hat{\theta} + \mathbf{K_d}\hat{\theta} \ = \ \mathbf{R_b} + \mathbf{R_s} \tag{4.4}$$

SUPG is a popular upwinding scheme. Many researchers have successfully ap-

plied this scheme to solve numerical problems in many fields, such as coupled heat and fluid flows [1], transient incompressible flow with velocity-pressure variables [27], transonic and supersonic flows [3], etc. SUPG has also been applied successfully to the triangular three-node finite element [19, 20].

A numerical solution to a problem using a method that incorporates SUPG procedure quite satisfactorily approximates a smooth function. However, when the function contains a shock front in the interior of the domain or a boundary layer, the numerical result contains overshoot and undershoot characteristics near the shock front or the boundary layer. To improve the result, beyond streamline upwind/Petrov-Galerkin upwinding scheme is introduced with an objective to smooth out the numerical result near a shock front or a boundary layer.

4.2 Beyond Streamline Upwind/Petrov-Galerkin (BSUPG)

A modification of SUPG, this scheme has an extra term called discontinuity-capturing operator [14]. The extra term only affects the numerical solution in the direction of the gradient of θ.

$\underline{v}_g$ is defined as follows

$$\underline{v}_g = \begin{cases} \dfrac{\underline{v} \cdot \underline{\nabla}\theta}{\parallel \underline{\nabla}\theta \parallel_2^2} \underline{\nabla}\theta & \text{if } \underline{\nabla}\theta \neq 0 \\ 0 & \text{if } \underline{\nabla}\theta = 0 \end{cases} \tag{4.5}$$

The vector $\underline{v}_g$ is a projection of the velocity vector in the direction of the gradient θ as shown in Fig. 4-3. The weighting function is modified to include the $\underline{v}_g$ term and is defined as follows

$$\overline{w} = w + \tau_1 \underline{v} \cdot \underline{\nabla}w + \tau_2 \underline{v}_g \cdot \underline{\nabla}w$$

The last term in the equation above is the discontinuity-capturing term which creates an artificial diffusivity in the gradient of θ direction. Applying the Galerkin procedure

43
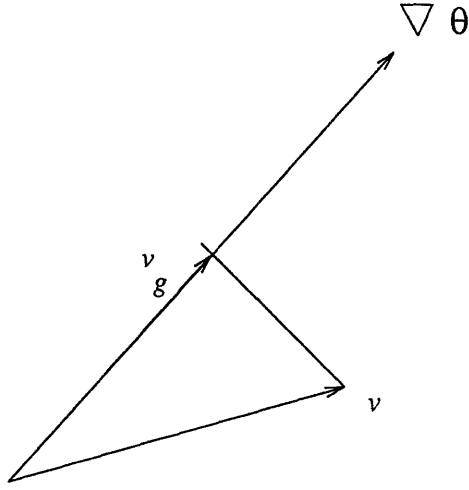
Figure 4-3: Projection of v in the direction of gradient θ $(\underline{v}_g)$

to eqn. 4.1 with the new weighting function, we obtain

$$\int_{Vol} \overline{w}(\theta_{,t} + \underline{v} \cdot \underline{\nabla}\theta - \alpha\nabla^2\theta - q)\, dVol = 0 \qquad (4.6)$$

Consider the weighting function $\overline{w}$ which interacts with the convective term in the convection-diffusion equation,

$$\int_{Vol} \overline{w}(... + \underline{v} \cdot \underline{\nabla}\theta + ...)\, dVol = ... \ + \int_{Vol} w\underline{v} \cdot \underline{\nabla}\theta\, dVol$$
$$+ \int_{Vol} \underline{\nabla}w\underline{v}\tau_1\underline{v} \cdot \underline{\nabla}\theta\, dVol$$
$$+ \int_{Vol} \underline{\nabla}w\underline{v}_g\tau_2\underline{v}_g \cdot \underline{\nabla}\theta\, dVol + ... \qquad (4.7)$$

In the expression above, the first term is the convective term obtained using the classical Galerkin method; the second, the artificial diffusivity term obtained using the original SUPG method; and the last, the extra term which is the artificial diffusivity term in the gradient of θ direction. For the last term, the relation of $\underline{v} \cdot \underline{\nabla}\theta = \underline{v}_g \cdot \underline{\nabla}\theta$

is used. The artificial diffusivities are

$$\tilde{\alpha}_1 = \underline{v}\tau_1\underline{v}^T$$

$$\tilde{\alpha}_2 = \underline{v}_g\tau_2\underline{v}_g^T$$

where $\tilde{\alpha}_1$ is acting in streamline direction originally from the SUPG scheme and $\tilde{\alpha}_2$ is acting in the direction of gradient θ to smooth out the numerical result around a shock front or a boundary layer.

The determinations of τ_1 and τ_2 are similar to those in the SUPG method except that the calculation for the characteristic length of an element is defined differently. Let

$$\underline{b}^e = (\underline{v} \cdot \underline{\nabla})\underline{\xi}^e$$

where $\underline{\xi}^e$ is the local coordinate system. Length of the vector $\underline{b}^e$ is defined using the p-norm definition,

$$|\underline{b}^e|_p = (b_1^p + b_2^p)^{\frac{1}{p}} \tag{4.8}$$

The characteristic length of an element is defined as follows

$$\frac{1}{2}l^e = \frac{|\underline{v}|_2}{|\underline{b}^e|_p} \tag{4.9}$$

When $p = 2$, $\frac{1}{2}l^e$ in the eqn. 4.9 can be interpreted as stretching a unit vector in the velocity direction on the global coordinate mapped onto the local coordinate system. So basically eqn. 4.9 defines the length of element in the velocity direction. Using this definition, the streamline factor τ_1 can be calculated directly,

$$\tau_1 = \frac{\gamma l^e}{2|\underline{v}|_2}$$

$$\gamma = \coth(\frac{Pe^e}{2}) - \frac{2}{Pe^e}$$

$$Pe^e = \frac{l^e|\underline{v}|_2}{\alpha}$$

$$|\underline{v}|_2 = \sqrt{v_x^2 + v_y^2}$$

45

Similarly, τ_2 is calculated as follows

$$
\begin{aligned}
\underline{b}_g^e &= (\underline{v}_g \cdot \underline{\nabla})\underline{\xi}^e \\
\frac{1}{2}l_g^e &= \frac{|\underline{v}_g|_2}{|\underline{b}_g^e|_p} \\
Pe_g^e &= \frac{l_g^e|\underline{v}_g|_2}{\alpha} \\
\gamma_g &= \coth(\frac{Pe_g^e}{2}) - \frac{2}{Pe_g^e} \\
\tau_2 &= \frac{\gamma_g l_g^e}{2|\underline{v}_g|_2}
\end{aligned}
$$

When $\underline{v}_g = \underline{v}$, double artificial diffusivity effect occurs. To avoid the double effect, the following condition is introduced

$$
\tau_2 = \max(0, \tau_2^{\cdot} - \tau_1)
$$

Applying the modified weighting function to eqn. 4.1, we obtain

$$
\int_{Vol} \overline{w}(\theta_{,t} + \underline{v} \cdot \underline{\nabla}\theta - \alpha\nabla^2\theta - q)\, dVol = 0 \tag{4.10}
$$

After applying integration by parts and the divergence rule to eqn. 4.10, we obtain

$$
\int_{Vol} \overline{w}\theta_{,t}\, dVol + \int_{Vol} \overline{w}\underline{v} \cdot \underline{\nabla}\theta\, dVol + \int_{Vol} \underline{\nabla}w\alpha\underline{\nabla}\theta\, dVol = \int_{Vol} \overline{w}q\, dVol + \int_{S_f} \overline{w}q^{\cdot}\, dS_f \tag{4.11}
$$

$\underline{\nabla}\overline{w} = \underline{\nabla}w$ because linear interpolation is considered. Eqn. 4.11 should yield a discrete equation at the node (j, k) for a uniform two dimensional mesh similar to the one obtained by SUPG procedure. However, the equation cannot be obtained because the gradient of θ is unknown. When this method is applied to the one dimensional case, the equation produces the same result as that from the SUPG method given the condition that $\tau_2 = 0$ when $\underline{v}_g = \underline{v}$. Eqn. 4.11 leads to the finite element matrix

46

equation

$$\mathbf{M}\dot{\hat{\theta}} + \mathbf{K_c}\hat{\theta} + \mathbf{K_d}\hat{\theta} = \mathbf{R_b} + \mathbf{R_s} \qquad (4.12)$$

Hughes and Mallet [13] extended this method to a multidimensional system.

BSUPG scheme requires that the gradient of variable θ in the above formulation be calculated iteratively and hence this makes the scheme expensive in terms of the CPU time.

Upwinding schemes have also been developed through the use of other finite element arguments such as control volume finite element method (CVFEM) with the expectation that the scheme will give a better numerical result.

4.3 Upwinding Schemes in Control Volume Finite Element Method

This section explains extended applications of the exponential upwinding schemes explained in section 3.3 to the two dimensional case. Three different upwinding formulations will be discussed in this section.

4.3.1 Original Formulation of CVFEM

The original CVFEM uses linear interpolation functions for the θ variable along the x and y grid lines [21] (See fig. 4-4 for a control volume applied to point P in the two dimensional case. W and E are nodes that lie in the same x-axis as point P where N and S are in the y-axis.) Using the linear interpolation functions produces oscillations in the numerical solutions to the convection-diffusion problems. Hence, an upwinding scheme is required to eliminate these oscillations. The first upwinding scheme used in the CVFEM formulation is a direct extension of the exponential upwinding scheme applied along each grid line.

The fluxes entering the control volume at node P from sides e, w, n and s shown in fig. 4-4 are defined using the exact solution to the one dimensional convection-
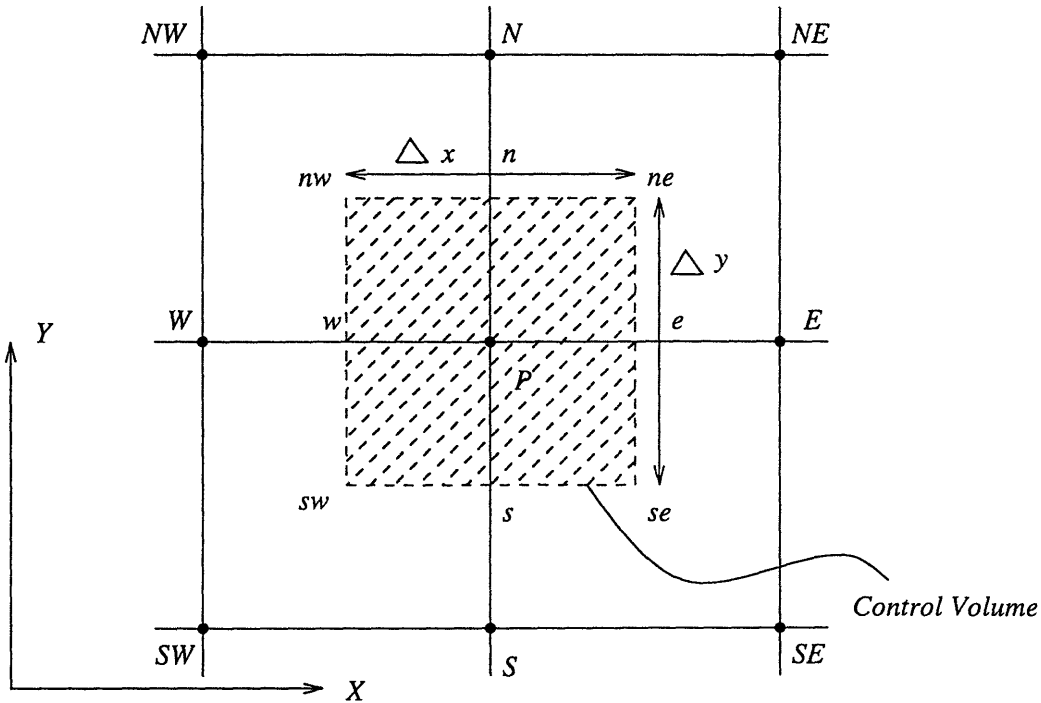
Figure 4-4: A control volume applied to the point P

diffusion equation,

$$f|_e = v_x \left[\theta_P + \frac{\theta_P - \theta_E}{c_x} \right] \qquad (4.13)$$

$$f|_w = v_x \left[\theta_W + \frac{\theta_W - \theta_P}{c_x} \right] \qquad (4.14)$$

$$f|_n = v_y \left[\theta_P + \frac{\theta_P - \theta_N}{c_y} \right] \qquad (4.15)$$

$$f|_s = v_y \left[\theta_S + \frac{\theta_S - \theta_P}{c_y} \right] \qquad (4.16)$$

where $c_x = \exp(Pe_x^e) - 1$ and $c_y = \exp(Pe_y^e) - 1$ (an alternative calculation of c_x and c_y uses the power law scheme [21] because exponential functions are expensive to calculate in terms of the CPU time.) Applying this upwinding formulation to eqn. 4.1 for the point P as shown fig. 4-4, we obtain

$$\int_{\Delta x} \int_{\Delta y} (\theta_{,t} + \underline{v} \cdot \underline{\nabla} \theta - \alpha \nabla^2 \theta - q) dx\, dy = 0$$

48

$$\triangle x \triangle y (\dot{\theta}_P - q) + f|_e \triangle y - f|_w \triangle y + f|_n \triangle x - f|_s \triangle x = 0 \qquad (4.17)$$

Substituting eqn. 4.13 to eqn. 4.16, we obtain

$$\triangle x \triangle y \, \dot{\theta}_P \; - \; \triangle x \triangle y \, q + \theta_P (v_x \triangle y + \frac{2v_x \triangle y}{c_x} + v_y \triangle x + \frac{2v_y \triangle x}{c_y}) - \theta_E (\frac{v_x \triangle y}{c_x})$$

$$- \; \theta_W (v_x \triangle y + \frac{v_x \triangle y}{c_x}) - \theta_N (\frac{v_y \triangle x}{c_y}) - \theta_S (v_y \triangle x + \frac{v_y \triangle x}{c_y}) = 0$$

The above equation can be rewritten as

$$m_P \dot{\theta}_P + a_P \theta_P + a_E \theta_E + a_W \theta_W + a_N \theta_N + a_S \theta_S = r_B \qquad (4.18)$$

where

$$
\begin{aligned}
m_P &= \triangle x \triangle y \\
a_P &= v_x \triangle y + \frac{2v_x \triangle y}{c_x} + v_y \triangle x + \frac{2v_y \triangle x}{c_y} \\
a_E &= -\frac{v_x \triangle y}{c_x} \\
a_W &= -v_x \triangle y - \frac{v_x \triangle y}{c_x} \\
a_N &= -\frac{v_y \triangle x}{c_y} \\
a_S &= -v_y \triangle x - \frac{v_y \triangle x}{c_y} \\
r_B &= \triangle x \triangle y q
\end{aligned}
$$

Applying the control volume to all other nodes in the domain, a complete matrix equation can then be assembled. The control volume edges contain fluxes produced by the boundary condition fluxes which contribute to the matrix $\mathbf{R_s}$, shown in the following equation

$$\mathbf{M}\dot{\hat{\theta}} + \mathbf{K}\hat{\theta} = \mathbf{R_b} + \mathbf{R_s} \qquad (4.19)$$

where the matrix $\mathbf{M}$ is a diagonal matrix containing the area of the control volumes, $\mathbf{K}$, the stiffness matrix and $\mathbf{R_b}$, the load vector.

49

This method guarantees the elimination of oscillations in numerical solutions around a shock front or a boundary layer, but nevertheless, it has a significant cross-wind diffusion defect. Furthermore, this method also gives a low accuracy for distorted meshes. To improve the numerical solutions, the interpolation functions defined in the finite element method within an element are used to interpolate θ in the control volume method. With these interpolation functions, a new upwinding scheme is required.

4.3.2 Positive Coefficient Upwinding Procedure for CVFEM

This upwinding scheme incorporated in the control volume method using the finite element interpolation functions was proposed by Schneider and Raw [15, 22]. The boundary of the control volume applied to the nodes is located at $r = 0$ and $s = 0$ of the element local coordinates as shown in fig 4-5. These boundaries divide every element into four subcontrol volumes (SCV). Through the use of linear interpolation, the average flux that enters through one side of the control volume boundary can be approximated by multiplying the value of the flux at the midpoint of the boundary surface with the boundary length. The convection-diffusion equation (eqn. 4.1) applied to the subcontrol volume 1 is derived as follows

$$\int_{scv_1} (\theta_{,t} + \underline{v} \cdot \underline{\nabla}\theta - \alpha\nabla^2\theta - q)dVol = 0$$

$$\int_{scv_1} (\theta_{,t} - q)dVol + Q_{2,1} + Q_{4,1} + Q_{c1,1} + Q_{c2,1} = 0 \tag{4.20}$$

where Qs are the fluxes that enter the subcontrol volume to be discussed later. The mass matrix, from the transient term, is obtained by evaluating the area of the control volume for every nodes, e.g. for node 1,

$$\int_{cv_1} \theta_{,t}\, dVol = A_{cv_1}\dot{\theta}_1$$

where A_{cv_1} is the area of the control volume 1. The source term for subcontrol volume SCV1 can be approximated by multiplying the midpoint value of the source function

50
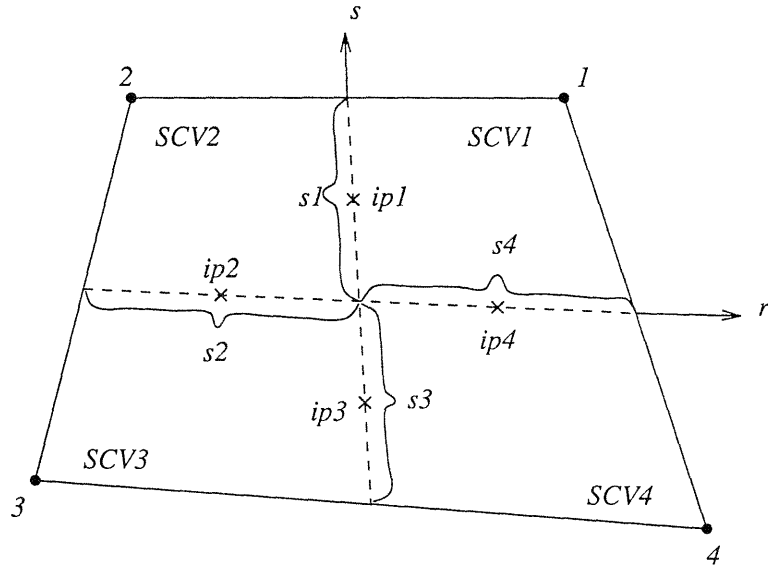
Figure 4-5: Subcontrol volumes within an element

in the SCV1 with the area of the SCV1, i.e., .

$$\int_{SCV1} q \, dVol = q|_{r=\frac{1}{2}; s=\frac{1}{2}} A_{SCV1}$$

The $Q_{j,i}$ term is the flux from the subcontrol volume i to j. The flux contains two parts, for example, for $i = 1$ and $j = 2$,

$$Q_{2,1} = Q_{2,1}^{d} + Q_{2,1}^{c}$$

where $Q_{2,1}^{d}$ and $Q_{2,1}^{c}$ are diffusive and convective fluxes respectively that flow from subcontrol volume 1 to subcontrol volume 2. Using the midpoint approximation (point $ip1$ as shown in fig. 4-5), the diffusive flux is calculated as follows

$$
\begin{aligned}
Q_{2,1}^{d} &= -\int_{S1} \alpha \underline{\nabla} \theta \cdot \underline{n} \, dS \\
&= -\sum_{i=1}^{4} (\alpha \frac{\partial h_i}{\partial x}|_{ip1} \triangle y_1 - \alpha \frac{\partial h_i}{\partial y}|_{ip1} \triangle x_1) \, \hat{\theta}
\end{aligned}
\qquad (4.21)
$$

Here, the function θ is approximated using the interpolation function h_i defined in chapter 2 for a two dimensional case. The normal vector of surface $s1$ for the sub-control volume 1 shown in fig. 4-6 is defined using the counter clockwise convention, i.e.

$$\underline{n} = \triangle y \hat{\underline{i}} - \triangle x \hat{\underline{j}}$$
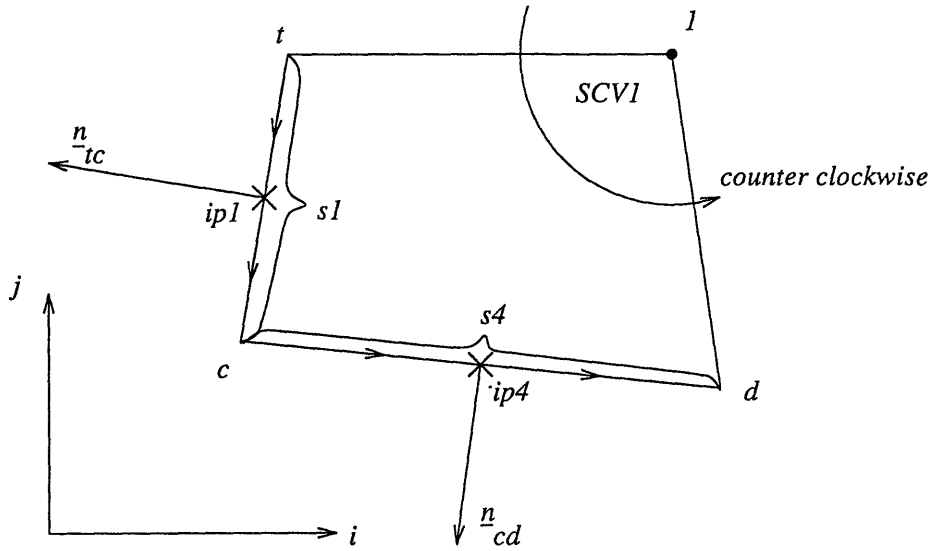
Figure 4-6: Normal vector convention for subcontrol volume 1.

$$\underline{n}_{tc} = (y_c - y_t)\hat{\underline{i}} - (x_c - x_t)\hat{\underline{j}}$$

$$\underline{n}_{cd} = (y_d - y_c)\hat{\underline{i}} - (x_d - x_c)\hat{\underline{j}}$$

Similarly,

$$
\begin{aligned}
Q_{2,1}^c &= \int_{S1} (\underline{v}\,\theta) \cdot \underline{n}\, dS \\
&= (v_x\theta)_{ip1}\triangle y - (v_y\theta)_{ip1}\triangle x \qquad (4.22)
\end{aligned}
$$

in the convective fluxes, the value of v and θ at the integration point are calculated in such a way as to obtain upwinding effect.

When v_x and v_y at the integration point $ip1$ are prescribed, as well as when we
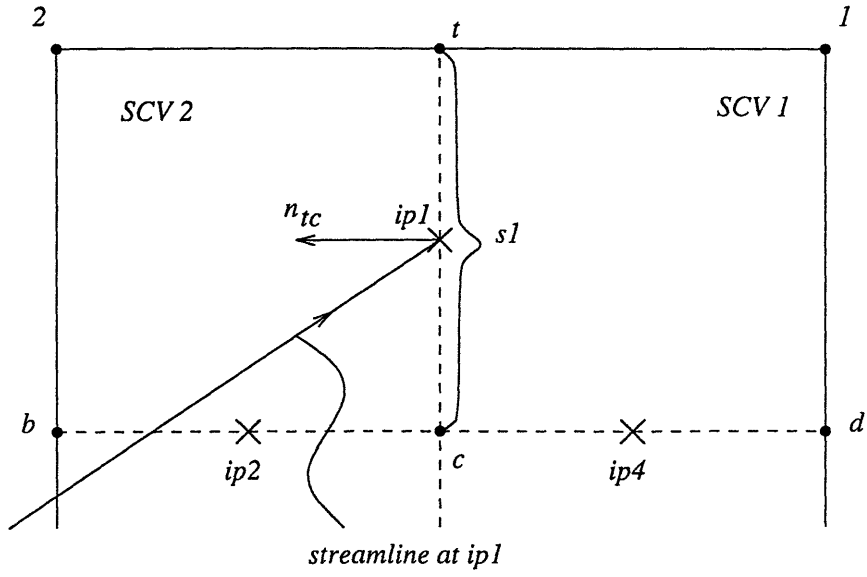
streamline at ip1

Figure 4-7: Streamline for the integration point ip1 when $\dot{m}_{tc} < 0$ (the flow is from the left) and normal vector of the surface tc in the subcontrol volume 1.

consider the subcontrol volume SCV1 and $\dot{m}_{tc} < 0$ (the flux is coming into SCV1 at $s1$ as shown in fig. 4-7), the value of θ_{ip1} is calculated as follows

$$\theta_{ip1} = (1 - f)\theta_2 + f\,\theta_{ip2}$$

$$f = -\frac{\dot{m}_{bc}}{\dot{m}_{tc}} \quad \text{and} \quad 0 \leq f \leq 1$$

where θ_2 and θ_{ip2} are the values of θ at node 2 and at integration point 2 respectively. $\dot{m}_{bc}$ and $\dot{m}_{tc}$ are mass fluxes passing through the line bc and tc in fig. 4-7 are calculated using the following equations

$$\dot{m}_{bc} = v_{x,ip2}\triangle y_{bc} - v_{y,ip2}\triangle x_{bc}$$

$$\dot{m}_{tc} = v_{x,ip1}\triangle y_{tc} - v_{y,ip1}\triangle x_{tc}$$

where $v_{x,ip1}$ and $v_{y,ip1}$ are values of v_x and v_y at the integration point $ip1$.

When $\dot{m}_{tc} > 0$ (the flux is going out from the subcontrol volume 1 at the surface

s1), θ_{ip1} is calculated as follows

$$\theta_{ip1} = (1 - f)\theta_1 + f\theta_{ip4}$$

where,

$$f = -\frac{\dot{m}_{cd}}{\dot{m}_{tc}} \quad \text{and} \quad 0 \le f \le 1$$

$$\dot{m}_{cd} = v_{x,ip4}\triangle y_{cd} - v_{y,ip4}\triangle x_{cd}$$

θ_{ip1} is connected to the other integration points and nodal values of θ which need to be condensed out.

Using this method, the appropiate upwinding scheme for the two dimensional case can be obtained by giving more weight to the node in the upstream direction for every flux that enters the control volume through its boundaries. Therefore, this method implements the idea of the full upwinding scheme for the two dimensional case.

Other Q terms with subscript ei in eqn. 4.20 are treated similarly, except that they are the given fluxes at the boundary conditions. These terms vanish for internal nodes because the nodes receive the fluxes from adjacent control volumes that will cancel each other as the fluxes come in pairs and in opposite directions.

The control volume method is applied to all the nodes in the domain so that the global mass, stiffness and load matrices can be assembled. Therefore we obtain the following matrix equation

$$\mathbf{M}\dot{\theta} + \mathbf{K}\theta = \mathbf{R}$$

where the mass matrix $\mathbf{M}$ is an assemblage matrix that consists of areas of the control volume for every node; the stiffness matrix $\mathbf{K}$ is obtained from a combination of the fluxes of the nodes, and load matrix $\mathbf{R}$ is from the source term and the boundary conditions.

This upwinding scheme is guaranteed to eliminate all of the oscillation difficulties, but its numerical result contains a slight crosswind diffusion.

4.3.3 SUPG in the CVFEM

CVFEM can be obtained by modifying the weighting function in the finite element method in such a way that a result identical to the one from the control volume method applied to the nodes in the domain is obtained. For the Galerkin method, the weighting function is the same as the interpolation function, but for CVFEM, the weighting function is defined as follows

$$\overline{w}_P = \begin{cases} 1 & \text{in the } P^{th} \text{ Control volume} \\ 0 & \text{elsewhere} \end{cases}$$

The weighting function is equal to one within the control volume boundary and zero elsewhere. Applying the Galerkin procedure on eqn. 4.1 using this weighting function definition, and integrating the results across the nodal control volumes and then summing the results for the whole domain, we obtain

$$\sum \int_{Vol_{cv}} (\theta_{,t} + \underline{v} \cdot \underline{\nabla}\theta - \alpha \nabla^2 \theta - q) \, dVol_{cv} = 0 \qquad (4.23)$$

Using integration by parts and the divergence rule to eqn. 4.23, we obtain

$$\sum \int_{Vol_{cv}} \theta_{,t} \, dVol_{cv} + \sum \int_{S_{cv}} (\underline{v}\theta - \alpha\underline{\nabla}\theta) \cdot \underline{\hat{n}} \, dS_{cv} + \int_{S_f} q' \, dS_f - \sum \int_{Vol_{cv}} q \, dVol_{cv} = 0$$
$$(4.24)$$

This equation poses a numerical difficulty when the convective term dominates the system as indicated by oscillations in the numerical result. To solve this difficulty, the SUPG upwinding method in the finite element method is modified for the use of the control volume method [25, 26]. The weighting function in the control volume is modified to create the SUPG upwinding scheme effect,

$$\overline{w} = w - p = w - \frac{\gamma h_e}{2 \parallel \underline{v} \parallel} \underline{\nabla} \cdot (\underline{v} \, w) = w - A\underline{\nabla} \cdot (\underline{v} \, w)$$
$$\gamma = \coth(\frac{Pe^e}{2}) - \frac{2}{Pe^e}$$
$$Pe^e = \text{Peclet number} = \frac{\parallel v \parallel h_e}{\alpha}$$

$$\| \underline{v} \| = \sqrt{v_x^2 + v_y^2} \text{ is magnitude of the average element velocity}$$

$$h_e = \text{characteristic length of the element}$$

In this equation, the perturbation function has a negative sign to correct the direction for the artificial diffusion term for the control volume method. Using the modified weighting function in eqn. 4.1, we obtain

$$\sum \int_{Vol_{cv}} \theta_{,t}\, dVol_{cv} + \sum \int_{S_{cv}} (\underline{v}\,\theta - \alpha\underline{\nabla}\theta) \cdot \hat{n}\, dS_{cv} + \int_{S_f} q^* dS_f$$

$$- \sum \int_{Vol_{cv}} q\, dVol_{cv} - \sum \int_{S_{cv}} A\underline{v} \cdot \hat{n}(\theta_{,t} + \underline{\nabla} \cdot (\underline{v}\,\theta) - q)dS_{cv} = 0 \qquad (4.25)$$

The perturbation function is not applied to the diffusion term because a linear interpolation function is used and the second derivative of linear function is zero. When this equation is applied to the control volume around the node P in fig. 4-4, we obtain

$$\left\{ \int_{p-e-ne-n} \left[\theta_{,t} - q\right] dVol + \int_e^{ne} \underline{j} \cdot \hat{n}\, dS + \int_{ne}^{n} \underline{j} \cdot \hat{n}\, dS \right\}_{P-E-NE-N}$$

$$+[\text{similar contribution from the other elements around the node P}]$$

$$+[\text{boundary condition fluxes for the edge element}] = 0$$

where $\underline{j}$ is the combination of the convective and diffusive fluxes, plus the perturbation term

$$\underline{j} = \underline{v}\,\theta - \alpha\underline{\nabla}\theta - A\underline{v}\left[\theta_{,t} + \underline{\nabla} \cdot (\underline{v}\theta) - q\right] \qquad (4.26)$$

For the transient term, the lumped mass matrix is used to avoid oscillations that appear when a consistent mass matrix is used [15]. The source term can be calculated by evaluating the value of q at $r = s = \frac{1}{2}$ which is the middle point of the subcontrol volume and multiplied by the control volume area. The flux $\underline{j}$ can be approximated by multiplying the value of $\underline{j}$ at the boundary surface midpoint with the length of the surface. The value of $\underline{j}$ at the midpoint is obtained by evaluating eqn. 4.26 and using the interpolating function for the θ variables.

The same procedure is then applied to all the nodal control volumes and the

matrix equation obtained is

$$\mathbf{M}\dot{\theta} + \mathbf{K}\theta = \mathbf{R}$$

4.4 Third Order Accuracy Upwinding in 2D

This is the extended application of the third order accuracy upwinding method that has been explained in chapter 3. The weighting function is generalized by using indix notation as follows

$$\overline{w}_i = w_i - \frac{1}{3}\triangle\xi_j^2 w_{i,jj} - \frac{1}{12}\beta\triangle\xi_j^3 \text{sign}(v_j)w_{i,jjj} \tag{4.27}$$

The modified weighting function is applied only to the convective term. Applying the weighting function to eqn. 4.1, we obtain

$$\int_{Vol} w_i(\theta_{,t} - \alpha\nabla^2\theta - q)dVol + \int_{Vol} \overline{w}_i\underline{v} \cdot \underline{\nabla}\theta \, dVol = 0$$

or, in indix notation,

$$\int_{Vol} w_i(\theta_{i,t} - \alpha\theta_{i,jj} - q_i)dVol + \int_{Vol} \overline{w}_i v_j \theta_{i,j} dVol = 0 \tag{4.28}$$

Similar to the one dimensional case, auxiliary variables are introduced to fit this formulation on bilinear interpolation functions. The following expression for the auxiliary variables are generalizations of eqn. 3.33 and 3.34,

$$\gamma_i = v_j \theta_{i,jj} \tag{4.29}$$

$$\lambda_i = \triangle\xi_j^2 w_{i,jj} \tag{4.30}$$

Substituting eqn. 4.29 and 4.30 into eqn. 4.27 and combining the result with eqn. 4.28, we obtain

$$\int_{Vol} w_i(\theta_{i,t} - \alpha\theta_{i,jj} - q_i)dVol + \int_{Vol} \left(w_i\gamma_i - \frac{1}{3}\lambda_i v_j\theta_{i,j} - \frac{1}{12}\lambda_{i,j}\beta\triangle\xi_j|v_j|\theta_{i,j}\right) dVol = 0 \tag{4.31}$$

57

Applying the Galerkin procedure to the auxiliary variable equation as defined in eqn. 4.29 and 4.30,

$$\int_{Vol} \bar{\gamma}_i \gamma_i \, dVol = \int_{Vol} \bar{\gamma}_i v_j \theta_{i,j} \, dVol$$

$$\int_{Vol} \bar{\lambda}_i \lambda_i \, dVol = -\int_{Vol} \bar{\lambda}_{i,j} \triangle x_j^2 w_{i,j} \, dVol + \int_{S_f} \bar{\lambda}_i \triangle x_j^2 w_{i,j} \, dS_f$$

Similar to the one dimensional case, the last term is assumed to be zero since we do not intend to calculate the auxiliary variable solutions. The above equations lead to the matrix equations

$$\mathbf{W}^T \mathbf{A}_1 \mathbf{\Gamma} - \mathbf{\Lambda}^T \mathbf{A}_2 \mathbf{\Theta} - \mathbf{\Lambda}^T \mathbf{A}_3 \mathbf{\Theta} + \mathbf{W}^T \mathbf{K} \mathbf{\Theta} = 0 \qquad (4.32)$$

$$\mathbf{M_o} \mathbf{\Gamma} = \mathbf{A}_4 \mathbf{\Theta}$$

$$\mathbf{M_o} \mathbf{\Lambda} = -\mathbf{A}_5 \mathbf{W}$$

where the matrices are defined as follows

$$\mathbf{A}_1 = \int_{Vol} \mathbf{H}^T \mathbf{H} \, dVol$$

$$\mathbf{A}_2 = \int_{Vol} \mathbf{H}^T \frac{1}{3} \mathbf{V} \mathbf{B} \, dVol$$

$$\mathbf{A}_3 = \int_{Vol} \mathbf{B}^T \frac{\beta}{12} \mathbf{D} \mathbf{B} \, dVol$$

$$\mathbf{A}_4 = \int_{Vol} \mathbf{H}^T \mathbf{V} \mathbf{B} \, dVol$$

$$\mathbf{A}_5 = \int_{Vol} \mathbf{B}^T \mathbf{D}^2 \mathbf{B} \, dVol$$

$$\mathbf{K} = \int_{Vol} \mathbf{B}^T \alpha \mathbf{B} \, dVol$$

$$\mathbf{V} = \begin{bmatrix} v_x & v_y \end{bmatrix}$$

$$\mathbf{D} = \begin{bmatrix} l_r & 0 \\ 0 & l_s \end{bmatrix}$$

where $\mathbf{H}$ and $\mathbf{B}$ are the interpolation and the gradient matrices respectively, that are defined in chapter 2 for the two dimensional case.

58

The matrix equations (eqn. 4.32) can be simplified to

$$\mathbf{A}^{*}\theta + \mathbf{K}^{*}\theta = 0$$

where

$$\mathbf{A}^{*} = \mathbf{A}_1 \mathbf{M}_o^{-1} \mathbf{A}_4 + \mathbf{A}_5^{\mathbf{T}} \mathbf{M}_o^{-\mathbf{T}} \mathbf{A}_2 + \mathbf{A}_5^{\mathbf{T}} \mathbf{M}_o^{-\mathbf{T}} \mathbf{A}_3$$
$$\mathbf{K}^{*} = \mathbf{K}$$

4.5 Other Upwinding Schemes

Similar to the Beyond SUPG method, Carmo and Galeao [6] have developed a method to improve SUPG numerical results. In this method, an algorithm is formulated to locate oscillations in the numerical solution obtained using the SUPG method. In iteration, more artificial diffusivity is applied to this area to supress the oscillations until an acceptable result is obtained. This method is not discussed in this thesis because the method is expensive in calculations, and so it is not efficient to solve the convection-diffusion problems.

Many upwinding methods have been developed to solve the convection-diffusion equation for the transient case. Dick [10], Bouloutas and Celia [4] modified the weighting function with a symmetric perturbation function. They proved that the modification led to a higher accuracy. However, oscillations still occurred in the numerical solution. Donea, Selmin and Quartapelle [11] used a method called the Taylor-Galerkin method to improve the numerical accuracy for transient analyses. The method used the Taylor expansion to approximate the first time derivative to second order accuracy. To suppress the oscillations in the numerical result, the method used the total variation diminishing (TVD) upwinding method. In TVD, a variable was introduced to detect a shock front or a boundary layer in a domain. This variable controlled the magnitude of artificial diffusivity required to avoid oscillations at a shock front or a boundary layer. The variable was designed to depend on the

gradient of the unknown variable. The TVD method is not discussed in this thesis because the method is similar to the BSUPG method because both methods use the gradient of θ in the formulations.

The Galerkin least squares method has been proven to be identical to the SUPG method for a bilinear interpolation element [12], so discussion of this method is not necessary.

The upwinding schemes explained in this thesis can also be expanded for application in three dimensional analysis, assuming that the eight-node three dimensional element would be used. To modify SUPG to a three dimensional application is simply to introduce another directional Peclet number corresponding to the z-axis direction. The calculation procedure applied to this added direction is similar to the calculations carried out for the other two directions. BSUPG can be modified in the way as SUPG but noting that the gradient θ is now a three dimensional vector. For the positive-coefficient upwinding procedure, the expression for θ at the integration point can be modified for three dimensinal fluxes. The expression should be able to maintain the coefficients of θ to be positive numbers. The third order accuracy upwinding scheme is directly expandable to three dimensional analysis by allowing the indices i and j to have values of $1, 2$, and 3. The third index corresponds to the third axis in the z-axis direction.

Chapter 5

Test Problem Descriptions

The test problems are designed to measure the stability and the accuracy of the upwinding schemes that have been explained in chapter 4. The stability of these schemes is very critical since unstable schemes would yield unrealistic results in high Peclet number flow problems even though the schemes may be very accurate in solving low Peclet number flow problems.

The main purpose of developing the finite element analysis is to help engineers to simulate and solve practical problems. Therefore it is important that the test problems enable to gage how dependable the upwinding schemes are in solving practical engineering problems.

To measure the stability of the upwinding schemes, both uniform and distorted meshes are used. In engineering practice, uniform meshes are hardly used since engineers commonly deal with complex geometries.

5.1   Test Problem 1

Test problem 1 has been studied by various researchers [5, 14, 19, 20, 22, 26]. The main purpose of this test is to show the crosswind characteristics of the upwinding schemes when a shock front is developed in the domain. The test problem is defined as follows.

Consider a (one-by-one) domain which is subdivided into 20x20 elements. The

boundary conditions for this domain are shown in fig. 5-1. The essential boundary conditions are applied to the left side and bottom side boundaries. The value of θ is fixed and is equal to 1 at the left and part of the bottom sides, while θ is equal to 0 at the remaining part of the bottom side. At the right and upper sides, the natural boundary conditions are applied. The diffusion fluxes at these sides are assigned to 0, see fig. 5-1.
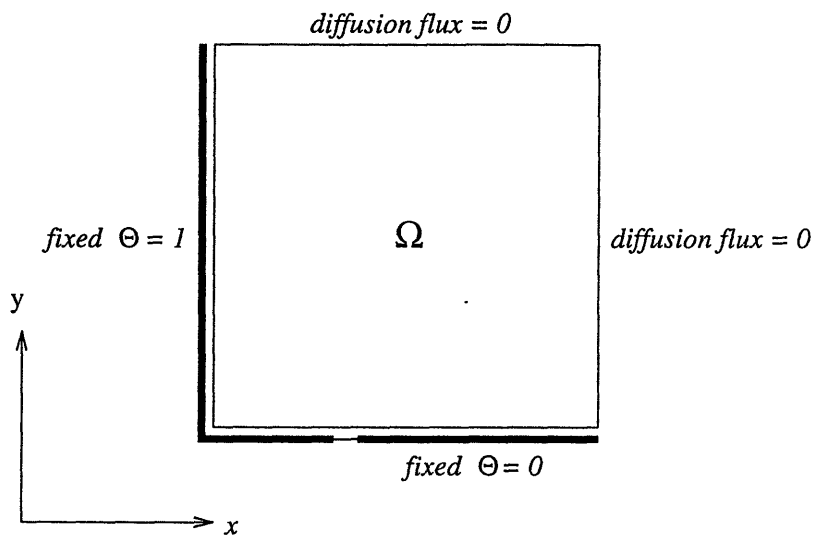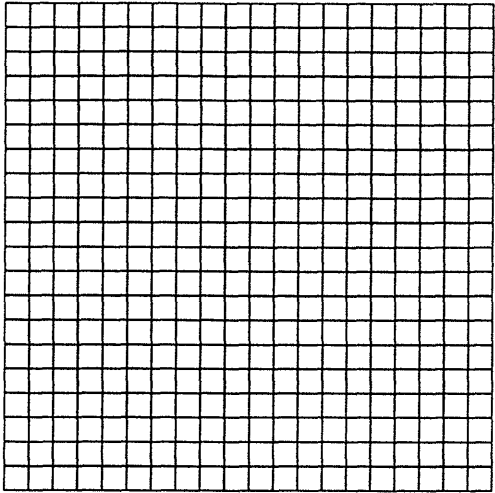

Figure 5-1: Boundary condition for the test problem 1.

meshes
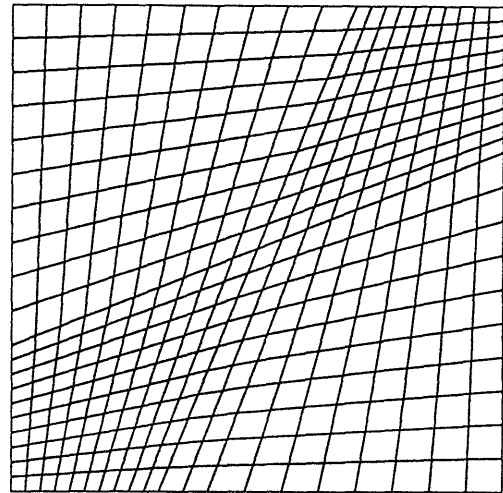
A uniform mesh and a distorted mesh are used for this test problem as shown in fig. 5-2.

velocity field

In this problem, a uniform velocity field is prescribed with a different fluid velocity direction for every run as shown in fig. 5-3. The direction of the velocity for every run

(a)   (b)

Figure 5-2: Meshes used for the test problem (a) Uniform mesh (b) distorted mesh.
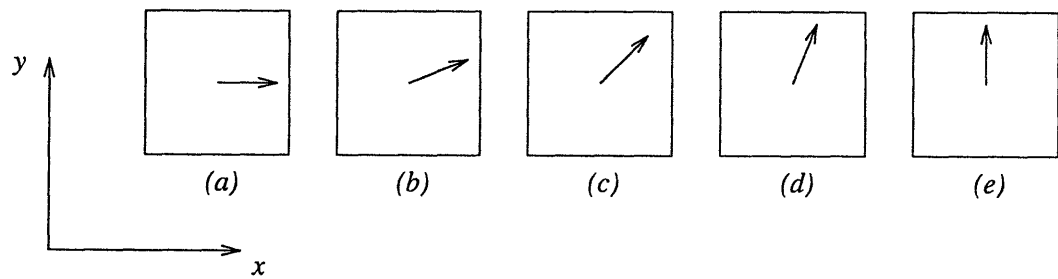
Figure 5-3: Prescribed velocity vector for (a) run 1 (b) run 2 (c) run 3 (d) run 4 (e) run 5.

can be decomposed into x and y velocity components. The coefficient of diffusivity is constant, $\alpha = 10^{-5}$, so the velocity and the Peclet number components for every run can be summarized as shown in table 5.1. V_x and V_y represent the velocity components in x and y directions. Pe_x and Pe_y are the Peclet number components in x and y directions. The Peclet number components are defined as

$$Pe_x = \frac{V_x L_x}{\alpha}$$

$$Pe_y = \frac{V_y L_y}{\alpha}$$

where $L_x = L_y = 1$. Graphical representation of the test problem is given in fig. 5-4.

Table 5.1: Summary of uniform velocity field and Peclet number components for every run.

Run number	V_x	V_y	α	Pe_x	Pe_y
1	1.0	0.0	10^{-5}	10^5	0.0
2	1.0	0.5	10^{-5}	10^5	0.5×10^5
3	1.0	1.0	10^{-5}	10^5	10^5
4	0.5	1.0	10^{-5}	0.5×10^5	10^5
5	0.0	1.0	10^{-5}	0.0	10^5

The expected solution of this test problem is simple. The shock front at the boundary is carried by the fluid to the interior of the domain. Since the Peclet number is very high the gradient of the temperature remains sharp. Fig. 5-5 shows a sketch of the expected solution for the test problem 1. Similarly, for a different prescribed velocity direction, the shock front is carried in the direction of the fluid velocity. The discretization of the domain will cause discrepancy from the exact solution, but reasonable solutions are still obtained using a good upwinding scheme.

Vector representation of velocity direction

Prescribed Θ *band*
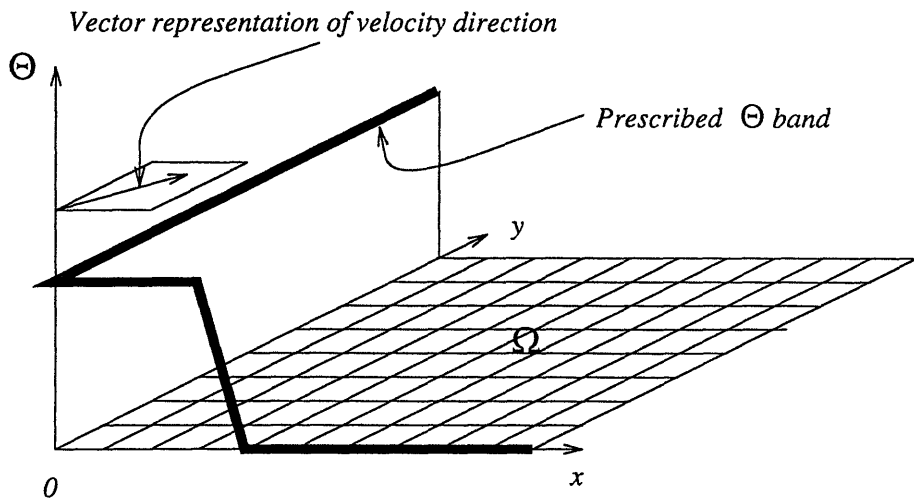
Figure 5-4: Summary of the test problem 1.

5.2   Test problem 2

In test problem 2, the uniform and distorted meshes defined in the test problem 1 are used. For consistency, the same velocity directions defined in the test problem 1 for run 1 through 5 are also used in this test problem. Boundary conditions are defined as shown in fig. 5-6. The test problem 2 is given in the graphical representation as shown in fig. 5-7.

The expected solution to this test problem is shown in fig. 5-8 for any prescribed velocity direction.

65
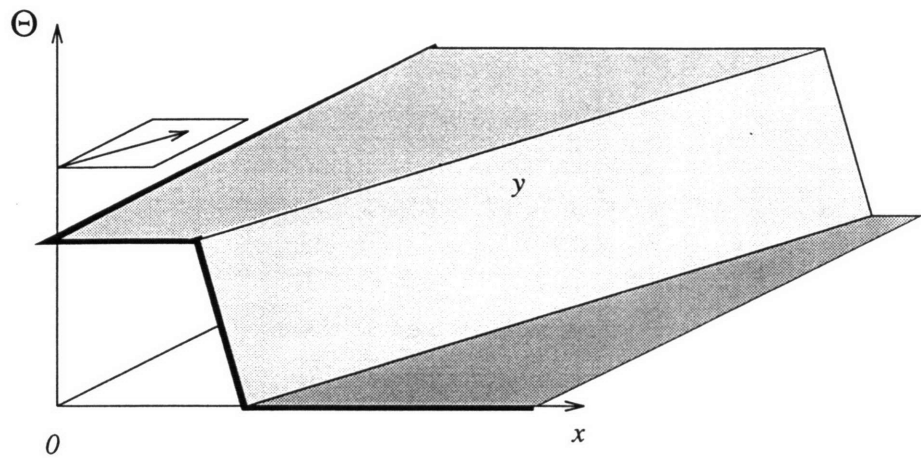
Figure 5-5: A sketch of expected solution of the test problem 1 for high Peclet number.
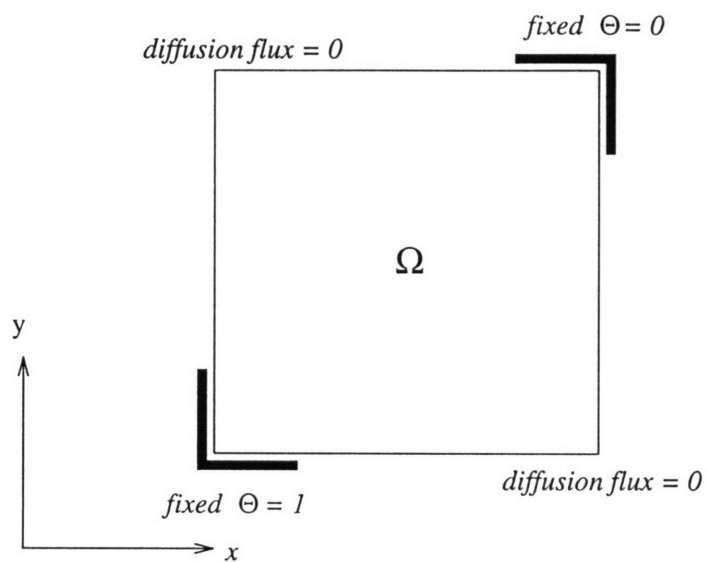
Figure 5-6: Boundary conditions for the test problem 2.
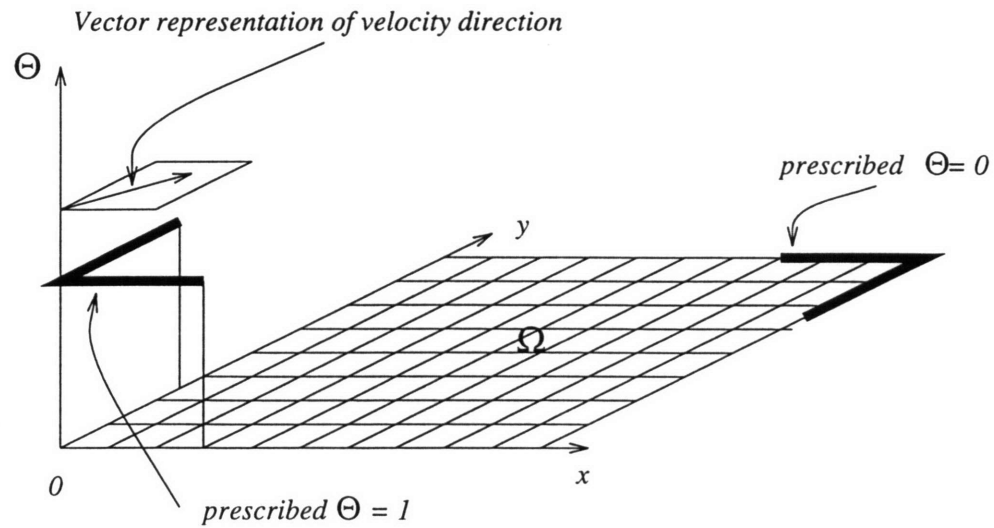
Figure 5-7: Summary of the test problem 2.
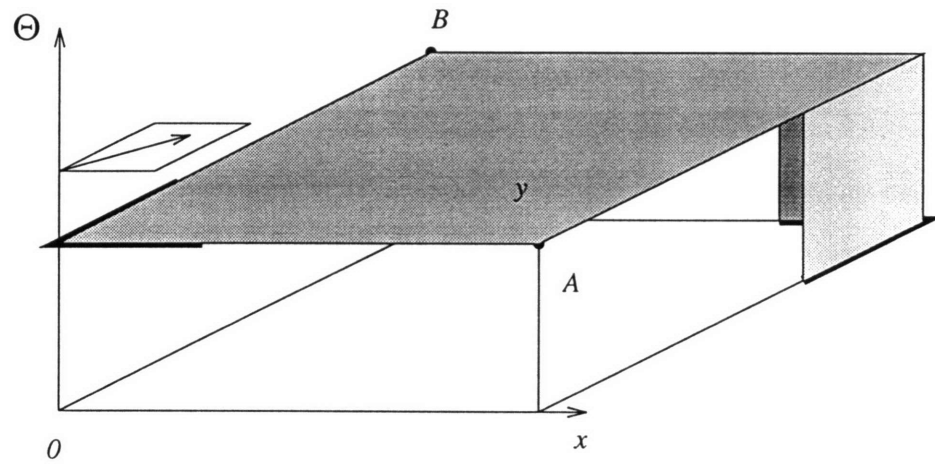
Figure 5-8: The sketch of expected solution to the test problem 2 for high Peclet number.

67

Chapter 6

Numerical Results

In this chapter, the numerical results of the upwinding schemes applied to the test problems explained in chapter 5 are presented. Four upwinding schemes will be discussed and compared, namely, the streamline-upwind/Petrov-Galerkin (SUPG), the beyond streamline-upwind/Petrov-Galerkin (BSUPG), the positive-coefficient upwinding procedure from the control volume finite element method, and the third order accuracy upwinding scheme. To complete the comparison, a commercial finite element method software, ADINA-F, is used to solve the test problems. Some conclusions are drawn based on these results.

Note that the test problem 1 is not a sufficient test problem because the classical Galerkin method can still obtain reasonable results. It does not indicate the necessity for developing any upwinding schemes. On the other hand, the test problem 2 shows the superiority of upwinding schemes compared to the Galerkin method. The Galerkin method cannot solve this problem because oscillations are observed in the solutions. The use of any upwinding scheme improves the results to this problem. Nevertheless, numerical solutions using many upwinding schemes show unstable signs of small oscillations near the boundary layer. This is not acceptable, when the schemes are applied to the Navier-Stokes equation, small oscillations will be amplified when iteration is used to calculate the velocity.

Streamline-Upwind/Petrov-Galerkin (SUPG)

Unlike many other upwinding schemes, the results using SUPG shows little crosswind diffusion. The solutions to both test problems using this method are shown in fig. 6-3 to 6-6. In the solutions to the test problem 1, the steepness of the shock front of θ at the boundary can be maintained in the interior of the domain. However, the solutions show small oscillations near the shock front. Test problem 1 run 1 shows the extreme of this characteristic where unacceptable oscillations occurs with up to 26% error at the shock front. The solutions to the test problem 2 display quite significant oscillations near the shock front. This confirms the conclusion of SUPG's oscillation characteristics.

Using distorted elements for the test problem 1 and 2, the accuracy of the numerical results deteriorate, and oscillations in the solutions are amplified.

Beyond Streamline-Upwind/Petrov-Galerkin (BSUPG)

The results of this method to the test problems show improvements compared to the results obtained using SUPG. The results are shown in fig. 6-7 to 6-10. In the solution to the test problem 1, this method eliminates the overshoot and undershoot characteristics near the shock front. However, in the solutions to the test problem 2, this scheme only reduces the oscillations near the shock front, but cannot eliminate them completely. On the other hand, a program that implements this method does not guarantee convergence when the gradient of θ is used in the iteration to obtain the solutions. To solve the test problem 2, iteration cannot converge to a certain limit, however, our experiments recommend the application of a maximum of three iterations to have "good" results. For solving steady state problems, iteration process is still required which makes this method expensive in computational time. Another remark is that the extra artificial diffusivity which acts in the direction of the gradient of θ is not based on physical interpretation. This extra diffusivity can cause the numerical results to depart from the exact solutions.

Similar to SUPG, the use of distorted elements deteriorates the accuracy of the numerical results. The amplitudes of oscillations in the results are amplified near the

shock front and the boundary layer.

Positive-Coefficient Upwinding Procedure for CVFEM

The positive-coefficient upwinding scheme produces the best numerical results to solve both test problems, see fig. 6-11 to 6-14. This method provides the exact solution for the test problem 1 for runs 1, 3 and 5 on the uniform mesh. It surpasses other upwinding schemes which give the exact solution for only run 5, and give poor results for run 1 with high overshoot characteristic at the shock front, and give a crosswind diffusion behavior for run 3. Using this method, oscillations in the solutions to both test problems can be eliminated completely, which shows the stability of this method. However, when the velocity field is between $0° - 45°$ or $45° - 90°$ to the mesh line, the numerical results contain a slight crosswind diffusion. It is indicated by the decreasing steepness of the shock front in the interior of the domain (see fig. 6-11 for run 2 and run 4).

Using distorted meshes, the results are slightly worse, yet acceptable, than those obtained using uniform meshes. The exact solutions of the test problem 1 for run 3 and 5 could not be obtained since the velocity directions are not aligned to the mesh line anymore.

Another advantage of this method, over the other previous upwinding schemes, is that it does not require calculating an adjusting variable, hence, it will save some computational time and may be more general in application.

Third Order Accuracy Upwinding Scheme

Generally, the results using the third order accuracy upwinding scheme for solving both test problems are not quite satisfactory. The results still contain oscillations near the shock front or the boundary layer, see fig. 6-15 and 6-18. Even though the amplitudes of the oscillations are less than SUPG's, the area affected by this behavior is wider. For the test problem 2, the results contain significant oscillations near the boundary layer for all runs.

A computer program that implements this method requires more memory space to

store global matrices than computer programs that implement other upwinding methods. Furthermore, multiplications performed on the global matrices consume a substantial amount of the CPU time, resulting in higher computational cost.

In this case, the use of distorted elements deteriorates the accuracy of the numerical results. However, the degree of deterioration is reasonable in case of the test problem 1. On the other hand, the results of the test problem 2, for runs 1 and 5, are not acceptable due to the occurence of a step-like θ drop in the domain (see fig. 6-18). This behavior does not take place in the solution when other upwinding methods are used.

In this formulation, an adjusting variable, β, is introduced as mentioned in chapter 4. The author of this method did not explain how to determine the value of this variable, but based on our experiments, $\beta = 1.5$ for one dimensional case, and $\beta = 3.0$ for two dimensional case will give the best numerical results for solving high Peclet number problems.

ADINA

The results to the test problems using ADINA-F are shown in figures 6-19 to 6-22. ADINA-F is proved to be very consistent based on the fact that oscillations in the numerical results are completely eliminated from the solutions to both test problems. However, the crosswind diffusion characteristics appear in the result of the test problem 1, run 5. In the uniform mesh, other upwinding schemes such as SUPG, BSUPG, the positive-coefficient upwinding scheme, and the third order accuracy scheme give the exact solutions for this run. This deficiency is due to the fact that in ADINA-F, a triangular element is used in the discretization where each quadrilateral domain is represented by four triangles. These triangles cannot capture the exact solution because the velocity field is not aligned with the element coordinate axes. While the use of triangular elements has this disadvantage, the triangular elements have the advantage of direct use in unstructured and highly graded meshes, and also they satisfy the inf-sup condition, see D. Chapelle and K.J. Bathe [7]. The four-node quadrilateral element tested in this thesis with the various upwinding methods does

71

not satisfy the inf-sup condition and would have to be used with caution in actual fluid flow analyses.
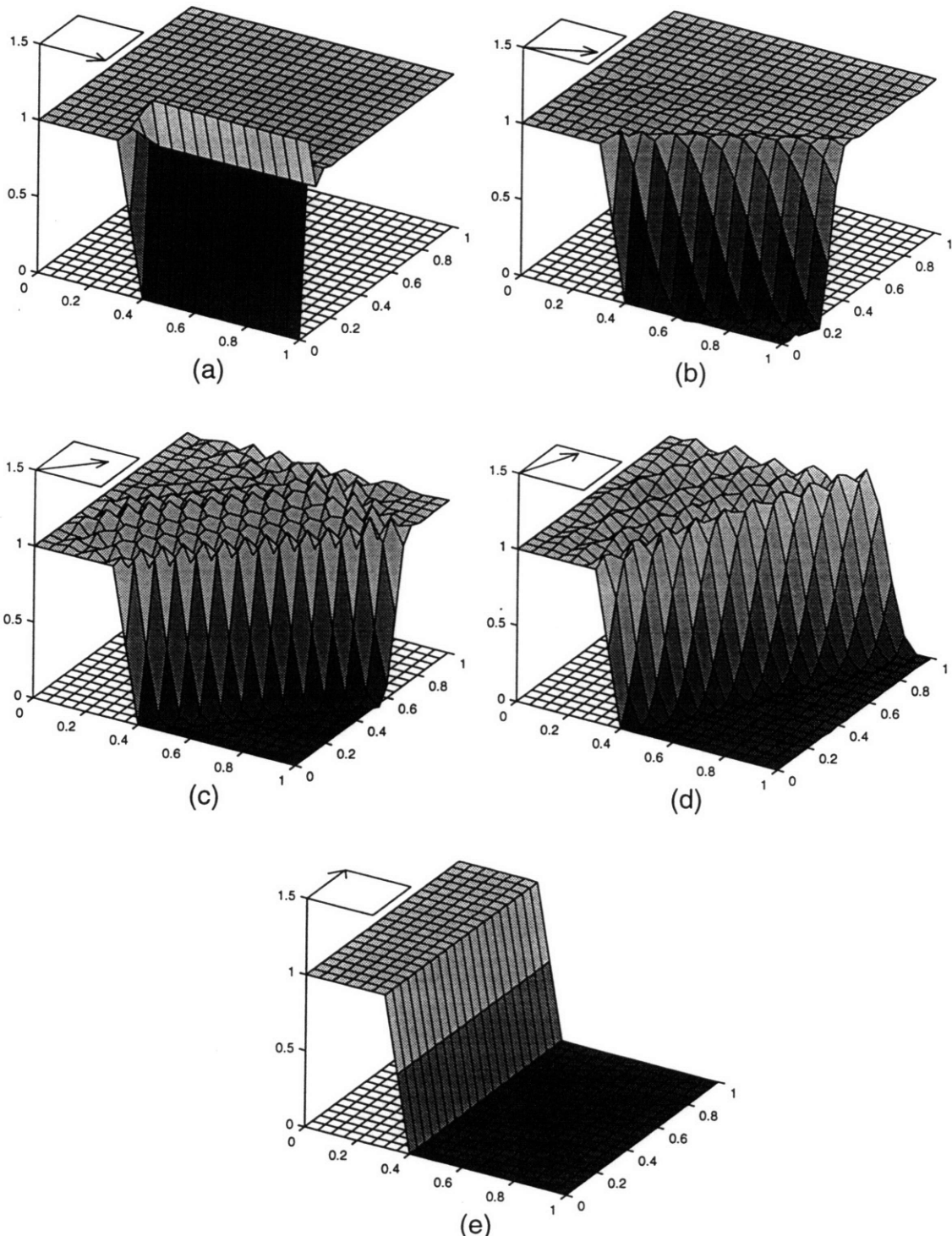
Figure 6-1: Numerical results of the Galerkin method for solving the test problem 1 on uniform mesh. (a) run 1 (b) run 2 (c) run 3 (d) run 4 (e) run 5
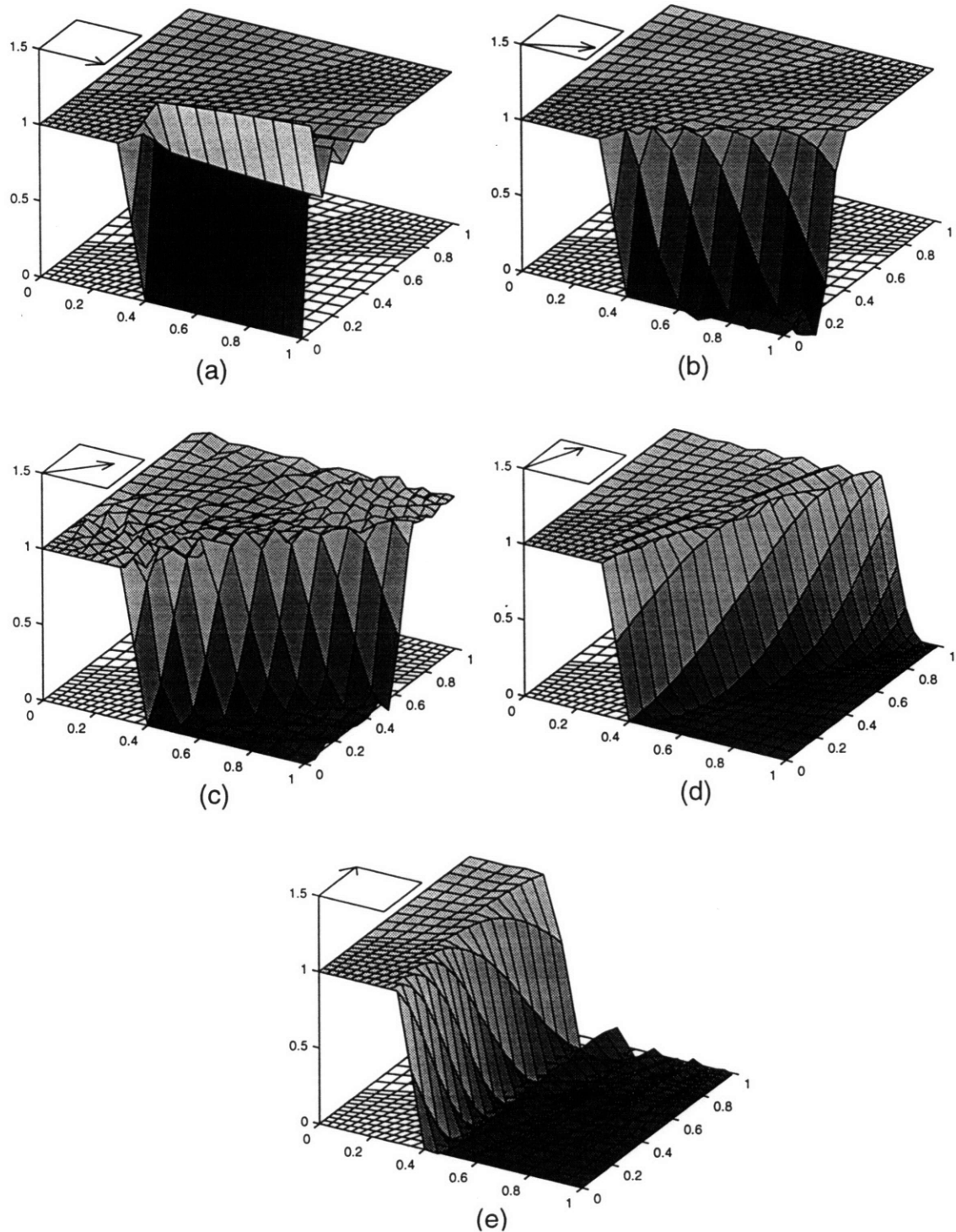
Figure 6-2: Numerical results of the Galerkin method for solving the test problem 1 on distorted mesh. (a) run 1 (b) run 2 (c) run 3 (d) run 4 (e) run 5
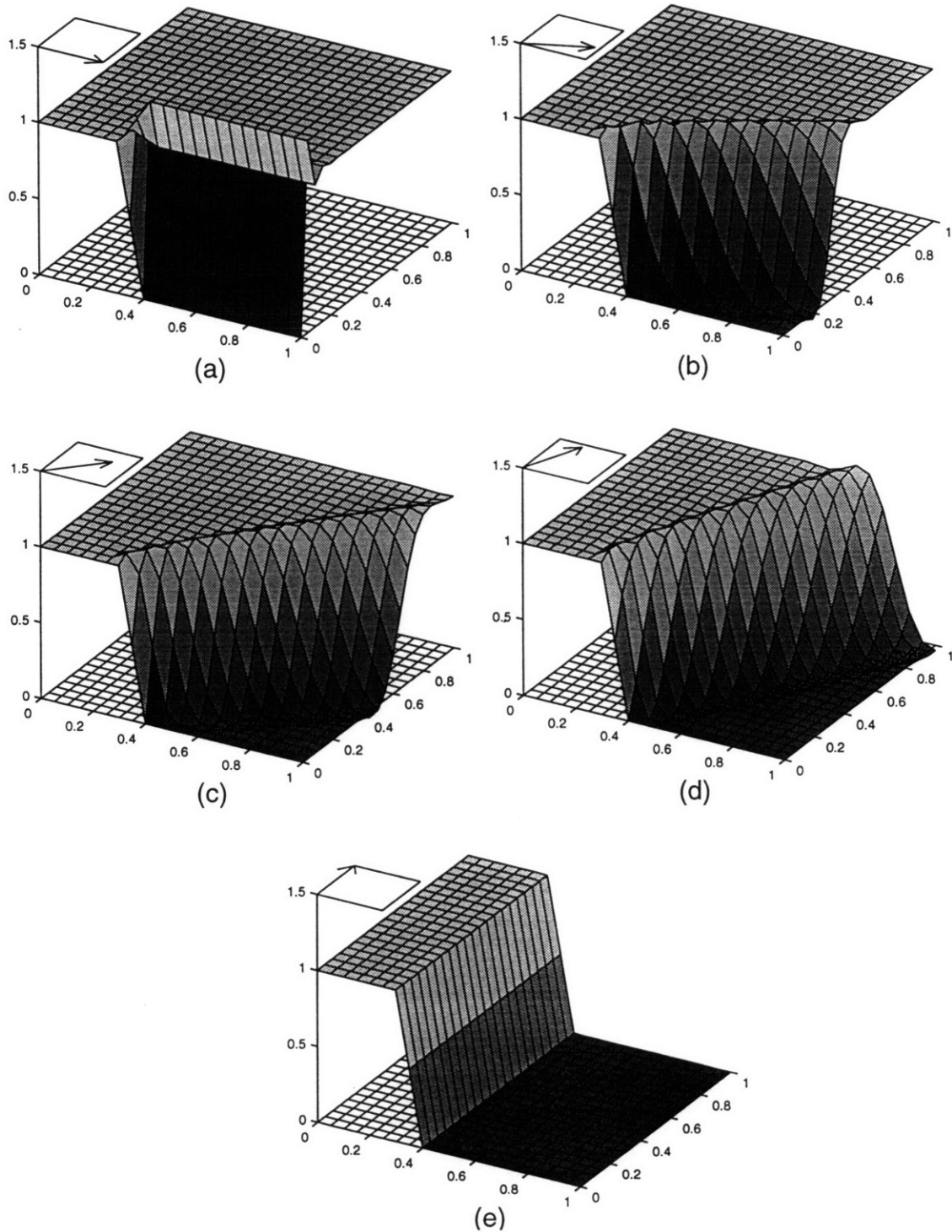
Figure 6-3: Numerical results of the streamline-upwind/Petrov-Galerkin method for solving the test problem 1 on uniform mesh. (a) run 1 (b) run 2 (c) run 3 (d) run 4 (e) run 5

75
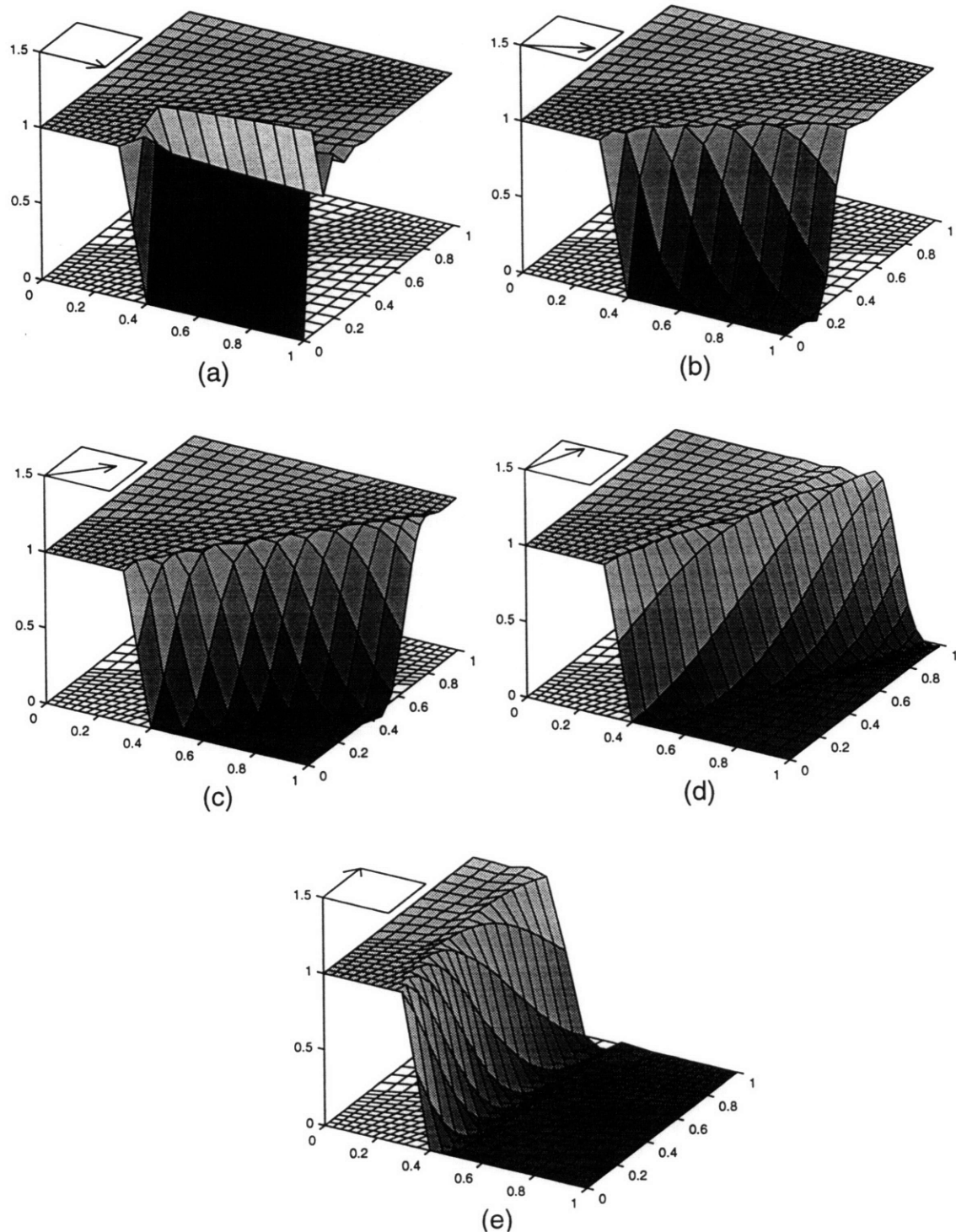
Figure 6-4: Numerical results of the streamline-upwind/Petrov-Galerkin method for solving the test problem 1 on distorted mesh. (a) run 1 (b) run 2 (c) run 3 (d) run 4 (e) run 5
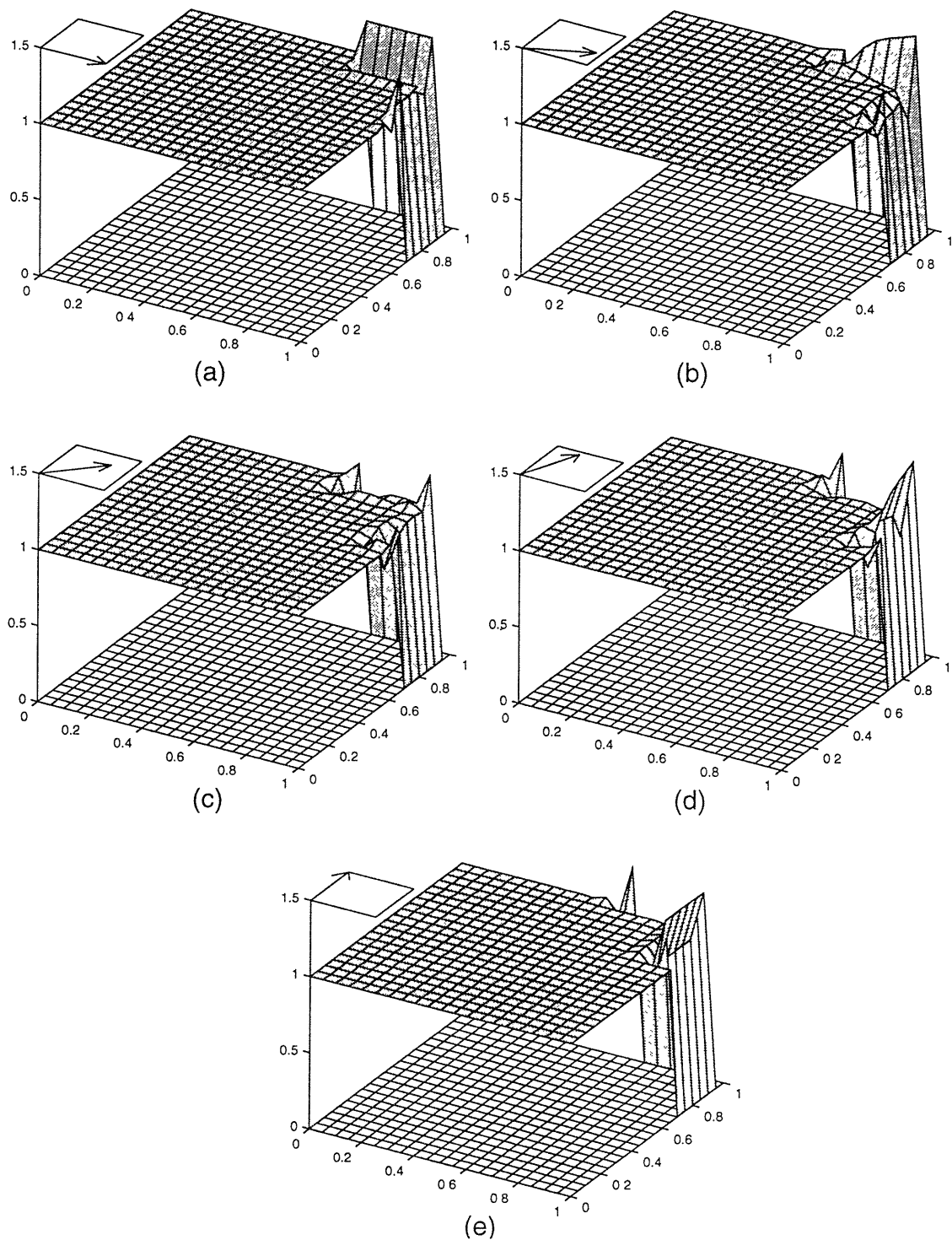
Figure 6-5: Numerical results of the streamline-upwind/Petrov-Galerkin method for solving the test problem 2 on uniform mesh. (a) run 1 (b) run 2 (c) run 3 (d) run 4 (e) run 5
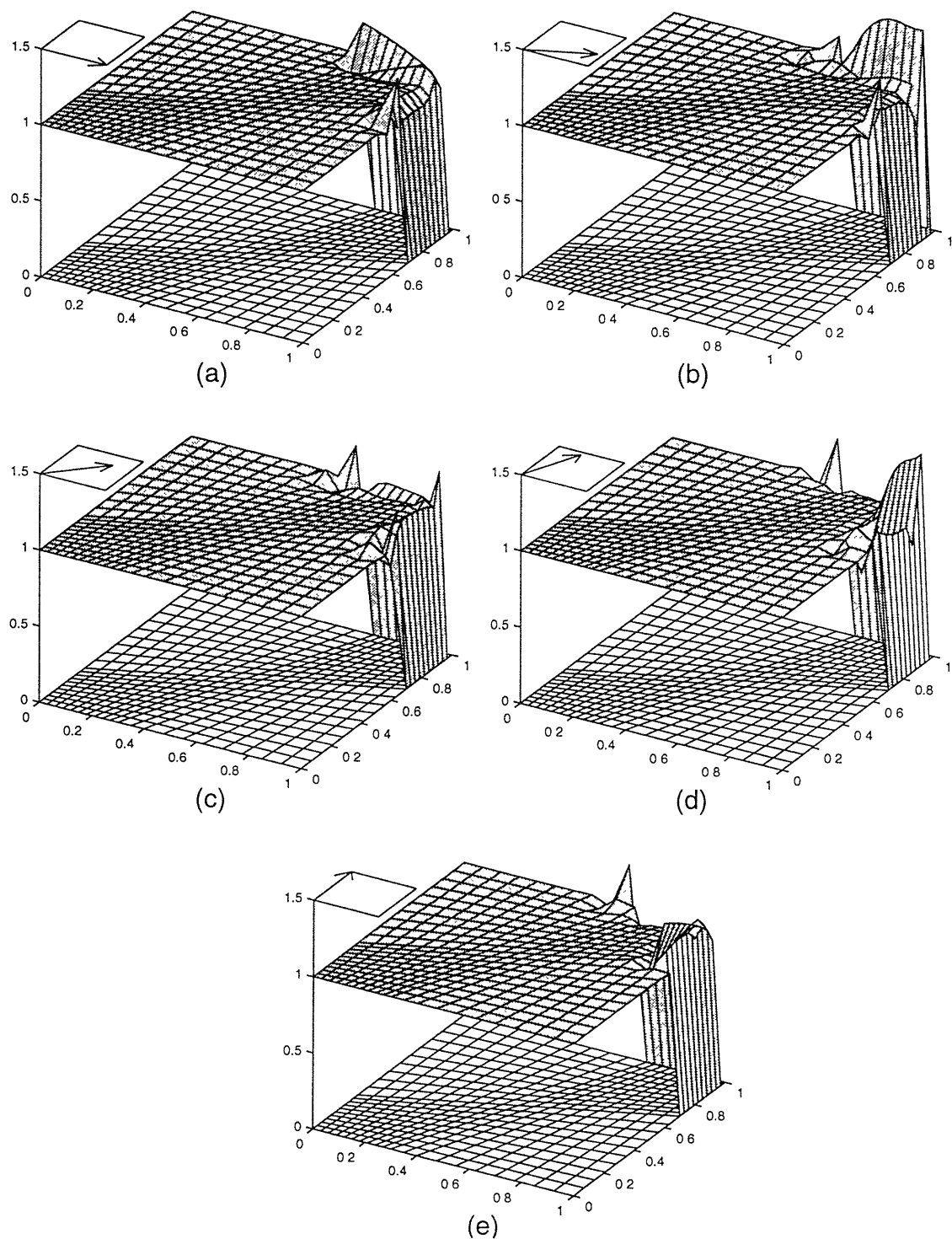
Figure 6-6: Numerical results of the streamline-upwind/Petrov-Galerkin method for solving the test problem 2 on distorted mesh. (a) run 1 (b) run 2 (c) run 3 (d) run 4 (e) run 5
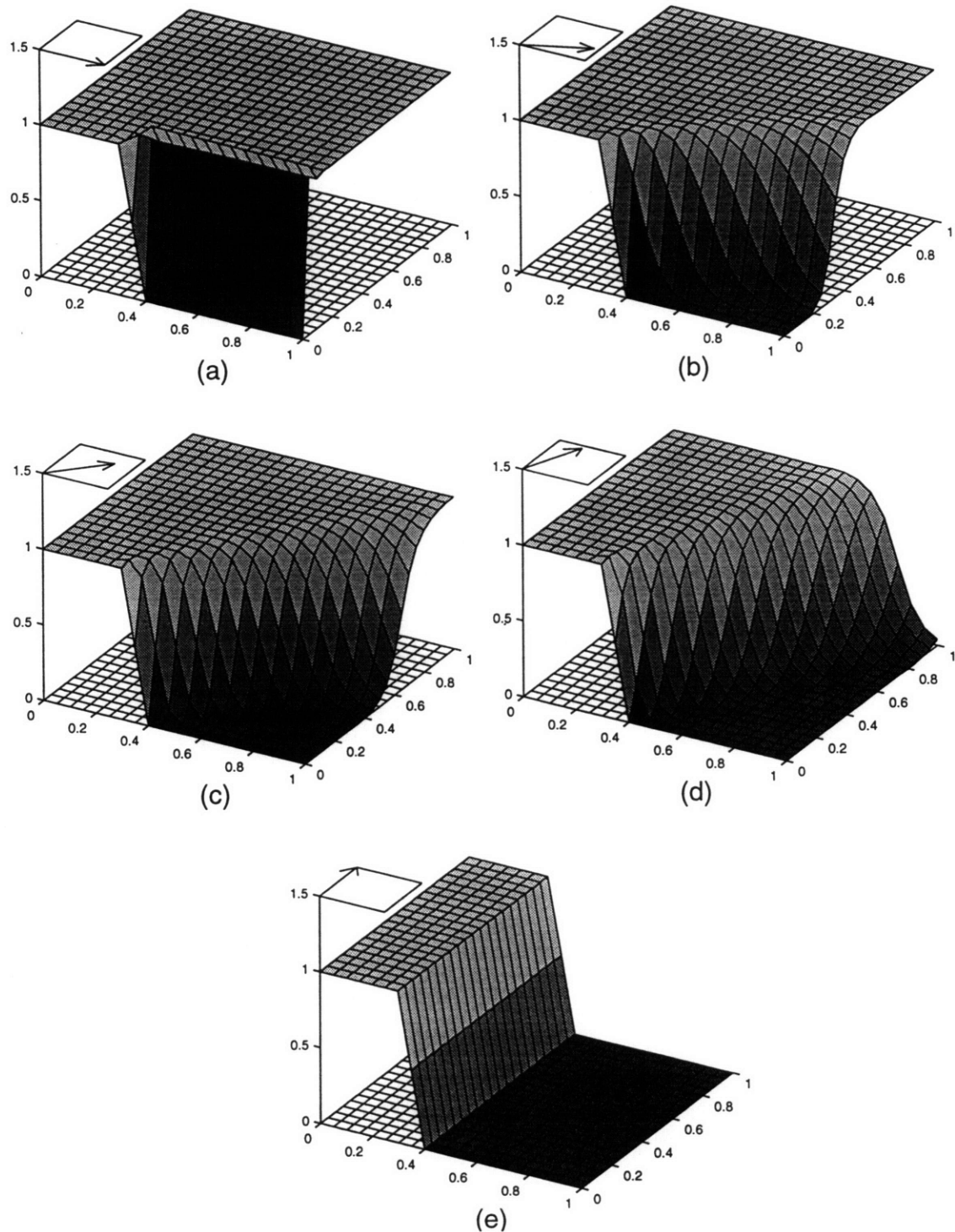
Figure 6-7: Numerical results of the beyond streamline-upwind/Petrov-Galerkin method for solving the test problem 1 on uniform mesh. (a) run 1 (b) run 2 (c) run 3 (d) run 4 (e) run 5
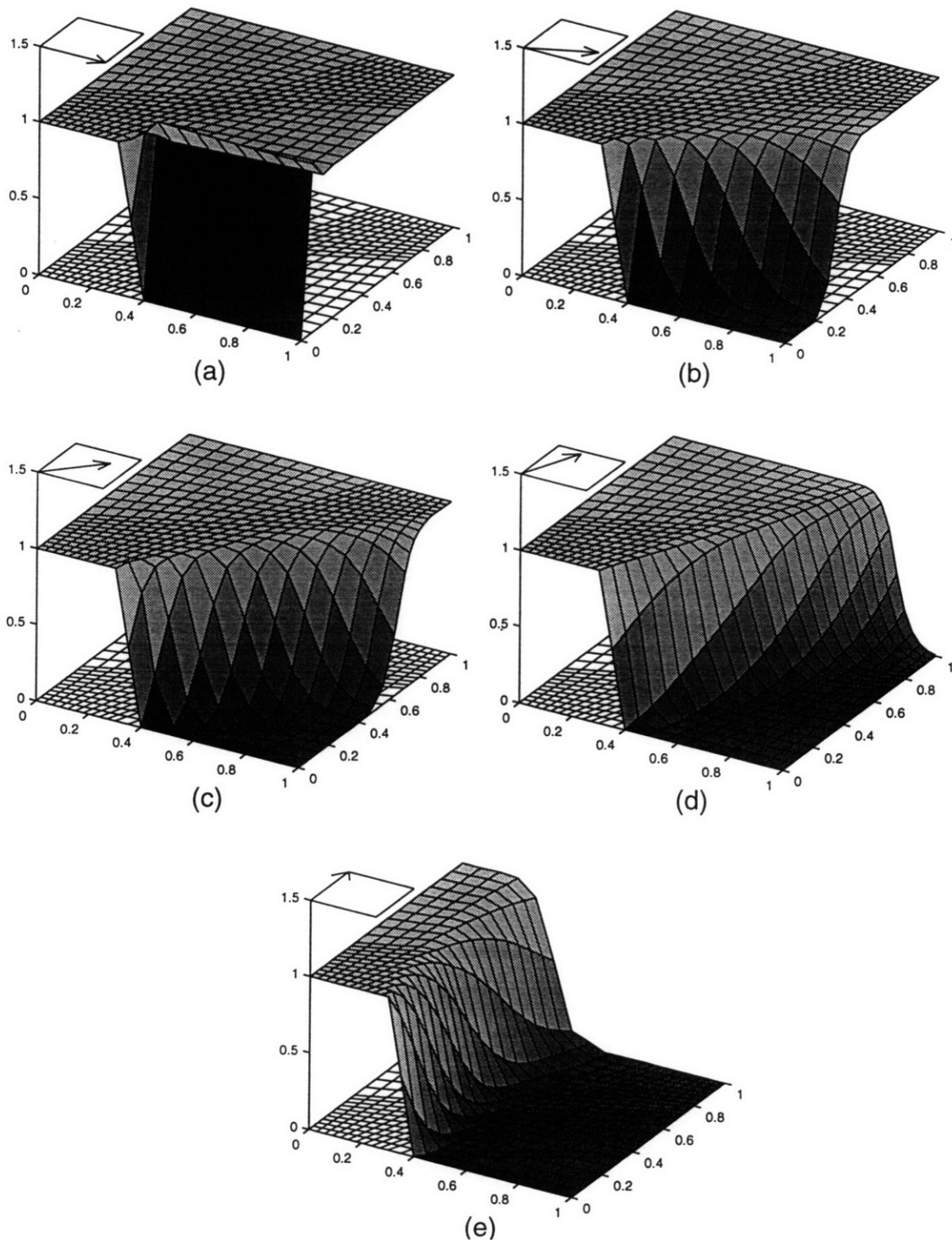
Figure 6-8: Numerical results of the beyond streamline-upwind/Petrov-Galerkin method for solving the test problem 1 on distorted mesh. (a) run 1 (b) run 2 (c) run 3 (d) run 4 (e) run 5
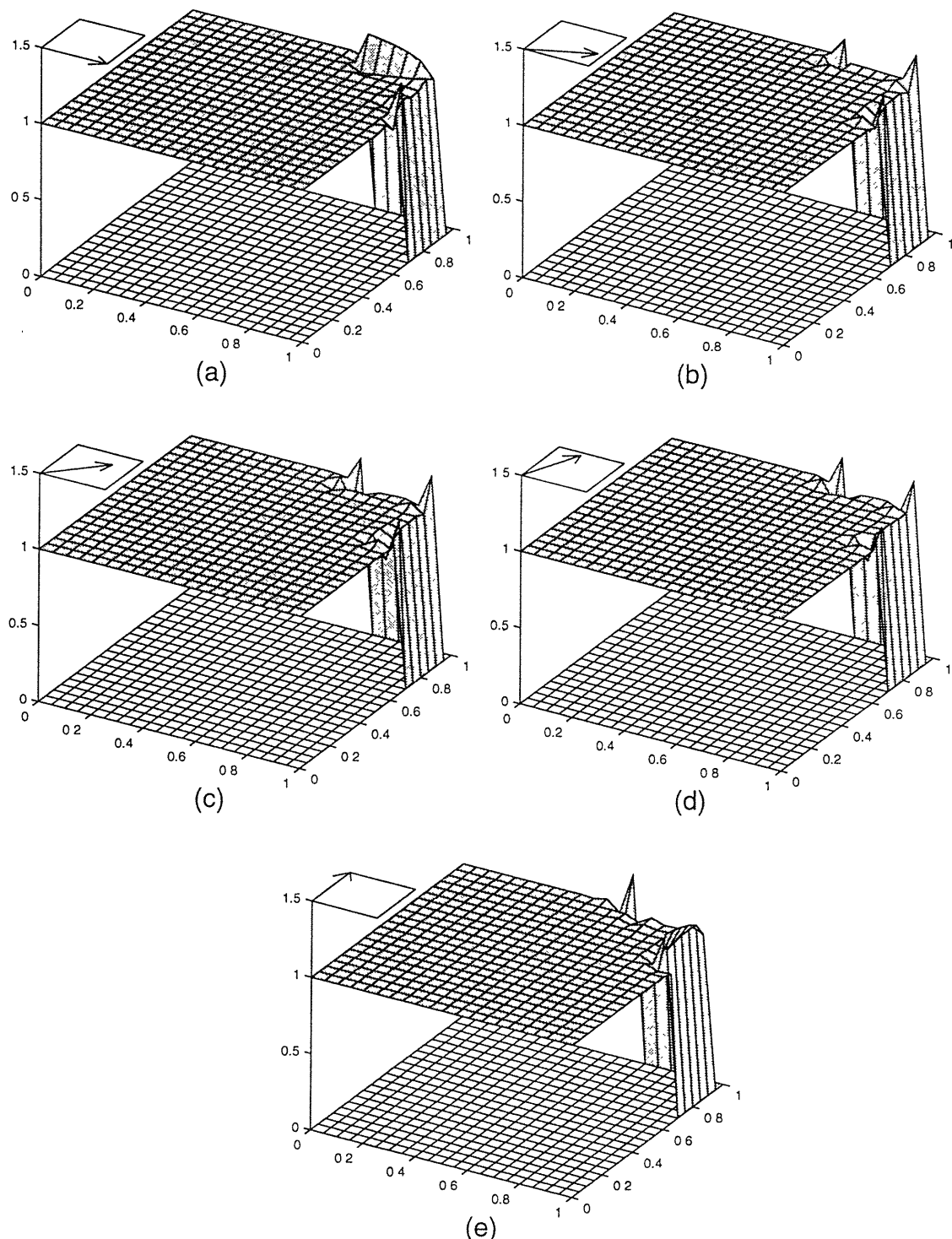
Figure 6-9: Numerical results of the beyond streamline-upwind/Petrov-Galerkin method for solving the test problem 2 on uniform mesh. (a) run 1 (b) run 2 (c) run 3 (d) run 4 (e) run 5
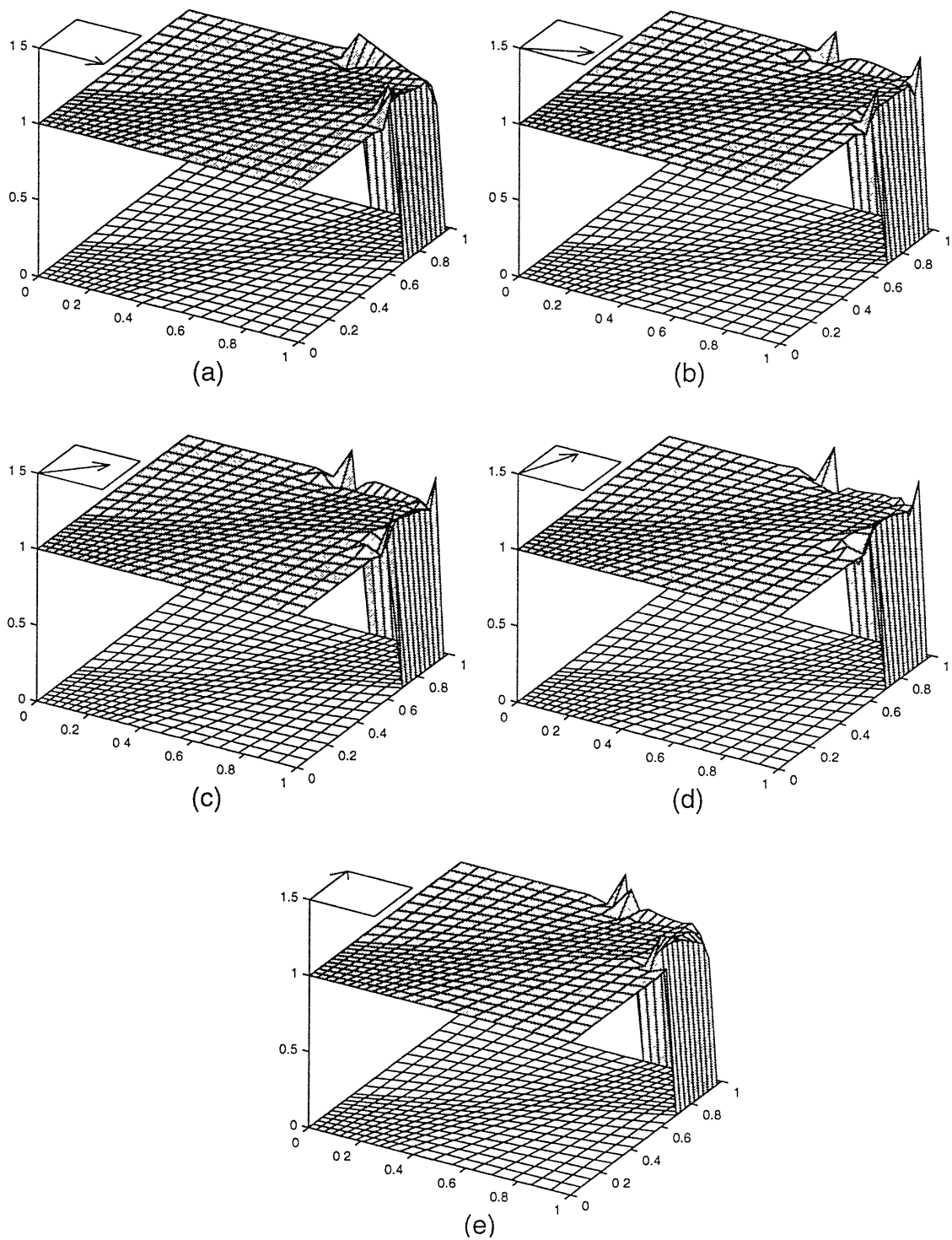
Figure 6-10: Numerical results of the beyond streamline-upwind/Petrov-Galerkin method for solving the test problem 2 on distorted mesh. (a) run 1 (b) run 2 (c) run 3 (d) run 4 (e) run 5
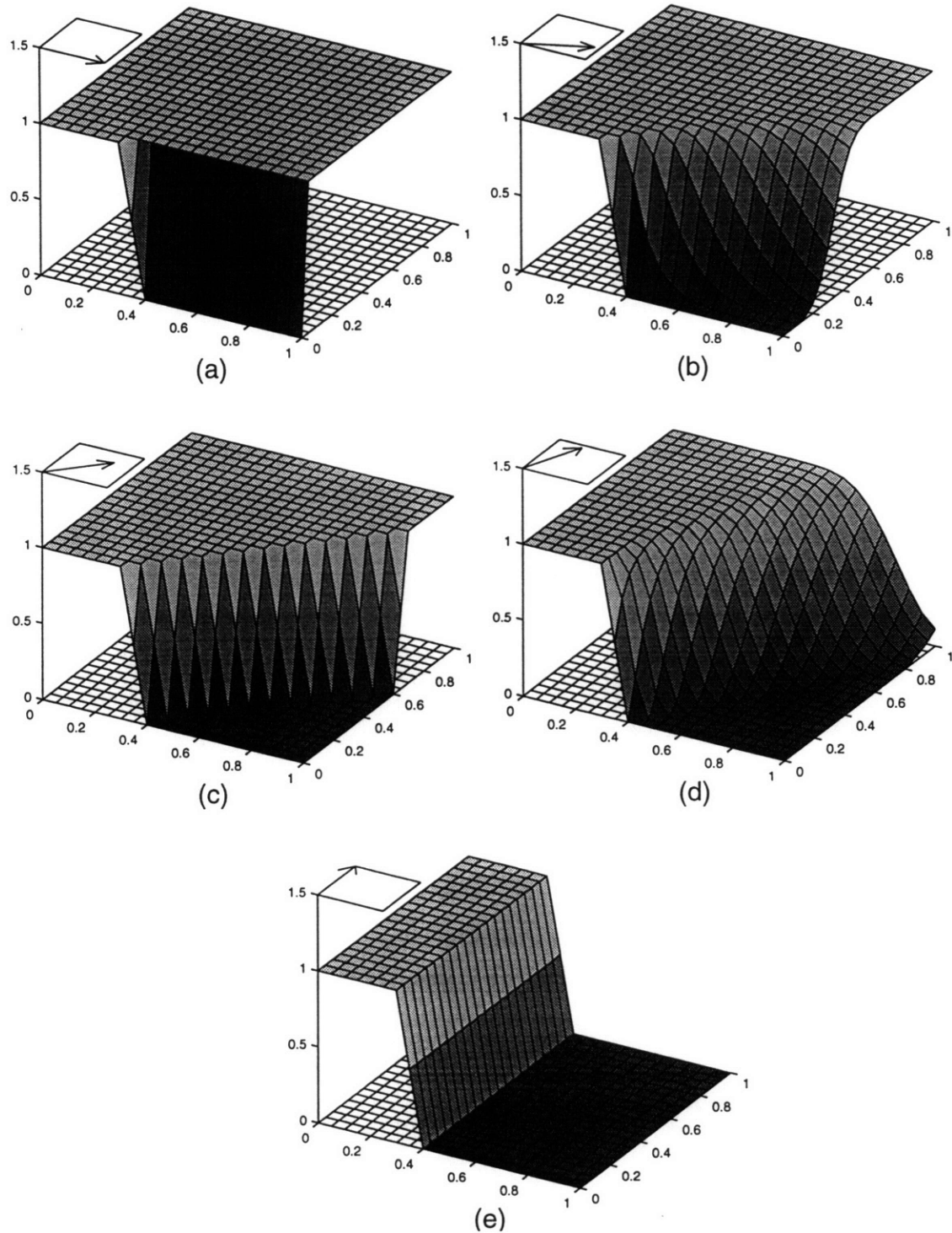
Figure 6-11: Numerical results of the positive-coefficient upwinding procedure for solving the test problem 1 on uniform mesh. (a) run 1 (b) run 2 (c) run 3 (d) run 4 (e) run 5
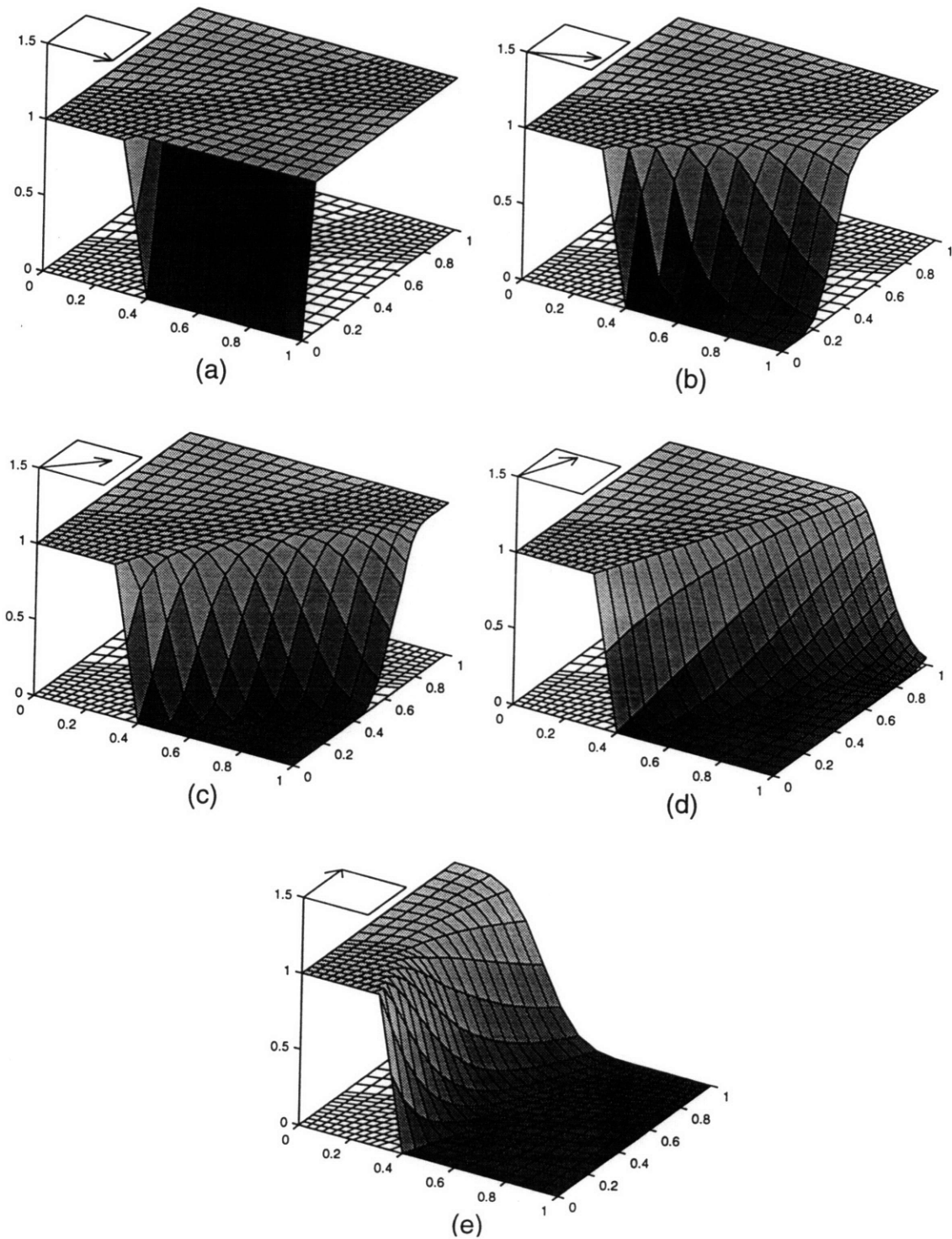
Figure 6-12: Numerical results of the positive-coefficient upwinding procedure for solving the test problem 1 on distorted mesh. (a) run 1 (b) run 2 (c) run 3 (d) run 4 (e) run 5
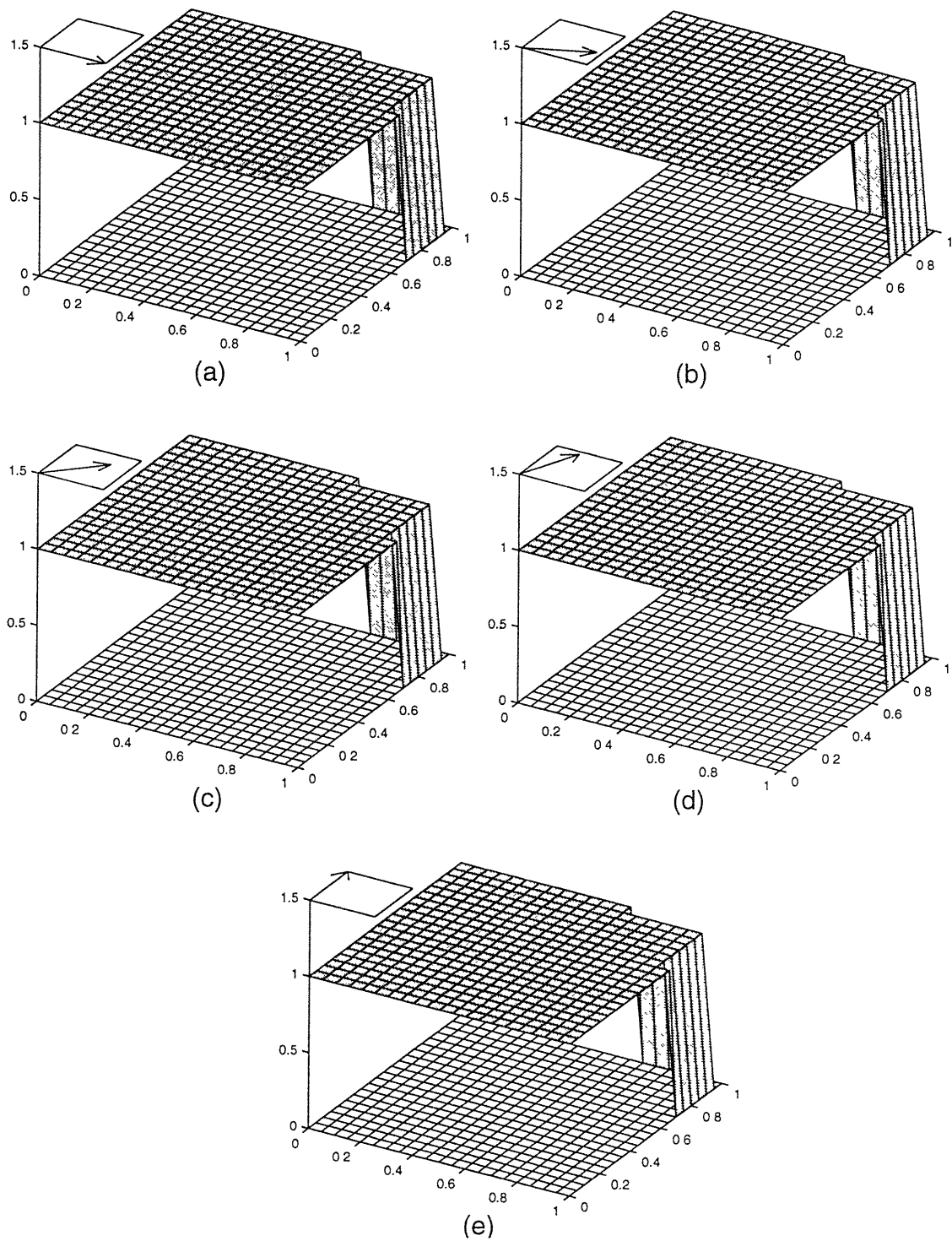
Figure 6-13: Numerical results of the positive-coefficient upwinding procedure for solving the test problem 2 on uniform mesh. (a) run 1 (b) run 2 (c) run 3 (d) run 4 (e) run 5
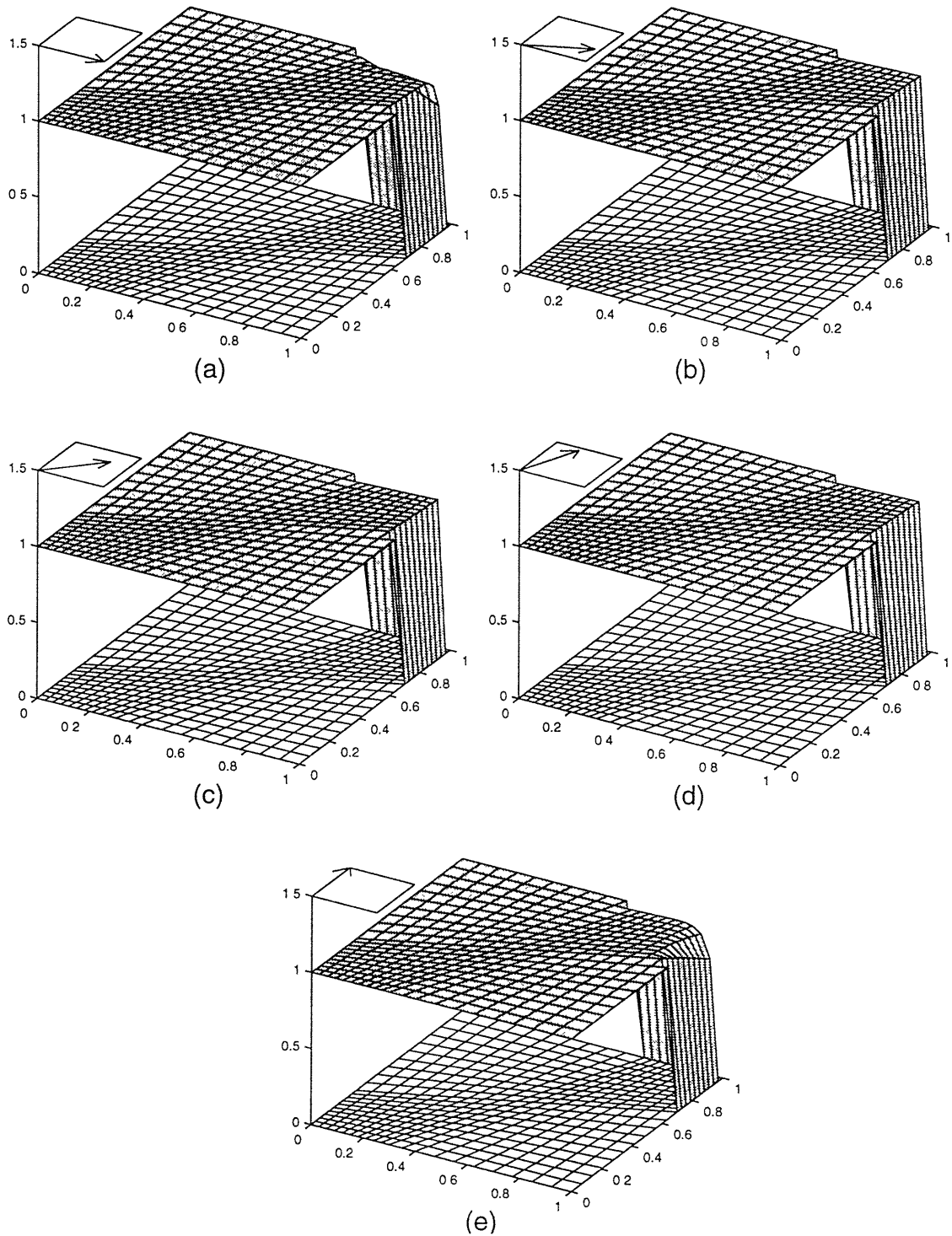
Figure 6-14: Numerical results of the positive-coefficient upwinding procedure for solving the test problem 2 on distorted mesh. (a) run 1 (b) run 2 (c) run 3 (d) run 4 (e) run 5
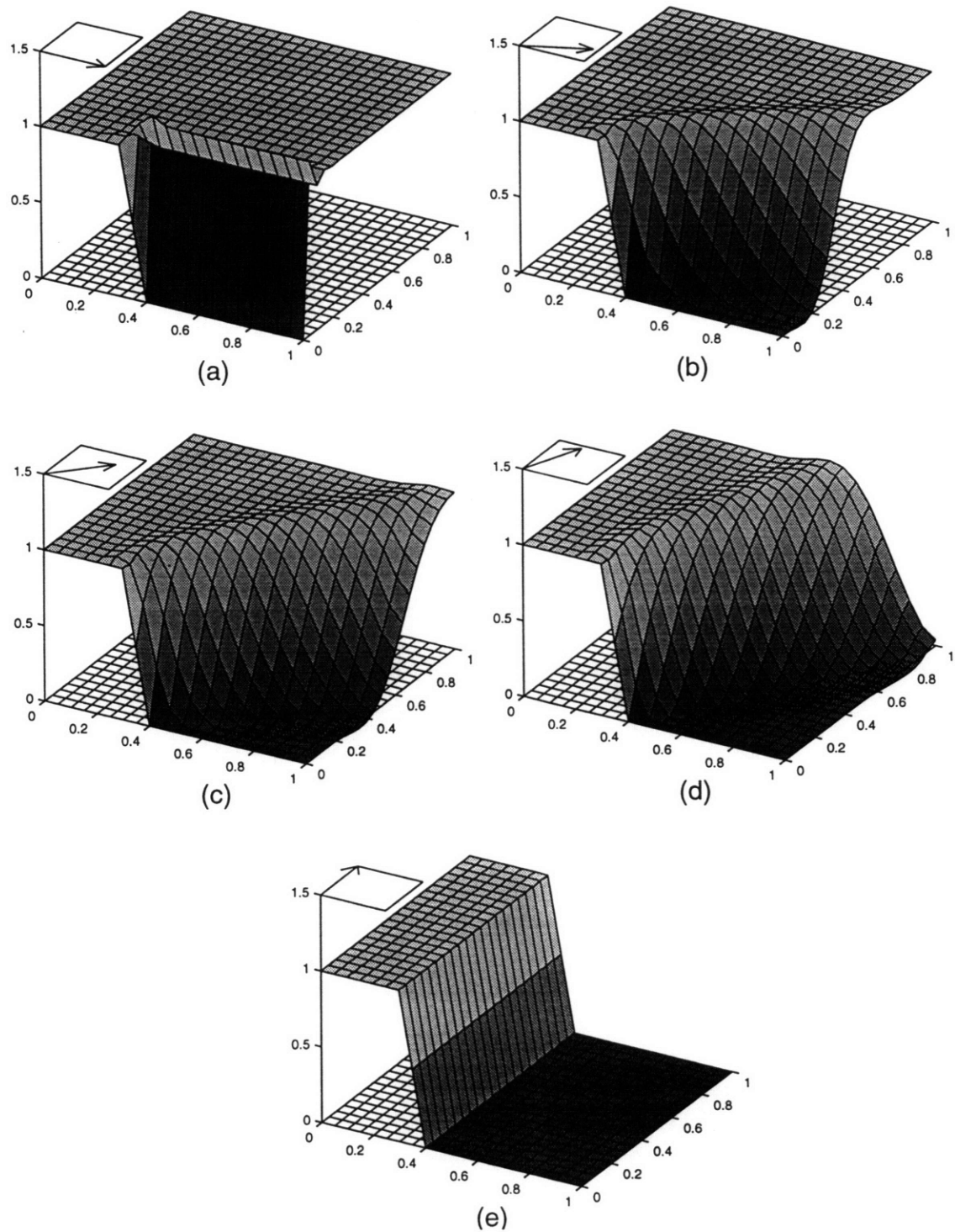
Figure 6-15: Numerical results of the third order accuracy upwinding method for solving the test problem 1 on uniform mesh. (a) run 1 (b) run 2 (c) run 3 (d) run 4 (e) run 5
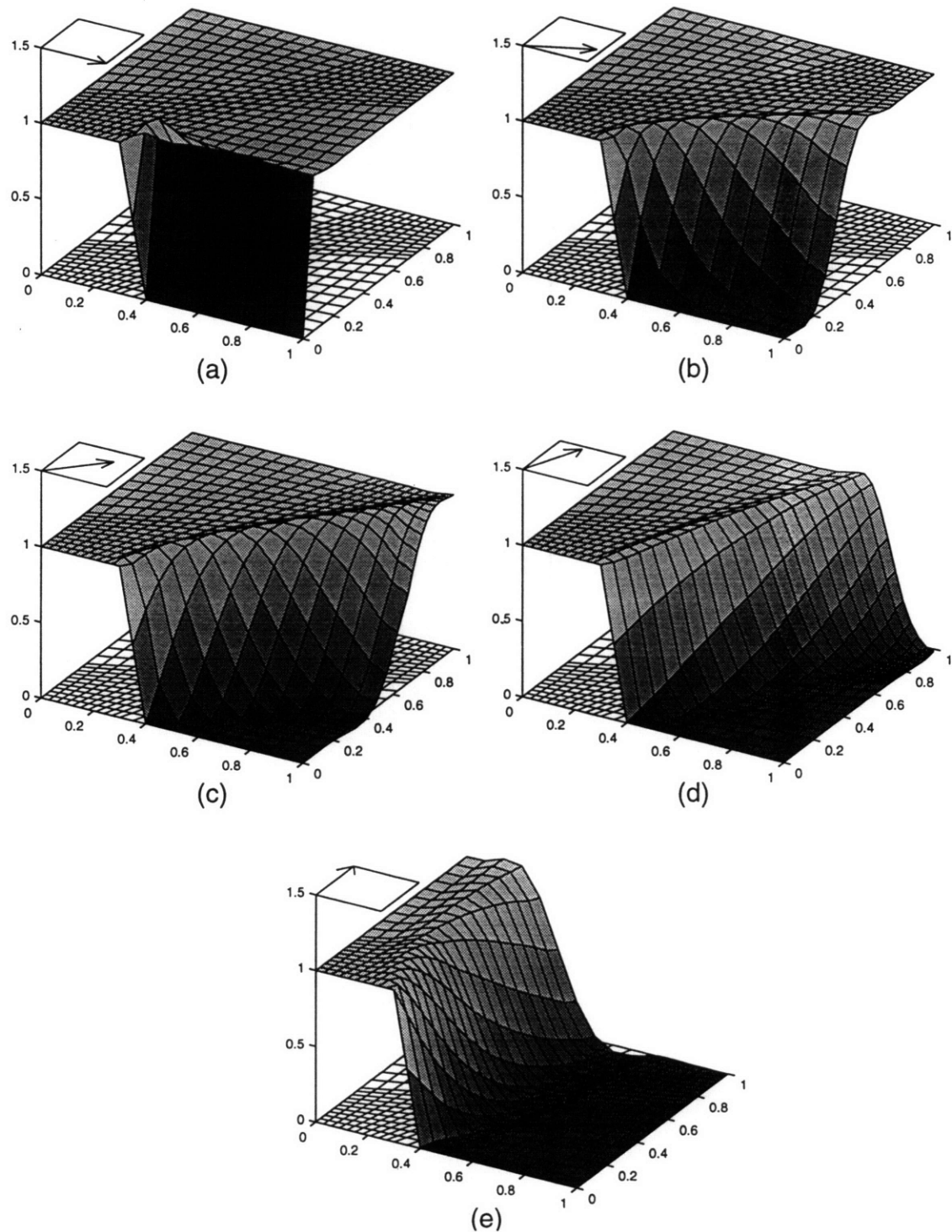
Figure 6-16: Numerical results of the third order accuracy upwinding method for solving the test problem 1 on distorted mesh. (a) run 1 (b) run 2 (c) run 3 (d) run 4 (e) run 5
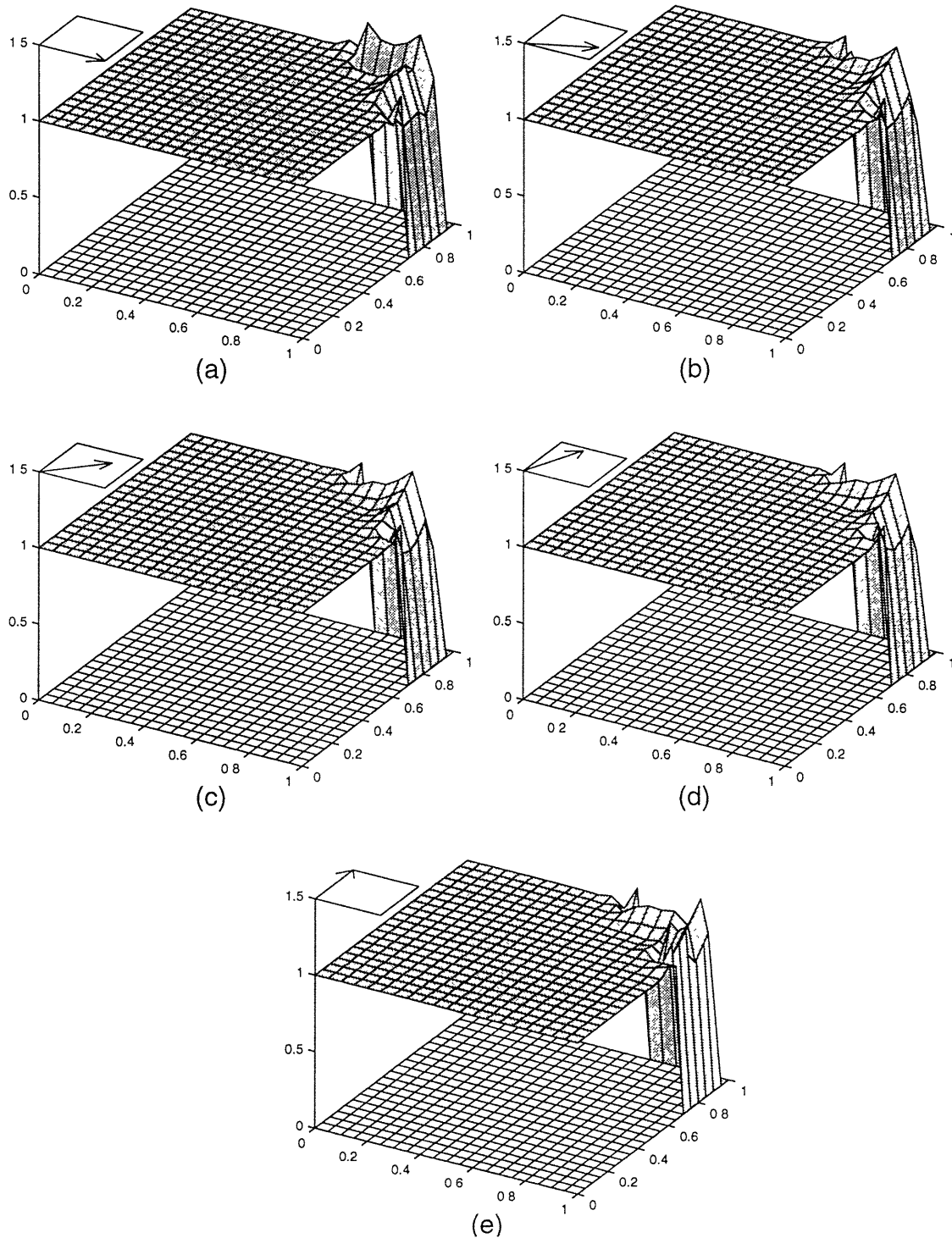
Figure 6-17: Numerical results of the third order accuracy upwinding method for solving the test problem 2 on uniform mesh. (a) run 1 (b) run 2 (c) run 3 (d) run 4 (e) run 5
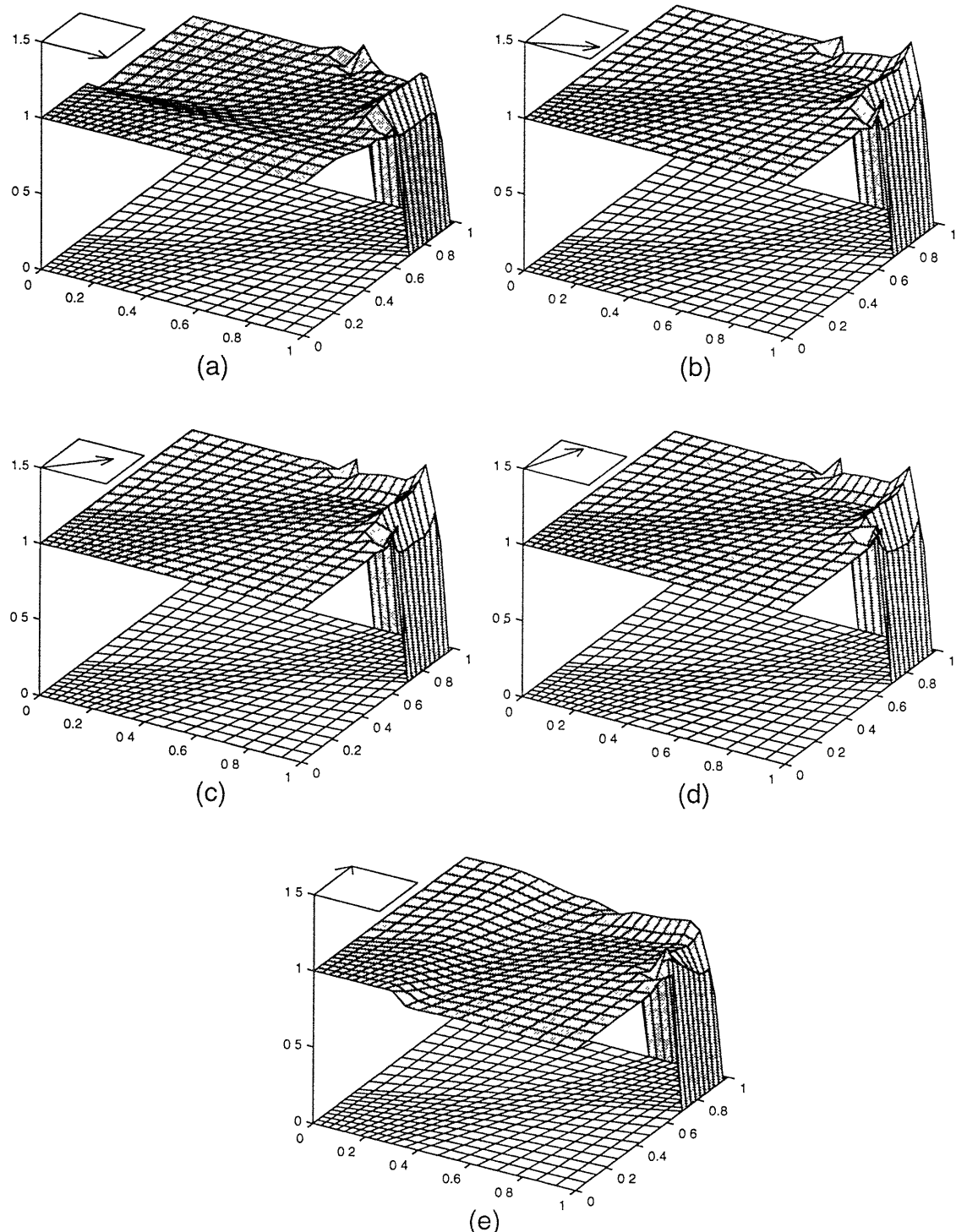
Figure 6-18: Numerical results of the third order accuracy upwinding method for solving the test problem 2 on distorted mesh. (a) run 1 (b) run 2 (c) run 3 (d) run 4 (e) run 5
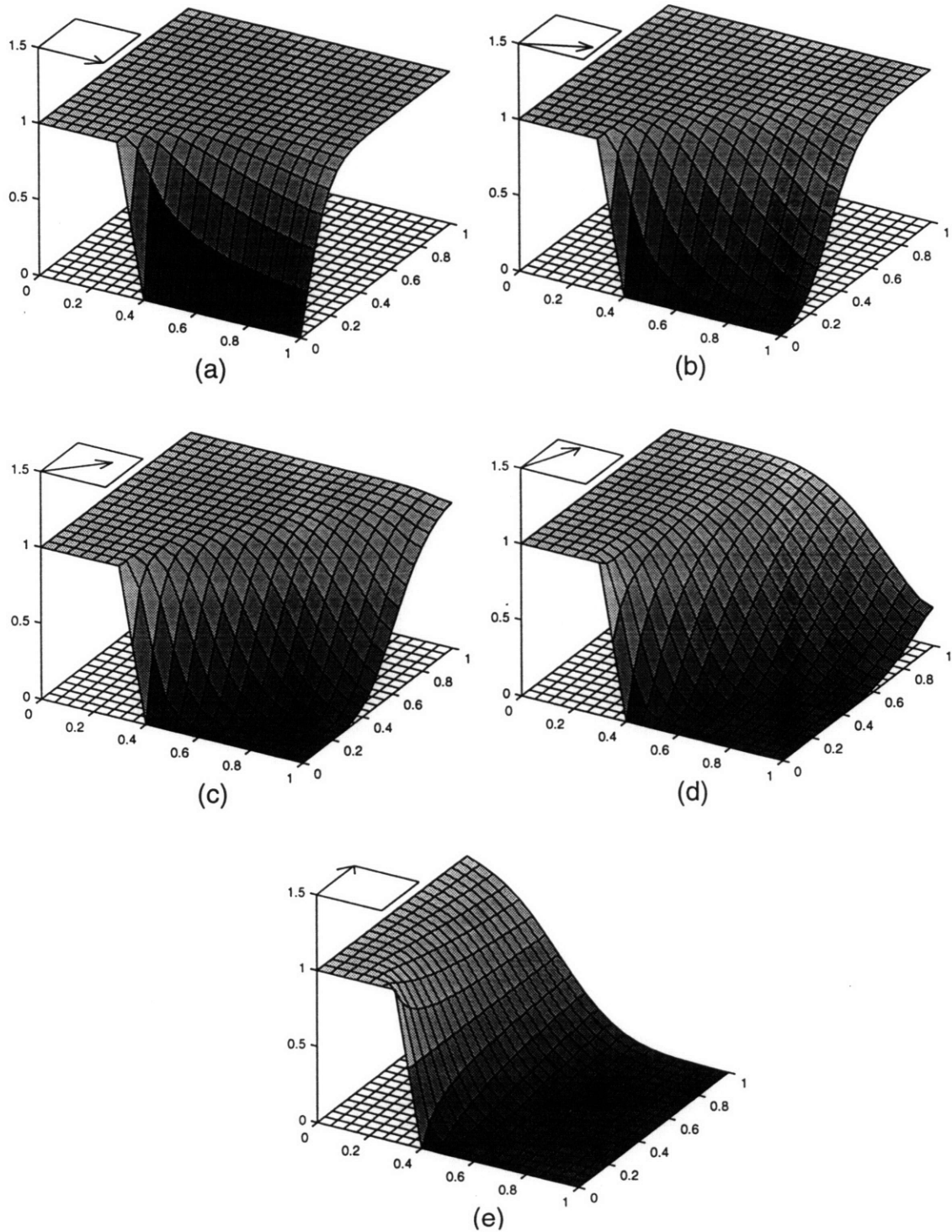
Figure 6-19: Numerical results of ADINA-F for solving the test problem 1 on uniform mesh. (a) run 1 (b) run 2 (c) run 3 (d) run 4 (e) run 5
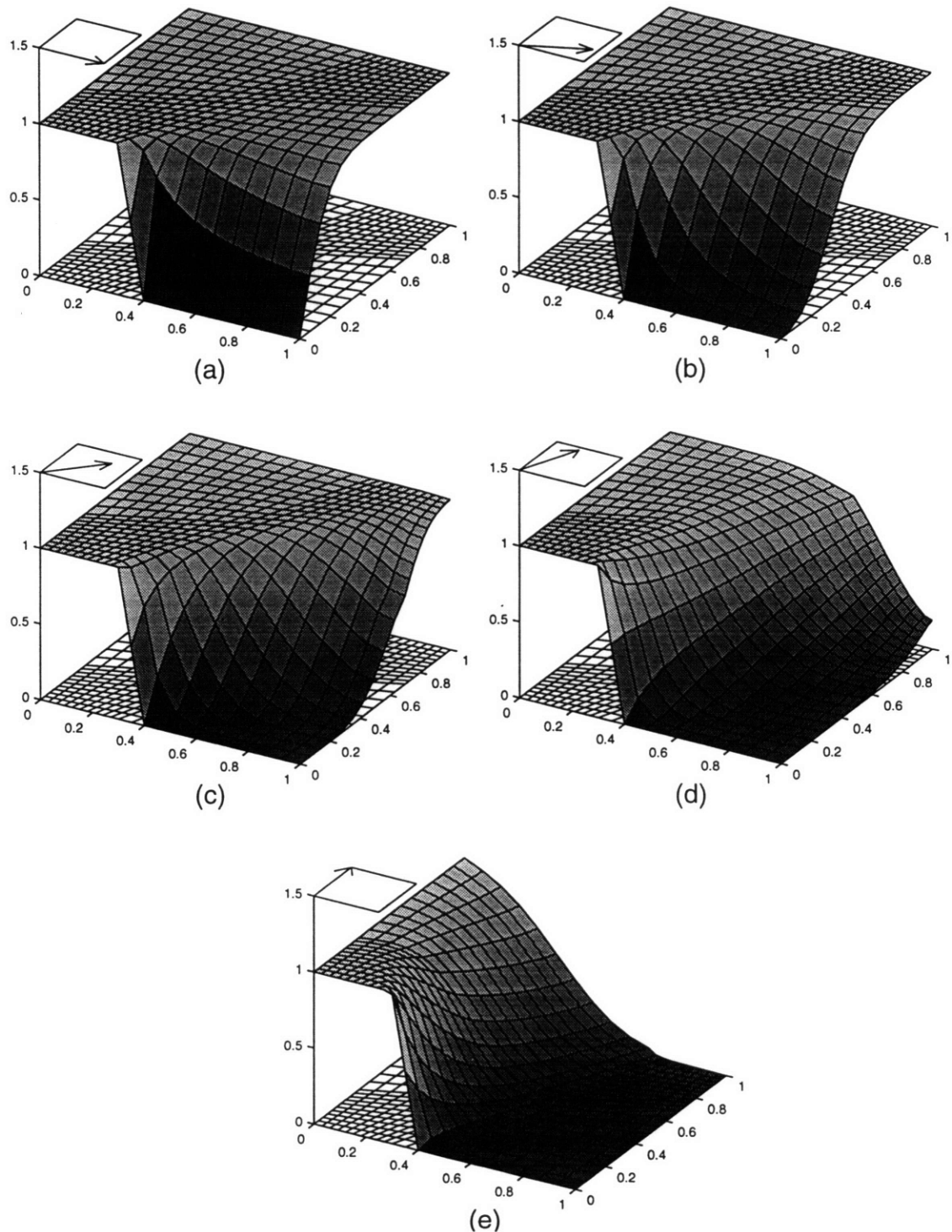
Figure 6-20: Numerical results of ADINA-F for solving the test problem 1 on distorted mesh. (a) run 1 (b) run 2 (c) run 3 (d) run 4 (e) run 5
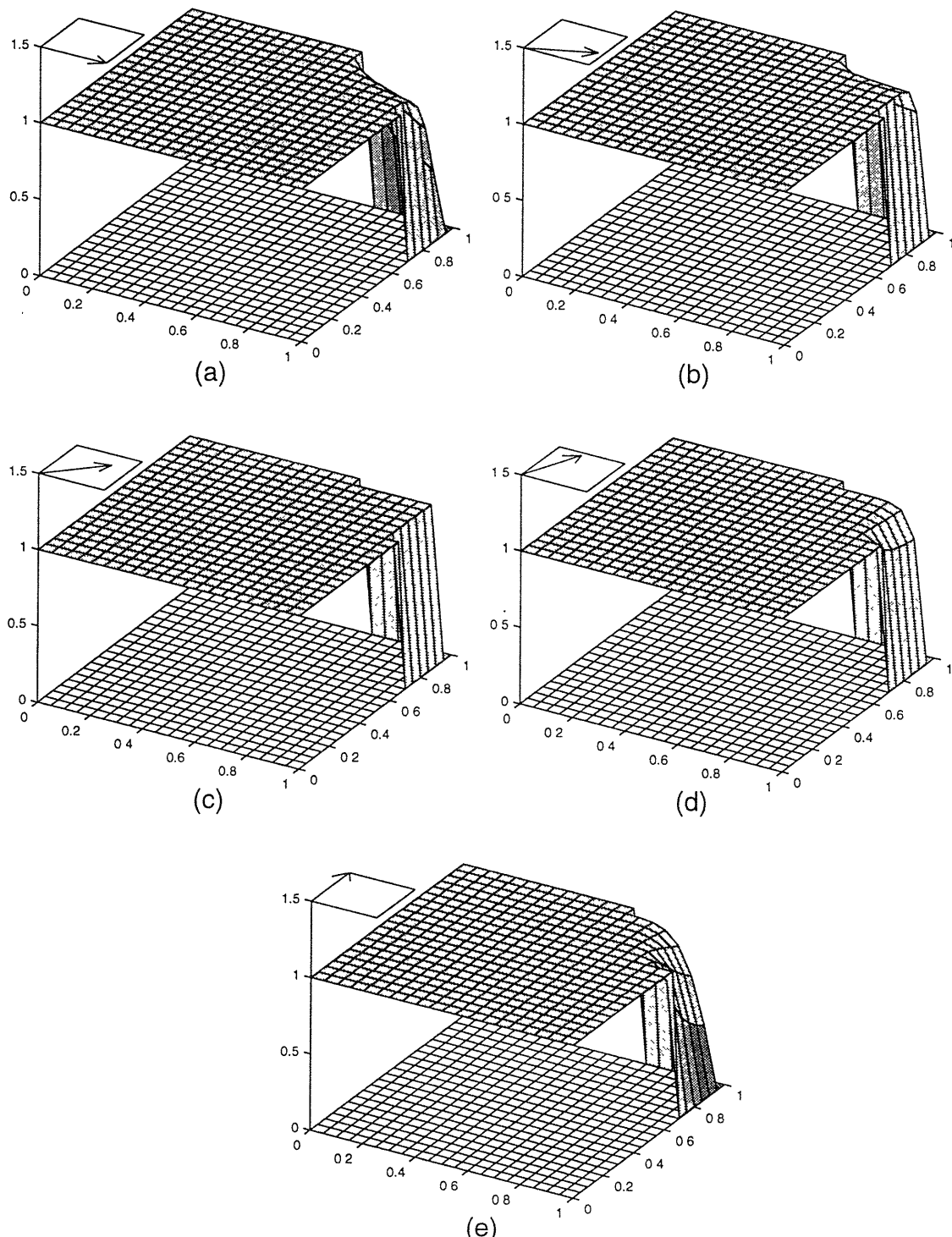
Figure 6-21: Numerical results of ADINA-F for solving the test problem 2 on uniform mesh. (a) run 1 (b) run 2 (c) run 3 (d) run 4 (e) run 5
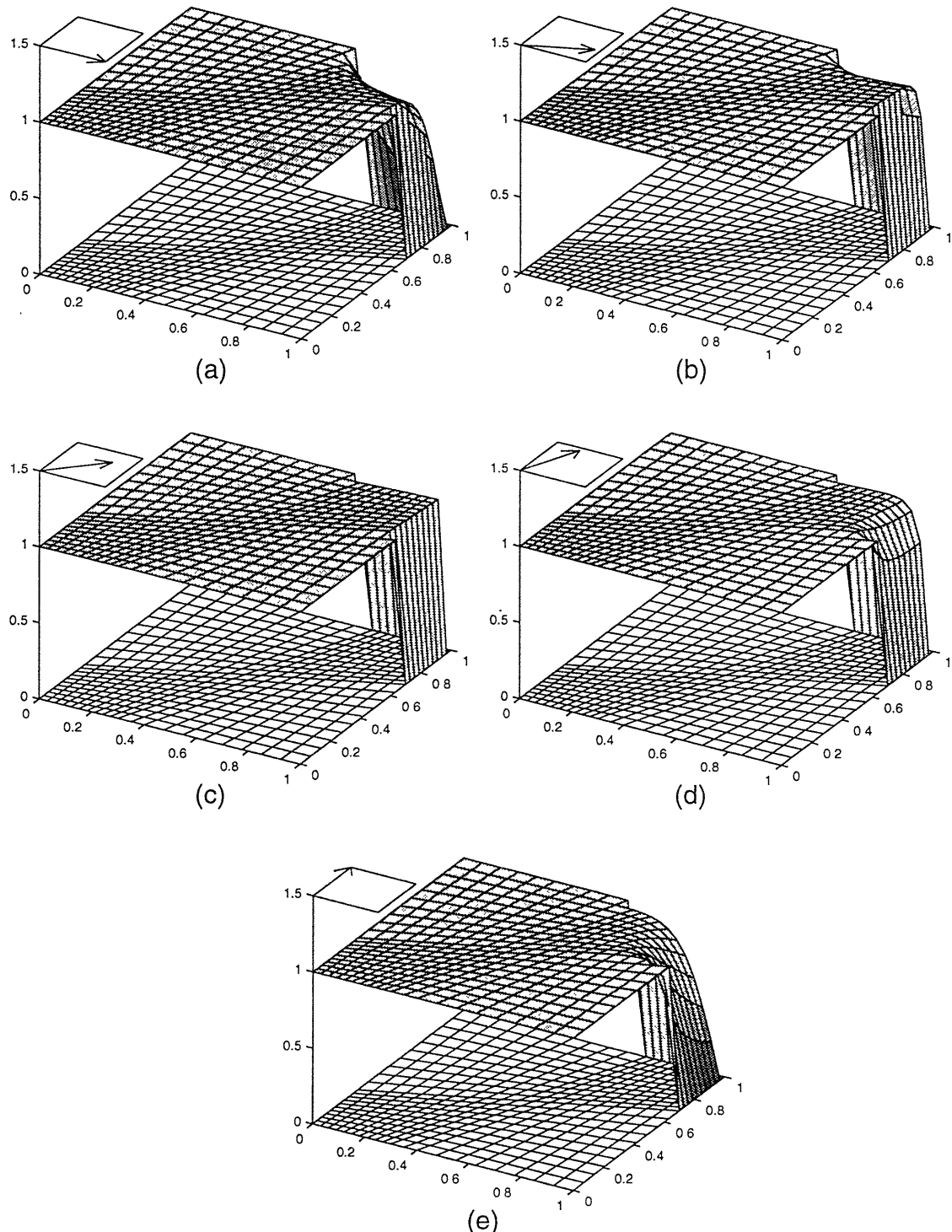
Figure 6-22: Numerical results of ADINA-F for solving the test problem 2 on distorted mesh. (a) run 1 (b) run 2 (c) run 3 (d) run 4 (e) run 5

Chapter 7

Conclusions

Based on the results given in the previous chapter, we have the following conclusions:

1. The SUPG and BSUPG upwinding procedures are easy to implement, however the results still contain small oscillations near shock fronts and boundary layers.

2. The third order accuracy upwinding scheme provides reasonable accuracy but is considerably more expensive in terms of memory space as well as computational time.

3. The ADINA-F upwinding method provides good stability. Since triangular elements are used, the accuracy near the shock fronts and boundary layers is less than that based on quadrilateral elements.

4. The overall best performing technique was the positive-coefficient upwinding procedure.

Of course, the upwinding schemes considered in this thesis were only tested on two analysis problems. For practical analyes, a discretization procedure must be sufficiently general to model very complex domains and be applicable to low and high Reynolds and Peclet number flows. It is then important that the discretization scheme also satisfy the inf-sup condition (to have a stable procedure for low Reynolds number flows) and this aspect was not addressed in this thesis.

Appendix A

Calculation of a control variable in Petrov-Galerkin method

The equation of discrete form for the ith node in a uniform mesh for one dimensional case using Petrov-Galerkin method (eqn. 3.24) is as follows

$$(-1 - (1 + \gamma)\frac{Pe^e}{2})\theta_{i-1} + (2 + \gamma Pe^e)\theta_i + (-1 + (1 - \gamma)\frac{Pe^e}{2})\theta_{i+1} = 0$$

This equation can be rewritten as

$$a\theta_{i-1} - (a + b)\theta_i + b\theta_{i+1} = 0$$

where $a = (-1 - (1 + \gamma)\frac{Pe^e}{2})$ and $b = (-1 + (1 - \gamma)\frac{Pe^e}{2})$, then manipulating this equation

$$
\begin{aligned}
\theta_{i+1} &= \frac{a+b}{b}\theta_i - \frac{a}{b}\theta_{i-1} \\
&= (1 + \frac{a}{b})\theta_i - \frac{a}{b}\theta_{i-1} \\
&= (1 + r)\theta_i - r\theta_{i-1}
\end{aligned}
$$

where $r = \frac{a}{b}$. Set $\theta_{-1} = K$ and $\theta_0 = L$, then

for $i = 0$

$$\theta_1 = (1+r)L - rK$$
$$= L + r(L - K)$$

for $i = 1$

$$\theta_2 = (1+r)(L + r(L-K)) - rL$$
$$= L + (r + r^2)(L - K)$$

for $i = 2$

$$\theta_3 = (1+r)(L + (r + r^2)(L-K)) - r(L + r(L-K))$$
$$= L + (r + r^2 + r^3)(L - K)$$

for $i = n$

$$\theta_{n+1} = L + (r + r^2 + r^3 + \ldots + r^{n+1})(L - K)$$
$$= L + (-1 + \sum_{k=0}^{n+1} r^k)(L - K)$$

Now consider,

$$\sum_{k=0}^{n+1} r^k - r \sum_{k=0}^{n+1} r^k = (1 + r + \ldots + r^{n+1}) - (r + r^2 + \ldots + r^{n+2})$$
$$= 1 - r^{n+2}$$

and also,

$$\sum_{k=0}^{n+1} r^k - r \sum_{k=0}^{n+1} r^k = (1 - r) \sum_{k=0}^{n+1} r^k$$

so,

$$\sum_{k=0}^{n+1} r^k = \frac{1 - r^{n+2}}{1 - r}$$

97

then, θ_{n+1} equation becomes

$$
\begin{aligned}
\theta_{n+1} &= -1 + \frac{1 - r^{n+2}}{1 - r} \\
&= \frac{r}{1 - r} - \frac{r}{1 - r} r^{n+1} \\
&= A_1 + B_1 r^{n+1}
\end{aligned}
$$

The exact solution for the convection-diffusion equation is

$$
\theta = \theta_L + \frac{\theta_R - \theta_L}{\exp(Pe^{e}) - 1}(\exp(\frac{Pe^{e} X}{L}) - 1)
$$

where θ_L is the given value of θ at the left boundary and θ_R at the right boundary. This equation can be rewritten as

$$
\theta = \theta_L - \frac{\theta_R - \theta_L}{\exp(Pe^{e}) - 1} + (\frac{\theta_R - \theta_L}{\exp(Pe^{e}) - 1})(\exp(\frac{Pe^{e}}{L}))^x
$$

Comparing the equation above to that obtained from discretization using the Petrov-Galerkin upwinding method, we obtain the relation that

$$
\begin{aligned}
A_1 &= \theta_L - \frac{\theta_R - \theta_L}{\exp(Pe^{e}) - 1} \\
B_1 &= \frac{\theta_R - \theta_L}{\exp(Pe^{e}) - 1} \\
r &= \exp(\frac{Pe^{e}}{L})
\end{aligned}
$$

The equation for A_1 and B_1 involve other variables, θ_L and θ_R, which are given values of θ at the boundary conditions. The last equation is used to determine the value of γ. Substituting the variable r with the expression defined in the discretized equation and assigning $L = 1$ since L is a non-dimensionalized length, we obtain

$$
\frac{-1 - (1 + \gamma)\frac{Pe^{e}}{2}}{-1 + (1 - \gamma)\frac{Pe^{e}}{2}} = \exp(Pe^{e})
$$

Manipulating the equation above, we obtain the equation for γ

$$\gamma = \coth(\frac{Pe^e}{2}) - \frac{2}{Pe^e}$$

Therefore, eqn. 3.25 is proved.

Appendix B

Calculation of a control variable in Galerkin least squares method

The equation in discrete form for the ith node in a uniform mesh for one dimensional case using the Galerkin least squares upwinding method (eqn. 3.28) is as follows

$$(-1 - \frac{Pe^e}{2} - \frac{\tau v^2}{\alpha})\theta_{i-1} + (2 + 2\frac{\tau v^2}{\alpha})\theta_i + (-1 + \frac{Pe^e}{2} - \frac{\tau v^2}{\alpha})\theta_{i+1} = 0$$

This equation can be rewritten as

$$a\theta_{i-1} - (a + b)\theta_i + b\theta_{i+1} = 0$$

where $a = (-1 - \frac{Pe^e}{2} - \frac{\tau v^2}{\alpha})$ and $b = (-1 + \frac{Pe^e}{2} - \frac{\tau v^2}{\alpha})$. The discretized equation is compared to the exact solution of the convection diffusion equation (refer to appendix A for a similar explanation), we obtain.

$$\frac{-1 - \frac{Pe^e}{2} - \frac{\tau v^2}{\alpha}}{-1 + \frac{Pe^e}{2} - \frac{\tau v^2}{\alpha}} = \exp(Pe^e)$$

Manipulating the equation above, we obtain

$$\tau = \frac{h}{2v}\coth(\frac{Pe^e}{2}) - \frac{\alpha}{v^2}$$

Therefore, eqn. 3.29 is proved.

Appendix C

Comparison of the Petrov-Galerkin method and the Galerkin least squares method

The Petrov-Galerkin method has the following equation

$$\int_{Vol} \overline{w}(\theta_{,t} + \underline{v} \cdot \underline{\nabla}\theta - \alpha \nabla^2 \theta - q) \, dVol = 0$$

where

$$\overline{w} = w + \lambda \frac{\underline{v} \cdot \underline{\nabla}w}{\parallel \underline{v} \parallel}$$

Applying integration by parts and the divergence rule, we obtain

$$\int_{Vol} w \, \theta_{,t} \, dVol \; + \; \int_{Vol} w \, \underline{v} \cdot \underline{\nabla}\theta \, dVol + \int_{Vol} \underline{\nabla}w \; \alpha \; \underline{\nabla}\theta \, dVol$$

$$+ \int_{Vol} \underline{\nabla}w \cdot \underline{v}\frac{\lambda}{\parallel \underline{v} \parallel}\theta_{,t} \, dVol \; + \; \int_{Vol} \underline{\nabla}w \cdot \underline{v}\frac{\lambda}{\parallel \underline{v} \parallel}\underline{v} \cdot \underline{\nabla}\theta \, dVol$$

$$- \int_{Vol} \underline{\nabla}w \cdot \underline{v}\frac{\lambda}{\parallel \underline{v} \parallel} \; \alpha \; \nabla^2 \theta \, dVol \; - \; \int_{Vol} \underline{\nabla}w \cdot \underline{v}\frac{\lambda}{\parallel \underline{v} \parallel} \; q \, dVol$$

$$= \; \int_{Vol} w \; q \, dVol + \int_{S_f} w \; q^* \, dS_f$$

For a linear interpolation element, terms of the second order spatial derivatives vanish, and so the above equation becomes

$$\int_{Vol} w\,\theta_{,t}\,dVol \;+\; \int_{Vol} w\,\underline{v}\cdot\underline{\nabla}\theta\,dVol + \int_{Vol} \underline{\nabla}w\,\alpha\,\underline{\nabla}\theta\,dVol$$

$$+\int_{Vol}\underline{\nabla}w\cdot\underline{v}\frac{\lambda}{\|\underline{v}\|}\theta_{,t}\,dVol \;+\; \int_{Vol}\underline{\nabla}w\cdot\underline{v}\frac{\lambda}{\|\underline{v}\|}\underline{v}\cdot\underline{\nabla}\theta\,dVol - \int_{Vol}\underline{\nabla}w\cdot\underline{v}\frac{\lambda}{\|\underline{v}\|}\,q\,dVol$$

$$= \int_{Vol} w\,q\,dVol + \int_{S_f} w\,q^{\bullet}\,dS_f$$

On the other hand, the Galerkin least squares method has the following equation

$$\int_{Vol} w\,(\theta_{,t}+\underline{v}\cdot\underline{\nabla}\theta-\alpha\nabla^2\theta-q)\,dVol + \int_{Vol}(L_{2m}\,[w])\tau(L_{2m}\,[\theta])\,dVol = 0$$

where

$$L_{2m}\,[w] \;=\; \underline{v}\cdot\underline{\nabla}w-\alpha\nabla^2 w$$

$$L_{2m}\,[\theta] \;=\; \underline{v}\cdot\underline{\nabla}\theta-\alpha\nabla^2\theta$$

Applying integration by parts and the divergence rule, we obtain

$$\int_{Vol} w\,\theta_{,t}\,dVol \;+\; \int_{Vol} w\,\underline{v}\cdot\underline{\nabla}\theta\,dVol + \int_{Vol}\underline{\nabla}w\,\alpha\,\underline{\nabla}\theta\,dVol$$

$$+\int_{Vol}\underline{\nabla}w\cdot\underline{v}\,\tau\,\theta_{,t}\,dVol \;+\; \int_{Vol}\underline{\nabla}w\cdot\underline{v}\,\tau\,\underline{v}\cdot\underline{\nabla}\theta\,dVol - \int_{Vol}\underline{\nabla}w\cdot\underline{v}\,\tau\,\alpha\,\nabla^2\theta\,dVol$$

$$-\int_{Vol}\underline{\nabla}w\cdot\underline{v}\,\tau\,q\,dVol \;-\; \int_{Vol}\nabla^2 w\,\alpha\,\tau\,\theta_{,t}\,dVol - \int_{Vol}\nabla^2 w\,\alpha\,\tau\,\underline{v}\cdot\underline{\nabla}\theta\,dVol$$

$$+\int_{Vol}\nabla^2 w\,\alpha\,\tau\,\alpha\,\nabla^2\theta\,dVol \;+\; \int_{Vol}\nabla^2 w\,\alpha\,\tau\,q\,dVol$$

$$= \int_{Vol} w\,q\,dVol + \int_{S_f} w\,q^{\bullet}\,dS_f$$

Similarly, for a linear interpolation element, terms of the second order spatial derivatives vanish, and the above equation becomes

$$\int_{Vol} w\,\theta_{,t}\,dVol \;+\; \int_{Vol} w\,\underline{v}\cdot\underline{\nabla}\theta\,dVol + \int_{Vol}\underline{\nabla}w\,\alpha\,\underline{\nabla}\theta\,dVol$$

$$+\int_{Vol}\underline{\nabla}w\cdot\underline{v}\,\tau\,\theta_{,t}\,dVol \;+\; \int_{Vol}\underline{\nabla}w\cdot\underline{v}\,\tau\,\underline{v}\cdot\underline{\nabla}\theta\,dVol - \int_{Vol}\underline{\nabla}w\cdot\underline{v}\,\tau\,q\,dVol$$

103

$$= \int_{Vol} w\, q\, dVol + \int_{S_f} w\, q^{\cdot}\, dS_f$$

For the linear interpolation element, these two schemes are identical where τ in the equation obtained using the Galerkin least squares method is equivalent to $\dfrac{\lambda}{\| \underline{v} \|}$ in the equation obtained using the Petrov-Galerkin method.

For the general element, these two schemes are not identical. The Galerkin least squares method results into an equation that contains extra terms.

Bibliography

[1] J. Argyris, A. Laxander, and J. Szimmat. Petrov-Galerkin finite element approach to coupled heat and fluid flows. *Comput. Methods Appl. Mech. Engrg*, 94:181–200, 1992.

[2] K.J. Bathe. *Finite Element Procedures* . Prentice-Hall, in press.

[3] C.E. Baumann, M.A. Storti, and S.R. Idelsohn. A Petrov-Galerkin technique for the solution of transonic and supersonic flows. *Comput. Methods Appl. Mech. Engrg*, 95:49–70, 1992.

[4] E.T. Bouloutas, and M.A. Celia. An improved cubic Petrov-Galerkin method for simulation of transient advection-diffusion processes in rectangularly decomposable domains. *Comput. Methods Appl. Mech. Engrg*, 92:289–308, 1991.

[5] A.N. Brooks and T.J.R. Hughes. Streamline upwind/Petrov-Galerkin formulations for convection dominated flows with particular emphasis on the incompressible Navier-Stokes equations. *Comput. Methods Appl. Mech. Engrg*, 32:199–259, 1982.

[6] E.G.D. Carmo and A.C. Galeao. Feedback Petrov-Galerkin methods for convection-dominated problems. *Comput. Methods Appl. Mech. Engrg*, 88:1–16, 1991.

[7] D. Chapelle, and K.J. Bathe. The Inf-Sup test. *Computers and Structures*, 47:537–545, 1993.

[8] I. Christie, D.F. Griffiths, A.R. Mitchell, and O.C. Zienkiewicz. Finite element methods for second order differential equations with significant first derivatives. *Internat. J. Numer. Methods Engrg.*, 10:1389–1396, 1976.

[9] R. Courant, E. Isaacson, and M. Rees. On the solution of nonlinear hyperbolic differential equations by finite differences. *Comm. on Pure and Applied Math.*, 5:243–255, 1952.

[10] E. Dick. Accurate Petrov-Galerkin methods for transient convective diffusion problems. *Inter. J. Num. Methods in Engrg*, 19:1425–1433, 1983.

[11] J. Donea, V. Selmin, and L. Quartapelle. Recent developments of the Taylor-Galerkin method for the numerical solution of hyperbolic problems. In *Numerical Methods for Fluid Dynamics III*, pages 171–185, New York, 1988. Oxford Univ. Press.

[12] T.J.R. Hughes, L.P. Franca, and G.M. Hulbert. A new finite element formulation for computational fluid dynamics: VIII. the Galerkin/least-squares method for advective-diffusive equations. *Comput. Methods Appl. Mech. Engrg.*, 73:173–189, 1989.

[13] T.J.R. Hughes and M. Mallet. A new finite element formulation for computational fluid dynamics : IV. a discontinuity-capturing operator for multidimensional advective-diffusive systems. *Comput. Methods Appl. Mech. Engrg*, 58:329–336, 1986.

[14] T.J.R. Hughes, M. Mallet, and A. Mizukami. A new finite element formulation for computational fluid dynamics: II. beyond SUPG. *Comput. Methods Appl. Mech. Engrg*, 54:341–355, 1986.

[15] G.E. Schneider. Elliptic Systems : Finite-Element Method I in W.J. Minkowycz E.M. Sparrow R.H. Pletcher and G.E. Schneider (eds). *Handbook of Numerical Heat Transfer*. Wiley, New York, 1988.

[16] N. Kondo, N. Tosaka, and T. Nishimura. Numerical simulation of viscous flows by the third-order upwind finite element method. *Theor. Appl. Mech.*, 39:237–250, 1990.

[17] N. Kondo, N. Tosaka, and T. Nishimura. Third-order upwind finite element formulations for incompressible viscous flow problems. *Comput. Methods Appl. Mech. Engrg.*, 93:169–187, 1991.

[18] N. Kondo, N. Tosaka, and T. Nishimura. Computation of incompressible viscous flows by the third-order upwind finite element method. *Inter. J. for Num. Methods in Fluids*, 15:1013–1024, 1992.

[19] A. Mizukami. An implementation of the streamline-upwind/Petrov-Galerkin method for linear triangular elements. *Comput. Methods Appl. Mech. Engrg*, 49:357–364, 1985.

[20] A. Mizukami and T.J.R. Hughes. A Petrov-Galerkin finite element method for convection dominated flows: an accurate upwinding technique for satisfying the maximum principle. *Comput. Methods Appl. Mech. Engrg*, 50:181–193, 1985.

[21] S.V. Patankar. *Numerical Heat Transfer and Fluid Flows*. McGraw-Hill, New York, 1980.

[22] G.E. Schneider and M.J. Raw. A skewed positive influence coefficient upwinding procedure for control-volume-based finite-element convection-diffusion computation. *Numerical Heat Transfer*, 9:1–26, 1986.

[23] F. Shakib. Finite element analysis of the compressible Euler and Navier-Stokes equations. *Ph.D. thesis, Stanford University*, 1988.

[24] D. B. Spalding. A novel finite difference formulation for differential expressions involving both first and second derivatives. *Internat. J. Numer. Methods Engrg.*, 4:551–559, 1972.

[25] C.R. Swaminathan and V.R. Voller. Streamline upwind scheme for control-volume finite element, part I. Formulations. *Numerical Heat Transfer, Part B*, 22:95–107, 1992.

[26] C.R. Swaminathan and V.R. Voller. Streamline upwind scheme for control-volume finite element, part II. Implementation and comparison with the SUPG finite-element scheme. *Numerical Heat Transfer, Part B*, 22:109–124, 1992.

[27] T.E. Tezduyar, S. Mittal, and R. Shih. Time-accurate incompressible flow computations with quadrilateral velocity-pressure element. *Comput. Methods Appl. Mech. Engrg*, 87:363–384, 1991.